National Library of Canada

Acquisitions and Bibliographic Services Branch

395 Wellington Street
Ottawa, Ontario
K1A 0N4

Bibliothèque nationale du Canada

Direction des acquisitions et des services bibliographiques

395, rue Wellington
Ottawa (Ontario)
K1A 0N4

Your file Votre référence

Our file Notre référence

NOTICE

The quality of this microform is heavily dependent upon the quality of the original thesis submitted for microfilming. Every effort has been made to ensure the highest quality of reproduction possible.

If pages are missing, contact the university which granted the degree.

Some pages may have indistinct print especially if the original pages were typed with a poor typewriter ribbon or if the university sent us an inferior photocopy.

Reproduction in full or in part of this microform is governed by the Canadian Copyright Act, R.S.C. 1970, c. C-30, and subsequent amendments.

AVIS

La qualité de cette microforme dépend grandement de la qualité de la thèse soumise au microfilmage. Nous avons tout fait pour assurer une qualité supérieure de reproduction.

S'il manque des pages, veuillez communiquer avec l'université qui a conféré le grade.

La qualité d'impression de certaines pages peut laisser à désirer, surtout si les pages originales ont été dactylographiées à l'aide d'un ruban usé ou si l'université nous a fait parvenir une photocopie de qualité inférieure.

La reproduction, même partielle, de cette microforme est soumise à la Loi canadienne sur le droit d'auteur, SRC 1970, c. C-30, et ses amendements subséquents.

Canada

UNIVERSITY OF ALBERTA

ANALYSIS OF CONFINING LAYER BEHAVIOUR

IN

WATER FLOODING AND FLUID DISPOSAL OPERATIONS

BY

© SYED AKHTAR-UL-HASAN WARSI

A THESIS
SUBMITTED TO THE FACULTY OF GRADUATE STUDIES AND RESEARCH IN
PARTIAL FULFILLMENT OF THE REQUIREMENT FOR THE DEGREE OF

MASTER OF SCIENCE

IN

PETROLEUM ENGINEERING

DEPARTMENT OF MINING, METALLURGICAL AND
PETROLEUM ENGINEERING

EDMONTON, ALBERTA
FALL 1994

National Library
of Canada

Acquisitions and
Bibliographic Services Branch

395 Wellington Street
Ottawa, Ontario
K1A 0N4

Bibliothèque nationale
du Canada

Direction des acquisitions et
des services bibliographiques

395, rue Wellington
Ottawa (Ontario)
K1A 0N4

Your file Votre référence

Our file Notre référence

THE AUTHOR HAS GRANTED AN IRREVOCABLE NON-EXCLUSIVE LICENCE ALLOWING THE NATIONAL LIBRARY OF CANADA TO REPRODUCE, LOAN, DISTRIBUTE OR SELL COPIES OF HIS/HER THESIS BY ANY MEANS AND IN ANY FORM OR FORMAT, MAKING THIS THESIS AVAILABLE TO INTERESTED PERSONS.

L'AUTEUR A ACCORDE UNE LICENCE IRREVOCABLE ET NON EXCLUSIVE PERMETTANT A LA BIBLIOTHEQUE NATIONALE DU CANADA DE REPRODUIRE, PRETER, DISTRIBUER OU VENDRE DES COPIES DE SA THESE DE QUELQUE MANIERE ET SOUS QUELQUE FORME QUE CE SOIT POUR METTRE DES EXEMPLAIRES DE CETTE THESE A LA DISPOSITION DES PERSONNE INTERESSEES.

THE AUTHOR RETAINS OWNERSHIP OF THE COPYRIGHT IN HIS/HER THESIS. NEITHER THE THESIS NOR SUBSTANTIAL EXTRACTS FROM IT MAY BE PRINTED OR OTHERWISE REPRODUCED WITHOUT HIS/HER PERMISSION.

L'AUTEUR CONSERVE LA PROPRIETE DU DROIT D'AUTEUR QUI PROTEGE SA THESE. NI LA THESE NI DES EXTRAITS SUBSTANTIELS DE CELLE-CI NE DOIVENT ETRE IMPRIMES OU AUTREMENT REPRODUITS SANS SON AUTORISATION.

ISBN 0-612-01789-3

Canada

UNIVERSITY OF ALBERTA

RELEASE FORM

NAME OF AUTHOR: Syed Akhtar-Ul-Hasan Warsi

TITLE OF THE THESIS: Analysis of Confining Layer Behaviour During Water Flooding and Fluid Disposal Operations

DEGREE FOR WHICH THESIS WAS PRESENTED: Master of Science

YEAR THIS DEGREE WAS GRANTED: Fall 1994

Permission is hereby granted to THE UNIVERSITY OF ALBERTA LIBRARY to reproduce single copies of this thesis and to lend or sell such copies for private, scholarly or scientific research only.

The author reserves other publication rights, and neither the thesis nor extensive extracts from it may be printed or otherwise reproduced without the author's written permission.

(SIGNED) _____

PERMANENT ADDRESS:

W4 - 104, 15508 - 84 Avenue
Edmonton, Alberta
T5R 3L6

DATED: July 16, 1994

THE UNIVERSITY OF ALBERTA

FACULTY OF GRADUATE STUDIES AND RESEARCH

This is to certify that they have read, and recommend to the Faculty of Graduate Studies and Research for acceptance, a thesis entitled ANALYSIS OF CONFINING LAYER BEHAVIOUR DURING WATER FLOODING AND FLUID DISPOSAL OPERATIONS submitted by SYED AKHTAR-UL-HASAN WARSI in partial fulfillment of the requirements for the degree of Master of Science in Petroleum Engineering.

Dr. W. S. Tortike (Supervisor)

Dr. R.G. Bentsen

Dr. D. Chan

Date: August 04/1994

ABSTRACT

Effective resource management is required to assure safe and environmentally responsible development of oil and gas fields. Hydraulic fractures which break out through the upper confining stratum can carry oil and gas up into the overlying formations, possibly contaminating water supplies. Similarly, the disposal of fluid waste by injection wells should ensure that it is confined to the intended injection zone.

To prevent any breakdown of the upper confining stratum during water flooding and waste disposal operations, an understanding of horizontal stress distribution in the confining layer and pore pressure distribution in the injection zone is required. The stress gradient in the underlying confining layer is usually higher than the injection zone, therefore it is less likely to break and has not been considered in the study. The pore pressure distribution in the injection zone was considered for Steady-State, transient, and pseudosteady-state flow systems. The radial and tangential stress profiles in the confining layer were developed under complete wellbore stress relief and under the conditions of applied wellbore stress. Analytical equations have been developed for the radius of the potential fracture region in the confining layer. Subsequently, the effect of pore pressure on the horizontal stresses in the confining layer has been studied to determine the potential fracture zones.

The radius of the potential fracture region in the confining layer at low wellbore injection pressures depends on the completion packer setting depth and the annulus pressure above the packer. When the packer is set below the confining layer and a certain minimum annulus pressure is maintained, the radius of the potential fracture region decreases compared to when the packer is set above the confining layer and wellbore pressure can be transmitted directly to the confining layer.

This is the first study combining petroleum engineering and geomechanical aspects to identify a potential environmental problem in injection and disposal operations. This study indicates that the minimum horizontal stresses in the confining layer should be considered when providing guidelines for safe injection pressure limitations for subsurface waste fluid disposal and water flooding operations.

ACKNOWLEDGMENTS

The author wishes to express his sincere gratitude and appreciation to Dr. W.S. Tortike for his guidance, encouragement and support throughout this study. Financial support for this work and my graduate studies was provided by the Central Research Fund of the University of Alberta, NSERC and CANMET, for which I am very thankful.

The author extends his thanks to Dr. D. Chan of the Department of Civil Engineering for providing his valuable expertise without which the study could not have been completed.

Finally, I would like to thank my family, especially my wife Ambreen, for their support, patience and understanding during my graduate studies.

TABLE OF CONTENTS

Page

Chapter 1: Introduction 1

Chapter 2: Review of Literature 3

Literature Review of Breakdown and Fracture Extension Pressure 3

Literature Review of Fracture Containment in Layered Formation 5

Tensile Fracture Criteria 8

Hydraulic Fracturing Process 8

Fracture Criteria 9

Comments 11

Chapter 3: Statement of the Problem 15

Statement of Problem 15

Chapter 4: Model Development 17

General Assumptions 17

Stress Field 18

Isotropic Stress around the Wellbore 18

Anisotropic Stresses around the Wellbore 20

Well Completions 21

Packer Set above the Confining Layer 21

Packer Set below the Confining Layer 21

Anisotropic Stresses and Fracture Azimuth 22

Chapter 5: Analytical Model of Radius of Potential Fracture Region—Steady-State Flow 29

Steady-State Flow 29

Analytical Model 30

Isotropic Stress Field, Stress Applied and Steady-State Flow Conditions 30

Isotropic Stress Field, Stress Relief and Steady-State Flow Conditions 33

Anisotropic Stress Field, Stress Applied and Steady-State Flow Conditions 33

Anisotropic Stress Field, Stress Relief and Steady-State Flow Conditions 35

Chapter 6: Analytical Model of Radius of Potential Fracture Region— Transient Flow 40

Transient Flow 40

Analytical Model 41

Isotropic Stress Field, Stress Applied and Transient Flow Conditions 41

Isotropic Stress Field, Stress Relief and Transient Flow Conditions 43

Anisotropic Stress Field, Stress Applied and Transient Flow Conditions 44

Anisotropic Stress Field, Stress Relief and Transient Flow Conditions 45

Chapter 7: Analytical Model of Radius of Potential Fracture Region—Pseudosteady-State Flow 50

Pseudosteady-State Flow 50

Analytical Model 52

Isotropic Stress Field, Stress Applied and Pseudosteady-state Flow Conditions 52

Isotropic Stress Field, Stress Relief and Pseudosteady-state Flow Conditions 54

Isotropic Stress Field, Stress Relief and Pseudosteady-state Flow Conditions 54

Anisotropic Stress Field, Stress Applied, and Pseudosteady-state Flow Conditions 55

Anisotropic Stress Field, Stress Relief and Pseudosteady-state Flow Conditions 56

Chapter 8: Investigation of the Limits of the Region of Potential Fracture 59

Effect of Injection and Injection Zone Pressure 59

Isotropic Stress Field and Stress Applied Conditions 60

Isotropic Stress Field and Stress Relief Conditions 61

Effect of Stress Relief Near the Wellbore 61

Anisotropic Stress Field and Stress Applied Conditions 62

Anisotropic Stress Field and Stress Relief Conditions 62

Effect of Stress Relief Near the Wellbore 63

Effect of Stress Contrast 64

Anisotropic Stress Field and Stress Applied Conditions 64

Anisotropic Stress Field and Stress Relief Conditions 64

Effect of Packer Setting Depth 65

Effect of Injection Rate 65

Effect of Injection Time 66

Effect of Injection Zone Porosity, Compressibility and Fluid Viscosity 66

Chapter 9: Conclusions and Recommendations 84

Conclusions 84

Recommendations 85

Bibliography 87

Appendix FORTRAN Programs 91

LIST OF TABLES

		Page
Table 2.1	Possible Shale Fracture	13
Table 5.1	Injection Zone and Confining Layer Parameters Used for Steady-State Flow Conditions	36
Table 6.1	Injection Zone and Confining Layer Parameters Used for Transient and Pseudosteady-State Flow Conditions	47

LIST OF FIGURES

		Page
Figure 2.1	Stress Condition in an Elemental Cube	14
Figure 4.1	Assumed Geological Conditions in the Ground	24
Figure 4.2	Isotropic Stresses Acting on a Formation	25
Figure 4.3	Stresses in a Hollow Cylinder	25
Figure 4.4	Radial and Tangential Stress Profile, Well Pressure Higher than Isotropic Stress Field	26
Figure 4.5	Anisotropic Stresses Acting on a Formation	26
Figure 4.6	Radial and Tangential Stress Profile, Isotropic Stress Field $\sigma_{h2}<p_w<\sigma_{h1}$	27
Figure 4.7	Packer Set Above the Confining Layer Stress Applied Conditions	27
Figure 4.8	Packer Set Below the Confining Layer Stress Relief Conditions	28
Figure 4.9	Effect of Stress Contrast on Fracture Orientation Around the Wellbore in Complete Stress Relief and Stress Applied Conditions	28
Figure 5.1	Steady-State Flow and Tangential Stresses in Isotropic Stress Field	37
Figure 5.2	Steady-State Flow and Radial Stresses in Isotropic Stress Field	37
Figure 5.3	Steady-State Flow and Radial Stresses in Anisotropic Stress Field	38
Figure 5.4	Steady-State Flow and Tangential Stresses in Anisotropic Stress Field	38
Figure 5.5	Steady-State Flow and Radial Stresses in Complete Stress Relief Conditions in Anisotropic Stress Field	39
Figure 6.1	Transient Flow and Tangential Stresses in Isotropic Stress Field	48
Figure 6.2	Transient Flow and Radial Stresses in Isotropic Stress Field	48
Figure 6.3	Transient Flow and Tangential Stresses in Anisotropic Stress Field	49.
Figure 7.1	Pseudosteady-State Flow and Tangential Stresses in Isotropic Stress Field	57
Figure 7.2	Pseudosteady-State Flow and Radial Stresses in Isotropic Stress Field	57.

Page

Figure 7.3 Pseudosteady-State Flow and Tangential Stresses Anisotropic Stress Field ..... 58.

Figure 8.1 Radius of Potential Fracture Region Steady-State Flow and Radial Stresses in Isotropic Stress Field 67

Figure 8.2 Radius of Potential Fracture Region Transient Flow and Radial Stresses in Isotropic Stress Field (Time 100 Hours) 67

Figure 8.3 Radius of Potential Fracture Region Pseudosteady-Steady-State Flow and Radial Stresses in Isotropic Stress Field (Time 1 Hour) 68

Figure 8.4 Radius of Potential Fracture Region Steady-State Flow and Radial Stresses in Complete and Partial Stress Relief Conditions 68

Figure 8.5 Radius of Potential Fracture Region Transient Flow and Radial Stresses in Complete and Partial Stress Relief Conditions (Time 100 Hours) 69

Figure 8.6 Radius of Potential Fracture Region Pseudosteady-State Flow and Radial Stresses in Complete and Partial Stress Relief Conditions (Time 1 Hour) 69

Figure 8.7 Comparison of Radius of Potential Fracture Region Near Wellbore in Complete and Partial Stress Relief Conditions Steady-State Flow and Radial Stresses 70

Figure 8.8 Comparison of Radius of Potential Fracture Region Near Wellbore in Complete and Partial Stress Relief Conditions Transient Flow and Radial Stresses (Time 100 Hours) 70

Figure 8.9 Comparison of Radius of Potential Fracture Region Near Wellbore in Complete and Partial Stress Relief Conditions Pseudo-Steady-State Flow and Stresses Radial (Time 1 Hour) 71

Figure 8.10 Radius of Potential Fracture Region Effect of Stress Contrast and Injection Zone Pressure Steady-State Flow and Tangential Stresses 71

Figure 8.11 Radius of Potential Fracture Region Effect of Stress Contrast and Injection Zone Pressure Transient Flow and Tangential Stresses (Time 100 Hours) 72

Figure 8.12 Radius of Potential Fracture Region Effect of Stress Contrast and Injection Zone Pressure Pseudosteady-State Flow and Tangential Stresses (Time 1 Hour) 72

Page

Figure 8.13 Radius of Potential Fracture Region Effect of Stress Contrast and Injection Zone Pressure Steady-State Flow and Tangential Stresses in Complete Stress Relief Conditions 73

Figure 8.14 Radius of Potential Fracture Region Effect of Stress Contrast and Injection Zone Pressure Transient Flow and Tangential Stresses in Complete Stress Relief Conditions (Time 100 Hours) 73

Figure 8.15 Radius of Potential Fracture Region Effect of Stress Contrast and Injection Zone Pressure Pseudosteady-State Flow and Tangential Stresses in Complete Stress Relief Conditions (Time 1 Hour)..... 74

Figure 8.16 Radius of Potential Fracture Region Effect of Stress Contrast and Injection Zone Pressure Steady-State Flow and Tangential Stresses in Partial Stress Relief Conditions 74

Figure 8.17 Radius of Potential Fracture Region Effect of Stress Contrast and Injection Zone Pressure Transient Flow and Tangential Stresses in Partial Stress Relief Conditions (Time 100 Hours) 75

Figure 8.18 Radius of Potential Fracture Region Effect of Stress Contrast and Injection Zone Pressure Pseudosteady-State Flow and Tangential Stresses in Partial Stress Relief Conditions (Time 1 Hour) 75

Figure 8.19 Comparison of Radius of Potential Fracture Region Near Wellbore in Complete and Partial Stress Relief Conditions Steady-State Flow and Tangential Stresses 76

Figure 8.20 Comparison of Radius of Potential Fracture Region Near Wellbore in Complete and Partial Stress Relief Conditions Transient Flow and Tangential Stresses (Time 100 Hours) 76

Figure 8.21 Comparison of Radius of Potential Fracture Region Near Wellbore in Complete and Partial Stress Relief Conditions Pseudosteady-State Flow and Stresses Radial (Time 1 Hour) 77

Figure 8.22 Effect of Horizontal Stress Contrast and Injection Pressure Steady-State Flow and Tangential Stresses 77

Figure 8.23 Effect of Horizontal Stress Contrast and Injection Pressure Transient Flow and Tangential Stresses (Time 100 Hours) 78

Figure 8.24 Effect of Horizontal Stress Contrast and Injection Pressure Pseudosteady-State Flow and Tangential Stresses 78

Page

Figure 8.25 Effect of Horizontal Stress Contrast and Injection Pressure Steady-State Flow and Tangential Stresses in Complete and Partial Stress Relief Conditions 79

Figure 8.26 Effect of Horizontal Stress Contrast and Injection Pressure Transient Flow and Tangential Stresses in Complete and Partial Stress Relief Conditions (Time 100 Hours) 79

Figure 8.27 Effect of Horizontal Stress Contrast and Injection Pressure Pseudosteady-State Flow and Tangential Stresses in Complete and Partial Stress Relief Conditions (Time 1 Hour) 80

Figure 8.28 Effect of Rate on the Radius of Potential Fracture Region Transient Flow Conditions (Time 100 Hours) 80

Figure 8.29 Effect of Rate on the Radius of Potential Fracture Region Pseudosteady-State Flow Conditions (Time 1 Hour) 81

Figure 8.30 Effect of Time on the Radius of Potential Fracture Region Transient Flow Conditions 81

Figure 8.31 Effect of Time on the Radius of Potential Fracture Region Pseudosteady-State Flow Conditions 82

Figure 8.32 Effect of Porosity, Viscosity and Compressibility on the Radius of Potential Fracture Region Transient Flow Conditions (Time 100 Hours) 82

Figure 8.33 Effect of Porosity, Viscosity and Compressibility on the Radius of Potential Fracture Region Pseudosteady-State Flow Conditions (Time 1 Hour) 83

NOMENCLATURE

Latin

c	compressibility [Pa^{-1}]
h	injection zone thickness [m]
k	injection zone permeability [m^2]
p_e	external boundary pressure at radius r_e [Pa]
p_i	initial reservoir pressure [Pa]
$p_{(r)}$	pore pressure at radial distance r from the wellbore [Pa]
$p(r,t)$	pore pressure at radial distance r and time t from the wellbore [Pa]
p_w	bottom hole well pressure [Pa]
q	injection rate at bottom hole conditions [m^3s^{-1}]
r	radial distance from well [m]
r_D	dimensionless radius
r_{fD}	dimensionless radius of potential fracture region
r_e	radius of affected domain or external boundary[m]
r_{eD}	dimensionless radius to external boundary
r_f	radius of potential fracture region [m]
r_w	radius of well [m]
t	time [s]
t_{Dw}	dimensionless time of injection defined by Equation 7.5

T_o	tensile strength in the horizontal direction [Pa]

Greek

ϕ	porosity [fraction]
γ	Euler constant ≈1.78
μ	viscosity [Pa.s]
σ_e	isotropic far field horizontal compressive stress [Pa]
σ_{h1}	maximum principal horizontal stress in anisotropic stress field [Pa]
σ_{h2}	minimum principal horizontal stress in anisotropic stress field [Pa]
σ_r	radial stress [Pa]
σ_{rw}	radial stress at the wellbore [Pa]
σ_v	principal vertical stress [Pa]
σ_w	stresses at the wellbore or wellbore internal pressure [Pa]
σ_θ	tangential stress [Pa]
$\sigma_{\theta w}$	tangential stress at the wellbore [Pa]
$\sigma_{\theta v}$	tangential stress in the vertical direction [Pa]
θ	angle of plane on which principal stress acts [radians]

SUBSCRIPTS

w	at the wellbore
v	in vertical direction
max	maximum
min	minimum

hmin	minimum horizontal
hmax	maximum horizontal

Chapter 1

INTRODUCTION

Hydraulic fractures which break out through the upper confining stratum can carry oil and gas into the overlying formations. Stress gradient in the underlying confining layer is usually higher than the injection zone, therefore it is less likely to break. Attempts are made to confine injection or disposal fluids in the desired injection zone for hydrocarbon conservation and ground water protection. For the confinement of disposal fluid, the classical approach emphasizes wellbore integrity and avoids interference with offset wells. Any fluid movement behind the pipe is usually attributed to bad cementing operations and, in an attempt to mitigate this problem, secondary cementing is usually recommended. The fluid movement behind the pipe could, however, be the result of local and regional stresses in the overlying formations.

Regulatory agencies such as the Alberta Energy Resources Conservation Board (ERCB) develop guidelines to ensure initial and ongoing confinement of disposal fluids in the injection zone. The information required to support an application to inject or dispose fluids, or for operating and monitoring purposes, also emphasizes well-bore integrity and the prevention of fluid migration to offset wells. To avoid fracturing in the injection zone, the ERCB specifies that the maximum wellhead injection pressure be limited to 90% of the injection zone fracture pressure, per ERCB guide G-51, March 1994. A step-rate injectivity test, in-situ stress test, or mini frac is recommended to determine the 90% wellhead pressure limit. If this 90% limit is based on actual formation breakdown pressure, then a situation exists where the confining layer can be fractured without fracturing the injection zone, even while the well pressure remains within the 90% limit. However, no information is requested for horizontal stress in the overlying formation. An assessment of the regional cap rock containment potential is required only if approval is requested to inject above the fracture pressure.

In the ground, one of two possible conditions exists: (1) there is no pre-existing opening, (2) a fracture starts from a pre-existing opening. To initiate a fracture in condition (1), the injection pressure should be higher than the tensile strength of the rock. However, in case the of condition (2), an injection pressure slightly higher than the least principal stresses would propagate the fracture if the crack is normal to the least principal stress.

When a fluid is injected into a permeable formation where there is no pre-existing crack, the pore pressure increases near the wellbore, and approaches the far field pressure away from the wellbore. If the injection pressure is lower than that required to reduce the compressive stresses across some plane in the premeable formation to zero, then there can be no fracture in that formation, but the high pore pressure can be transmitted into the impermeable confining stratum, if there exists a small defect in the form of a crack or notch at the interface between the confining layer and the permeable injection zone.

As the pore pressure increases to a value slightly higher than the minimum horizontal stresses at this point in the confining layer, a fracture may be propagated through the notch at the interface, even while the wellhead pressure remains within the 90% limit. The amount of fracture propagation depends on the fracture toughness of the confining layer. If the fracture toughness of confining layer is neglected, then the fracture may penetrate through the confining layer into the overlying formation. This situation is environmentally hazardous because it allows fluids from the injection zone to contaminate the overlying formation. This situation is absolutely undesirable if the overlying formation were a potable aquifer or if radio-active materials or carcinogenic chemicals are being disposed of in the injection zone.

The extent of this potential fracture region from the wellbore depends on the injection fluid pressure and the in-situ stresses in the confining stratum. The problem is further complicated by the horizontal stress contrast around the wellbore and the type of completion.

In this study the effect of underlying injection zone pressure, horizontal stress contrast, and type of completion on the extent of the potential fracture region is presented. The pore pressure distribution in the permeable injection zone is considered for steady-state, pseudosteady-state and transient flow conditions.

Chapter 2

REVIEW OF LITERATURE

Whether the fractures are created deliberately or whether they are formed during water flooding or waste disposal operations, the bounding layers are relied upon to confine the fractures. To identify the factors affecting behaviour of the confining layers, an understanding of the relationship between the fluid injection pressure and the local and regional stresses is required. Therefore this chapter has been divided into three sections. The first part presents a literature review of fracture breakdown and fracture extension pressure. The second part presents a literature review of fracture containment in layered formations. A brief discussion of some background information on tensile fracture criteria is presented in the third part. As the confining layer is usually a shale, comments on underground situations where shale may not be effective as a confining layer when there is high pore pressure in the injection zone are also presented.

2.1 Literature Review of Breakdown and Fracture Extension Pressures

Hubbert and Willis (1957) demonstrated the planes of fracture using a gelatin model, and suggested two types of pressure behaviour with respect to fracturing. The first is a breakdown pressure which is higher than both the horizontal stresses and the tensile strength of the rock. Since the tensile strength of most rocks subjected to hydraulic fracturing is effectively zero, the breakdown pressure is that required to reduce the compressive stresses across some plane in the rock to zero. The second type of behaviour is the fracture propagation or extension pressure, and is used when a fracture initiates from a pre-existing crack. Since the fracture propagates in the

direction normal to the least principal stress, the propagation pressure is merely higher than the least principal stress, but is lower, perhaps substantially, than the breakdown pressure.

Haimson and Fairhurst (1969) verified the fracturing concept, presented by Hubbert and Willis, through laboratory experiments on hydrostone, and found that breakdown occurs when the tangential stresses make the compressive stresses effectively zero. The fractures were generated at points $\theta = 0$ and $\theta = \pi$ along the wellbore, perpendicular to the least horizontal stress.

Hagoort et al. (1978) presented a theoretical analysis of hydraulic fracturing pressures in a two dimensional system consisting of permeable rock overlain by an impermeable material. Fluid was injected into the permeable rock and a fracture was created. He concluded that the fracture initiation pressure required to part undamaged rock was higher than the fracture extension pressure required to open the existing fracture or crack.

Kry and Gronseth (1982) studied the influence of the in-situ stresses on hydraulic fracturing in the Esso Kelly gas reservoir in the Alberta Deep Basin. Hydraulic fractures were created in the field and two types of pressure behaviour were observed— a fracture breakdown pressure and the pressure in the fracture as it closes. The breakdown pressure was higher. The pressure in the fracture as it closed was equal to the minimum horizontal stress.

Warpinski et al. (1985) conducted several hydraulic fracture stress tests in sandstone and shale for in-situ stress measurement in the Mesaverde Group, Rifle, Colorado. The minimum horizontal stresses were determined by analysis of the pressure time record and were found equal to the instantaneous shut-in pressure in the hydraulic fracture. The data were compared with the calculated stresses and were found to be similar in magnitude.

Nolte (1988) performed a series of pump tests in a permeable formation and analyzed the pressure data. From this he defined the fluid pressure required to initiate an opening from existing cracks as equal to the minimum principal stress.

Fjaer et al. (1992) defined the fracturing pressures. The breakdown pressure is defined as the peak pressure observed before the formation fractures and the well starts to take fluid. They suggested that the breakdown pressure is observed only in unparted rocks. After a fracture is created, the pressure remains constant and this pressure is the fracture extension pressure. If now the well is closed, the pressure falls off to a level where it balances the formation stresses and the fracture is closed. This pressure is called the instantaneous shut-in pressure (ISIP). To reopen the fracture an injection pressure slightly higher than the ISIP is required. This is called the fracture closure pressure. For small fractures the ISIP is approximately equal to the closure pressure.

Guo et al. (1993) evaluated various existing models of fracture breakdown pressure theoretically and experimentally and suggested that breakdown pressure is the peak bottom hole pressure induced during injection of fracture fluid. The bottom hole pressure decreases after the breakdown. The rock is intact at the start of injection, so it must be broken first (if no pre-existing crack is present) by overcoming the tensile strength of the rock. A fracture exists in the formation during subsequent injection cycles so the tensile strength is effectively zero. Therefore, tensile strength should not be calculated from the fracturing reopening pressure in the subsequent cycles. The tensile strength obtained from experiments on fracture reopening pressure was too variable and found to depend on applied stress and the injection rate.

2.2 Literature Review of Fracture Containment in Layered Formations

The literature on fracture containment in layered formations was reviewed to understand the of behaviour of confining layer during hydraulic fracturing. Some authors have studied fracture containment in a sandstone formation bounded by shales. Others have performed laboratory

experiments using layers of different materials. These other results can still be applied to the behaviour of fracture containment in sandstone formations bounded by shales.

Sidney et al. (1973) studied the stress-strain behaviour of silty shale and coarse grained sandstone through an experiment. The sandstone deformed more at high pressure than did shale. The main structural difference between the two rocks appeared to be the grain size. The sandstone, with a larger grain size, was composed of quartz and the shale was composed mainly of clay minerals. At high pressure the large grains will carry more of the load and can be deformed more than the clay minerals.

Simonson et al. (1976) studied the effect of in-situ stress on fracture propagation. They found that a layer of greater in-situ stress provides an effective barrier because of the increase in fracturing pressure necessary to continue propagating a fracture in this layer. The greater the difference in in-situ stress between the two regions the more effective the barrier is. Since the shales typically have in-situ stress higher than in sandstone, a shale boundary can be considered an effective barrier to further fracture growth.

Anderson and Larson (1978) performed a laboratory experiment on Nugget sandstone and Indiana limestone, finding, that in addition to the tensile or shear strength of the material on either side of an interface, the shear strength of the interface itself is important in determining whether a crack will propagate through it. With weak bonding, shear fracture containment is possible and is associated with slippage at the interface. Daneshy (1978) also reported that a difference in rock properties alone is insufficient to stop fracture growth. Instead he suggested that fracture containment may be more a result of the nature of the interface itself. As low frictional forces exist only at shallow depths, crack propagation is arrested by this mechanism only at shallower depths.

Cleary (1978) suggested that weak bonding between sandstone and shale results in a partial blunting of the crack tip by frictional slippage perpendicular to the propagation direction. This provides a mechanism to arrest fracture propagation.

Warpinski et al. (1980) conducted several experiments using ash-fall tuff and a welded tuff interface to delineate the vertical and horizontal distribution of in-situ stress, and to determine its effect on fracture growth and geometry. He reported that the minimum principal in-situ stress is the dominant influence on hydraulic fracture containment. Fractures are arrested wherever there is a sufficiently large difference in stress gradient between the two layers. Since the minimum principal in-situ stresses in shales are expected to be much higher than in sandstone, they tend to arrest the fracture growth from sandstone.

Eekelen (1980) performed a theoretical analysis of fracture containment in layered formations. He suggested that the shale layer often seemed to contain hydraulic fractures because the in-situ stress was higher than that in the sandstone. He pointed out that interface slippage can occur only at a shallow depths. At greater depths, high frictional resistance due to overburden weight probably prevent, interface slippage. Therefore this crack arrest mechanism will not be present.

Veatch (1983) stated that the local stress field and variation in stresses between adjacent formations are the dominant parameters in controlling fracture orientation and vertical growth. The difference between horizontal and vertical stresses affects the plane of orientation of a fracture. Control of vertical fracture growth may be dominated by high lateral stresses existing in the formation above and below the fracture initiation zone. He also reported that most measurements in sand shale sequences indicate that shale generally has higher stresses than sandstone.

Teufel and Clark (1984) performed laboratory experiments on Arizona, Berea, and Tennessee sandstone and Lueders limestone to study the effect of hydraulic fracture propagation in layered formations. He concluded that an important condition for containment is an increase in the minimum horizontal stress at the bounding layer, so that the fracture is be bounded by two high stress layers.

Whitehead et al. (1987) also reported in-situ stress data for the Travis Peak formation in the Waskom field of East Texas. The measured values of in-situ stress were determined with mini-

fractures and compared with log-derived values. The fracture gradient was higher in shales indicating that the shales have higher in-situ stress than sandstone. Therefore, in these fields, fracture propagation should be arrested as it approaches the shales.

Garon et al. (1988) investigated the mechanism associated with fracturing resulting from thermally induced in-situ stress reduction from water flooding. They found that vertical permeability barriers (e.g. shales) often maintain a higher horizontal stress than the adjacent sandstone as no cool fluid can enter them, and provide a barrier to further vertical fracture growth.

Boone and Detournay (1990) performed a theoretical analysis of vertical fracture response to quantify the role of poroelastic effects during the propagation of a hydraulic fracture. They found that impermeable layers that are stiffer than the permeable ones accelerate fracture closure.

2.3 Tensile Fracture Criteria

Hydraulic fracturing plays a major role in enhancing petroleum production. The technique itself is mechanically related to other phenomena such as pressure parting in water injection or waste disposal wells, lost circulation during drilling and breakdown of formations during squeeze cementing operations. A brief discussion of the fracturing process and criteria is presented in this section.

2.3.1 Hydraulic Fracturing Process

The term hydraulic fracturing is used for fluid injection into a sealed borehole to induce and propagate a tensile fracture. As water pressure increases, the critical compressive stress in the rock are reduced and at some point become tensile. When the stress reaches the uniaxial tensile strength, a crack is formed. According to the theory of elastic deformation, the crack width is controlled by

the fluid pressure drop in the fracture. Thus a higher pressure drop in the crack due to a high injection rate and viscous fluids results in relatively wider cracks. As the pumping is continued the crack extends and, if the pumping is stopped but the section kept sealed, the crack extends until the equilibrium is reached at some pressure, called the shut-in pressure. At this pressure the crack begins to close. We assume that three mutually perpendicular principal stresses σ_{h1}, σ_{h2} and σ_v in the ground are unequal, as shown in Figure 2.1. Here σ_{h1}, σ_{h2} are respectively the greatest and least horizontal principal stresses, and σ_v is the vertical stress. It is expected that induced fracture extends in the direction perpendicular to that of the smallest compressive stress or along the path of least resistance.

2.3.1 Fracture Criteria

For a material that behaves as linearly elastic, the fracture is generated at diametrically opposite points along the wellbore where the maximum stress difference between the applied stresses and the original stresses is developed. For a vertical borehole in a formation with isotropic horizontal stress, tangential stress at the borehole wall first become negative when the well pressure is sufficiently large. The pressure adds tensile stresses to all points around the hole; thus, for a vertical fracture to form, the stress must be equal and opposite to the uniaxial tensile strength. Therefore a tensile fracture will occurs at the wellbore wall when:

$$\sigma_\theta = 2\sigma_e - p_w + T_o \tag{2.1}$$

or

$$p_w = 2\sigma_e + T_o \tag{2.2}$$

Therefore a tensile failure will occurs at the borehole wall if the well pressure is increased above the value given by Equation 2.2.

When the horizontal stress is anisotropic a tensile fracture occurs at the position where the tangential stress is smallest which is at $\theta = 0$ and $\theta = \pi$ along the direction of maximum principal stress. If σ_{h1} and σ_{h2} are the maximum and minimum horizontal stress, respectively, then the tensile failure criteria for anisotropic stress is :

$$\sigma_{\theta} = 3\sigma_{h2} - \sigma_{h1} + T_0 \qquad (2.3)$$

or

$$p_w = 3\sigma_{h2} - \sigma_{h1} + T_0 \qquad (2.4)$$

Therefore a tensile failure occurs at the borehole wall if the well pressure is increased above the value given by Equation 2.4.

Once the crack has formed, fluid penetrates the parting and pressure is applied to the walls of the fracture. This reduces the stress concentration that previously existed in the vicinity of the well bore and the pressure required to hold the fracture open is then equal to the component of the undisturbed stress field normal to the plane of the fracture. A pressure slightly higher than this extends the fracture indefinitely; that is,

$$p_w > \sigma_{h2} \qquad (2.5)$$

is required to propagate the existing fracture. The fracture grows until it reaches the bounding zone and then begins to be constrained in the vertical direction. The high stress at the top and bottom tend to close the fracture. The fracture extends into the bounding zones until the opposing forces

counter balance one another. If these bounding zones are not thick enough, or if the pressure drop in the fracture gets high enough, then the fracture could penetrate into other zones.

Horizontal fractures can be initiated by vertical effective stresses overcoming the tensile strength of the rock in the vertical direction, T_v. Therefore,

$$\sigma_{\theta_v} = \sigma_v - p_w + T_v \tag{2.6}$$

or

$$p_w = \sigma_v + T_v \tag{2.7}$$

Hence a tensile failure occurs at the borehole wall if the well pressure is increased above the value of the sum of the principal stress in the vertical direction and the tensile strength of the rock in the vertical direction. Away from the wellbore, initiation of a horizontal fracture is possible only in the case of fluid penetration into the rock.

2.3.2 Comments

Many authors have identified the in-situ stress difference, between shale and sandstone, as the major parameter affecting fracture containment, but the presence of a shale bounding layer by itself is not always indicative of a large stress contrast. Further field observations have shown that stress variations of 6-8 MPa over a short interval are required for fracture containment. (Wyman et al., 1980). Table 2.1 shows some of the cases where difference in horizontal stresses is less than 6 MPa. Therefore, unless appropriate conditions are maintained, shale does not always act as

confining layer for hydraulic fractures. All the above cases discussed in the literature review depend on the premise that a fracture is first initiated in the sandstone and only then propagates into the confining layer. Another situation can exist where there is no fracture in the sandstone but there is a defect in the form of crack in the shale. If fluid is injected in the sandstone then high pore pressure in the sandstone would be transmitted to the shale and, according to the fracture propagation pressure given by Equation 2.5, may initiate a fracture as soon as it becomes greater than the minimum horizontal stress in the shale. Since there is no pre-existing fracture or crack in the sandstone, the breakdown pressure given by Equation 2.1 would be required to initiate a fracture in the sandstone, if an isotropic stress field is assumed. This breakdown pressure would be much higher than the fracture propagation pressure as shown in the last column of Table 2.1

TABLE 2.1

POSSIBLE SHALE STRUCTURE

Data Source	Field	Depth Interval (m)	Minimum Horizontal Stress (MPa) Sandstone			Minimum Horizontal Stress (MPa) Shale			Stress Difference (MPa)			Frac. Pressure (MPa)	
			Measured	Log.	Calc.	Measured	Log.	Calc.	Measured	Log.	Calc.	Sand	Shale
WARPINSKI 1985	Rifle Colorado	7850 7760	45.8	–	45.2	–	–	47.7	–	–	2.5	91.6	48
ROSEPILER 1979	Cotton Valley	10350 10280	–	50.0	–	–	52.0	–	–	2.0	–	100.0	52.1
	Cotton Valley	9970 9920	–	42.0	–	–	44.0	–	–	2.0	–	84.0	44.1
KRY 1983	Esso Kelly	8910 8850	43.0	–	–	43.0	–	–	0.0	–	–	86.0	43.1

Figure 2.1 - Stress Condition on an Elemental Cube

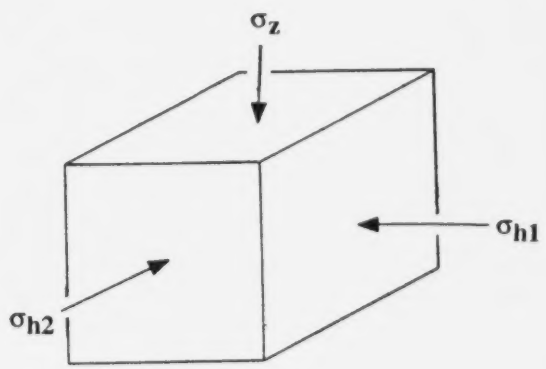

Chapter 3

STATEMENT OF THE PROBLEM

Hubbert and Willis (1957), in their classical paper "Mechanics of Hydraulic Fracture", described the two types of down-hole pressure behaviour reviewed in Section 2.1. The difference in the definition for the two types of behaviour can lead to circumstances where unsafe conditions arise during injection and disposal operations. The investigation of these circumstances is the motivation for this study.

3.1 Statement of Problem

The object of this research is to identify potential unsafe and environmentally hazardous conditions inherited from the 90% wellhead pressure limit set by the Energy Resources Conservation Board. The results can be used as a valuable diagnostic tool to predict the potential fracture region and to provide safer injection pressure guidelines.

The objectives require:

1) the development of radial and tangential stresses profiles around the wellbore and in the confining layer under complete and partial stress relief, and under conditions of applied stress;

2) the pore pressure distribution profile in the injection zone considering steady-state, pseudo-steady-state and transient flow conditions;

3) the development of equations for the radius of the potential fracture region for isotropic and anisotropic horizontal stresses, and for steady-state, pseudosteady-state, and transient flow conditions;

4) and the development of curves for the potential fracture region and for observing the effects of horizontal stress contrast, injection zone pressure and injection pressure on the radius of the potential fracture region.

Once the curves have been developed, they can be used as a diagnostic tool to determine the extent of the potential fracture region under different field conditions. This research is the first pilot study which combines petroleum engineering and geomechanical aspects to identify a potential environmental problem in deliberate hydraulic fracturing, and in injection and disposal operations.

Chapter 4

MODEL DEVELOPMENT

The development of a mathematical model requires an understanding of the horizontal stress distribution in the confining layers and the pore pressure distribution in the permeable injection zone. Only overlying confining layer is considered because the stress gradient, in the underlying confining layer is usually higher than the injection zone and therefore the derlying confining layer is less likely to fracture. The object of this chapter is to present the basic assumptions, stress distribution, and the type of completion considered in developing the mathematical model. This information is incorporated in subsequent chapters to develop the mathematical model for the radius of fracture region in steady-state, pseudosteady-state, and transient flow conditions.

4.1 General Assumptions

i) The injection zone is assumed to be underlying the confining layer. A permeable formation is overlying the confining layer as shown in Figure 4.1. The overlying, impermeable, nonporous confining layer has a defect, in the form of a pre-existing crack at the injection zone and confining layer interface, The orientation of stresses around the crack is the same as the stresses around the wellbore.

ii) The radius of a smooth cylindrical vertical wellbore (r_w) is very small compared to the radius of the affected domain (r_e).

iii) Far-field horizontal stresses in the confining layer and the boundary pressure in the permeable injection zone are not affected by changes in well pressure, except in the case of pseudosteady- steady-state flow conditions.

iv) Fluid is injected into a permeable injection zone which does not have any pre-existing crack.

v) Fluid is not injected directly into the confining layer. Radial and hoop stresses develop in the confining layer due to an increase in wellbore pressure.

vi) The injection pressure is always higher than the minimum horizontal stress in the confining layer and may act as a fracture propagation pressure as described in the previous chapter. Isothermal conditions prevail in the injection zone and in the confining layer.

vii) The horizontal stresses in the permeable injection zone and the confining layer are modelled on the Esso Kelly formation in the Deep Basin gas exploration area of Alberta.

viii) A linear elastic formation is assumed around the wellbore. A tensile fracture criterion is assumed. Shear fractures are beyond the scope of this study.

ix) The stresses are axisymmetrical. The compresive stresses are positive and the tensile stresses are negative.

4.2 Stress Field

Underground formations are always subject to a stress field, due to overburden pressures and tectonic stresses. When a well is drilled into a formation, stressed solid material is removed and replaced by a fluid under pressure. Both isotropic and anisotropic stress fields are considered when examining the stress state surrounding the wellbore.

4.2.1 Isotropic Stress around the Wellbore

A vertical borehole in a linear elastic formation with equal horizontal stresses around it is considered as shown in Figure 4.2. The vertical stress is in the plane parallel to the borehole. The wellbore radius is r_w, and the radius of the investigated domain is r_e. There are no shear forces acting on the surface of the borehole. The internal pressure in the wellbore is σ_w and the external far-field stresses are σ_e. The solution to this type of problem is the same as that given for a thick-walled cylinder of infinite wall thickness, subjected to internal and external pressure as shown in Figure 4.3. The solution can be obtained by finding the stresses at any point in the material in

terms of internal pressure, external pressure, and the radii of the internal and external surfaces. The mathematical solution given by Scott et al. (1953) was used to calculate the tangential and radial stress around the wellbore and in the confining layer. In their solution for tangential stress a positive value is a tensile stress. In our research a positive value is a compressive stress. Therefore multiplying tangential stress by a minus sign:

$$\sigma_\theta = -\frac{\sigma_w r_w^2 - \sigma_e r_e^2 + \frac{r_w^2 r_e^2}{r^2}(\sigma_w - \sigma_e)}{r_e^2 - r_w^2}, \quad r_w \le r \le r_e \tag{4.1}$$

.

and

$$\sigma_r = \frac{\sigma_e r_e^2 - \sigma_w r_w^2 + \frac{r_w^2 r_e^2}{r^2}(\sigma_w - \sigma_e)}{r_e^2 - r_w^2}, \quad r_w \le r \le r_e \tag{4.2}$$

where a positive value of radial stress is a compressive stress.

When $r = r_w$ the tangential and radial stresses at the wellbore are given by

$$\sigma_{\theta w} = 2\sigma_e - \sigma_w \tag{4.3}$$

and

$$\sigma_{r_w} = \sigma_w \tag{4.4}$$

The radial stresses are higher than the tangential stresses at the wellbore because the well pressure is assumed always to be higher than the horizontal stresses in the confining layer. An increase in well pressure produces an increase in radial stress and an equal reduction in the tangential stresses. The variation of stresses as a function of r is shown in Figure 4.4. It is obvious that the largest stress difference from the initial stress state is found at the borehole; hence, rock failure is expected to initiate at or close to the wellbore. Away from the wellbore both stresses tend to the far-field values.

4.2.2 Anisotropic Stresses around the Wellbore

This represents a more general situation in which horizontal stresses around a vertical wellbore are not equal in all directions. The largest horizontal stress is represented by σ_{h1} and the least horizontal stress by σ_{h2}. The orientation of stresses is such that the largest horizontal stress is parallel to the *x*-axis, the least horizontal stress is parallel to *y*-axis and the vertical stress is parallel to the borehole. The direction of the *x*-axis is horizontal and that of the *z*-axis is vertical, as shown in Figure 4.5. Since the well is vertical and the stresses are principal stresses, there are no shear stresses applied under these conditions. Therefore using Bradley's (1979) solution for stress in anisotropic conditions and neglecting the shear component, the radial and tangential stresses with well pressure σ_w are given by:

$$\sigma_\theta = \tfrac{1}{2}\left(\sigma_{h_1} + \sigma_{h_2}\right) + \frac{r_w^2}{2r^2}\left(\sigma_{h_1} + \sigma_{h_2} - 2\sigma_w\right) - \tfrac{1}{2}\left(\sigma_{h_1} - \sigma_{h_2}\right)\left(1 + \frac{3r_w^4}{r^4}\right)cos\,2\theta \qquad (4.5)$$

$$\sigma_r = \tfrac{1}{2}\left(\sigma_{h_1} + \sigma_{h_2}\right) + \frac{r_w^2}{2r^2}\left(-\sigma_{h_1} - \sigma_{h_2} + 2\sigma_w\right) + \tfrac{1}{2}\left(\sigma_{h_1} - \sigma_{h_2}\right)\left(1 - \frac{4r_w^2}{r^2} + \frac{3r_w^4}{r^4}\right)cos\,2\theta \qquad (4.6)$$

When $r = r_w$ the tangential and radial stresses at the wellbore are given by

$$\sigma_{\theta w} = \sigma_{h_1} + \sigma_{h_2} - \sigma_w - 2\left(\sigma_{h_1} - \sigma_{h_2}\right)\cos 2\theta \qquad (4.7)$$

and

$$\sigma_{r_w} = \sigma_w \qquad (4.8)$$

An increase in wellbore pressure produces an increase in radial stress and a reduction in the tangential stress. The variation of stress as a function of *r* is shown in Figure 4.6. It is obvious

that the largest stress difference from the initial stress state is found at the borehole; hence, rock failure is again expected to initiate at the wellbore when tangential stress is smallest, which is at $\theta = 0$ and $\theta = \pi$ Thus fracture occurs in the direction of maximum horizontal stress, or perpendicular to the direction of the least horizontal stress. (Hubbert and Willis, 1957). Away from the wellbore, the radial stress tends to the value of the maximum horizontal stress, and the tangential stress approaches the value of the least horizontal stress.

4.3 Well Completions

Stress acting on the confining layer due to the application of borehole pressure depends on the packer setting depth. In the case of anisotropic stress, the packer setting depth also determines the horizontal stress ratio at which the confining layer may fracture in tension. Two types of completions are considered: the packer set above the confining layer, and the packer set below the confining layer.

4.3.1 Packer Set above the Confining Layer

When the packer is set above the confining layer, as shown in Figure 4.7, the change in the wellbore pressure is transmitted to the confining layer. Therefore, an increase in the wellbore pressure increases the radial stresses and causes an equal decrease in the tangential stresses. In the case of isotropic stresses around the wellbore, the tangential and radial stresses can be calculated using Equations 4.1 to 4.4, and for anisotropic stresses Equations 4.5 to 4.8 can be used to calculate the tangential and radial stresses. Setting the packer above the confining layer is referred to as the "stress applied condition". The radius of the potential fracture region is calculated for this condition considering both isotropic and anisotropic stresses around the wellbore.

4.3.2 Packer Set below the Confining Layer

When a packer is set below the confining layer, as shown in Figure 4.8, the waste fluid is disposed of down the tubing with the annulus isolated from high bottom-hole pressures. In this situation the casing across the confining layer is not exposed to changes in wellbore pressure, and the stresses in

the confining layer remain the same as they were at the time of completion, assuming no further pressure is applied to the annulus. Depending on the fluid gradient in the annulus the stresses in the confining layer can be calculated by keeping σ_w constant in Equations 4.1 to 4.8. Two cases are considered:

i) $\frac{\sigma_w}{\sigma_{h_2}} = 0.0$

and

ii) $\frac{\sigma_w}{\sigma_{h_2}} = 0.5$

where σ_{h2} is the minimum horizontal stress.

The first case is referred as "complete stress relief", and the second case as "partial stress relief". The radius of the potential fracture region is calculated for each case considering both isotropic and anisotropic stress fields.

4.4 Anisotropic Stresses and Fracture Azimuth

Whenever the stress field is anisotropic, there is a preferred fracture azimuth perpendicular to the minimum principal in-situ stress (Hubbert and Willis, 1957). The fracture prefers to take the path of least resistance and therefore opens up against the smallest stress. At near isotropic conditions the rock fabric probably controls the fracture azimuth.

Hubbert and Willis (1957) and Haimson and Fairhurst (1969) suggested that the breakdown pressure is related to $(3\sigma_{h\min} - \sigma_{h\max})$. In the earlier sections it has been shown that tangential stresses are effective in creating the tensile fracture. According to Equation 4.7, σ_θ varies from $(3\sigma_{h2} - \sigma_{h1} - \sigma_w)$ at $\theta = 0$ to $(3\sigma_{h1} - \sigma_{h2} - \sigma_w)$ at $\theta = \pi / 2$. As the internal pressure in the pre-existing crack is increased, σ_θ first becomes negative when $p(r) = 3\sigma_{h_2} - \sigma_{h_1}$, and a tension

fracture in the plane $\theta = 0$ becomes possible. Here $p(r)$ is the pressure in the pre-existing crack at a distance r from the wellbore. At $\theta = \pi / 2$ the tangential stresses increase. To determine the horizontal orientation of fracture graphically, the tangential stresses normalized by the least horizontal stress are plotted against the stress field ratio. The stress field ratio was varied from 0.3 to 1. Figure 4.9 shows that the tangential stress at $\pi / 2$ radians is always higher than the stress at 0 radians Therefore the fracture first initiates in the direction of 0 radians.

Figure 4.9 also shows that, under the complete stress relief conditions $(\sigma_w / \sigma_{h2} = 0)$, a horizontal stress ratio $(\sigma_{h2} / \sigma_{h1})$ of 0.3 or lower results in fracturing the confining layer in tension. Therefore injection or waste disposal is not desirable at this or lower horizontal stress ratios. Under the stress-applied condition $(\sigma_w / \sigma_{h2} = 1.04)$ as the stress contrast increases, the permeable injection zone fractures in tension at a horizontal stress ratio of 0.5.

Note that at a horizontal stress ratio of 0 to 0·5 the injection zone fractures first under the stress applied condition. If the same horizontal stresses are assumed in the injection zone and in the confining layer, then setting the injection disposal pressure limit at 90% of this fracturing pressure results in safe operating conditions. However, when the horizontal stress ratio is greater than 0·5, which is a more frequent occurrence, the 90% fracture pressure limit may be greater than the least horizontal stress in the confining layer. In this case, if a pre-existing crack exists in the confining layer, a fracture is created in the confining layer prior to fracturing the injection zone. Therefore an injection or disposal pressure limit of 90% of the target zone fracturing pressure may not be effective in preventing fluid migration to the overlying formation when the horizontal stress ratio varies between 0.5 and 1. In subsequent chapters the effect of stress contrast on the radius of the potential fracture region is examined when the horizontal stress ratio varies between 0.5 and 1.

Figure 4.1 - Assumed Geological Conditions in the Ground

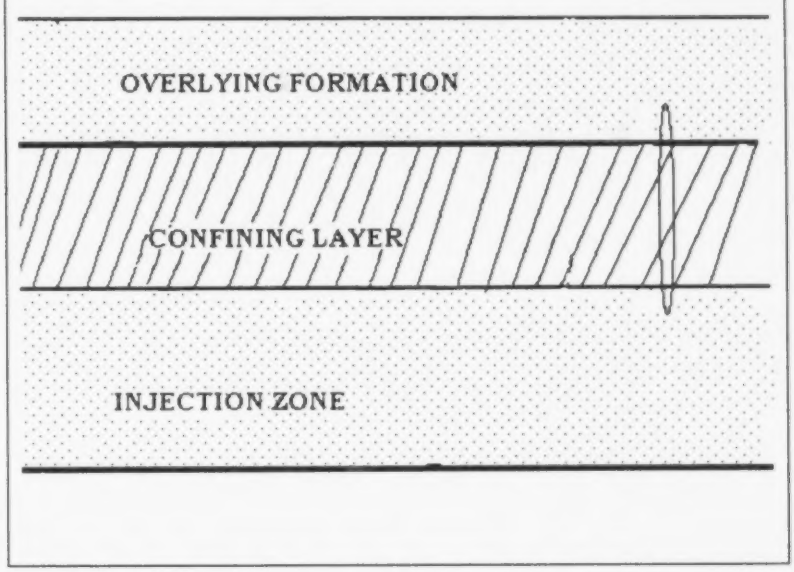

Figure 4.2 - Isotropic Stresses Acting on a Formation

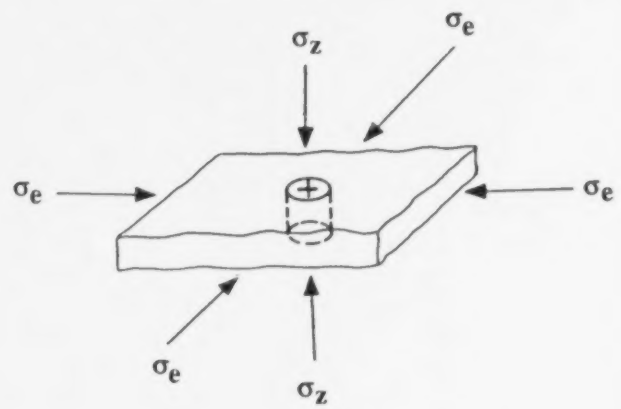

Figure 4.3 - Stresses in a Hollow Cylinder

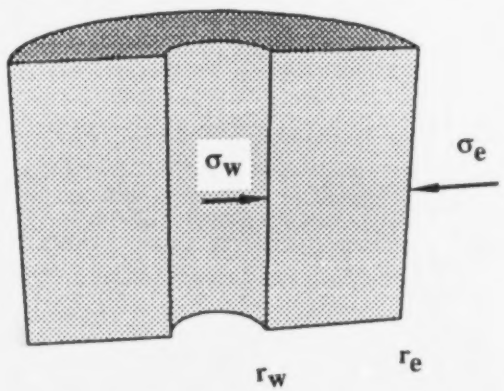

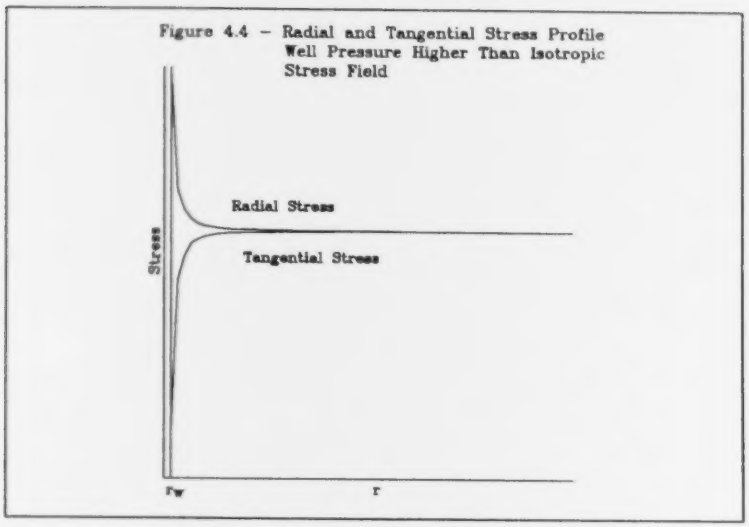
Figure 4.4 – Radial and Tangential Stress Profile
Well Pressure Higher Than Isotropic
Stress Field
Radial Stress
Tangential Stress
Stress
r
r

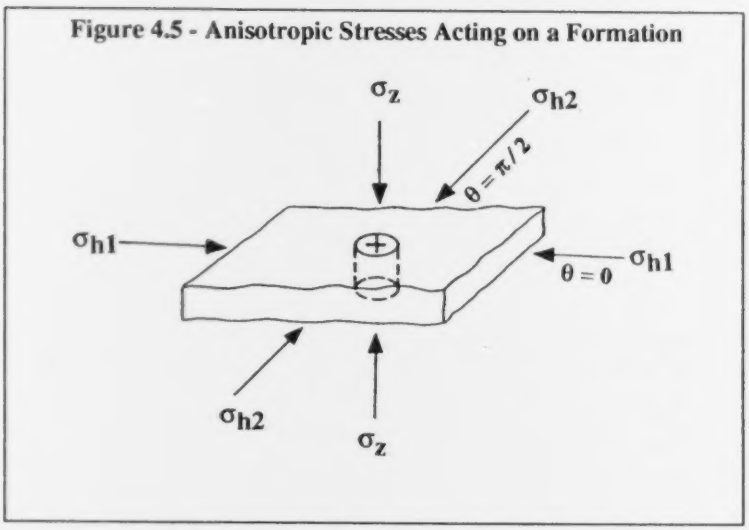
Figure 4.5 - Anisotropic Stresses Acting on a Formation
σz
σh2
θ = π/2
σh1
σh1
θ = 0
σh2
σz

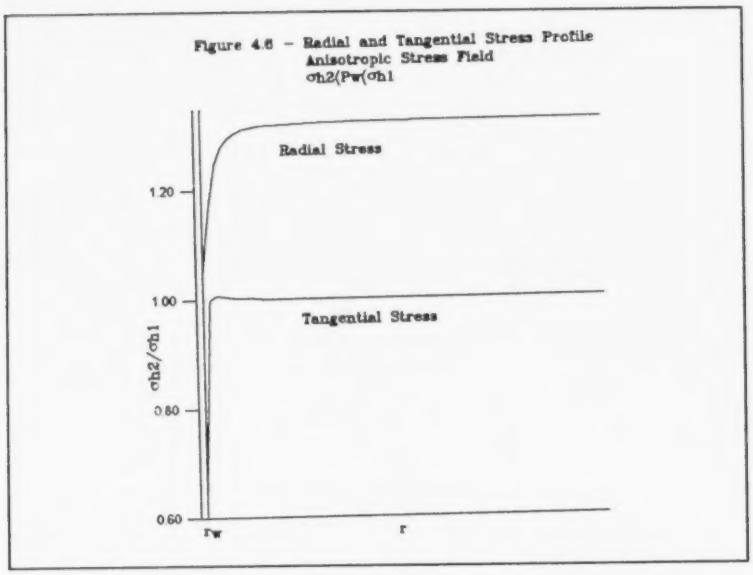
Figure 4.6 – Radial and Tangential Stress Profile
Anisotropic Stress Field
σh2(Pw(σh1
Radial Stress
Tangential Stress
1.20
1.00
0.80
0.60
σh2/σh1
Pw
r

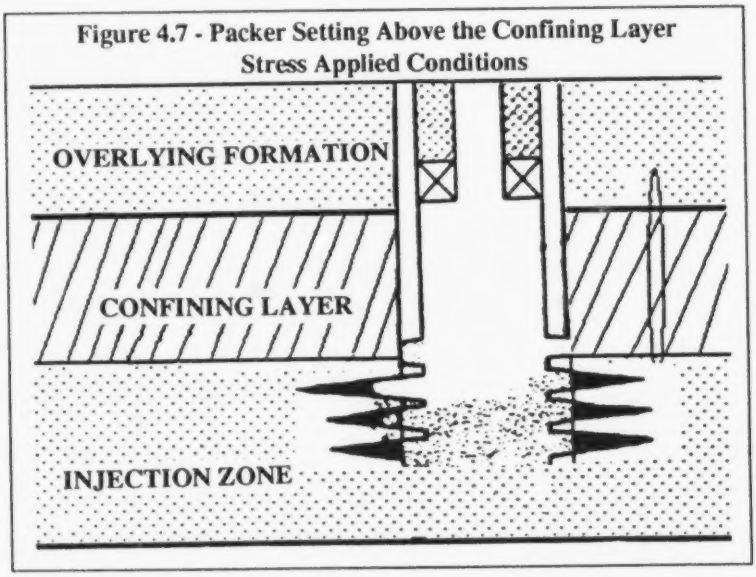
Figure 4.7 - Packer Setting Above the Confining Layer
Stress Applied Conditions
OVERLYING FORMATION
CONFINING LAYER
INJECTION ZONE

Figure 4.8 - Packer Setting Below the Confining Layer Stress Relief Conditions

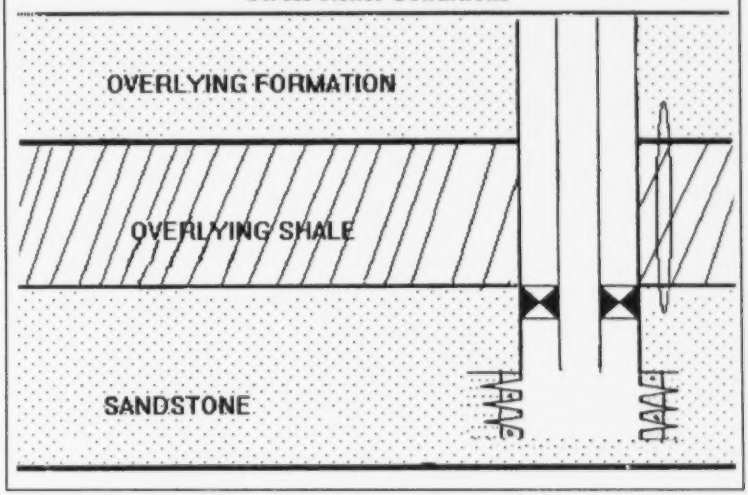

Figure 4.9 – Effect of Stress Contrast on Fracture Orientation Around the Wellbore in Complete Stress Relief and Stress Applied Conditions

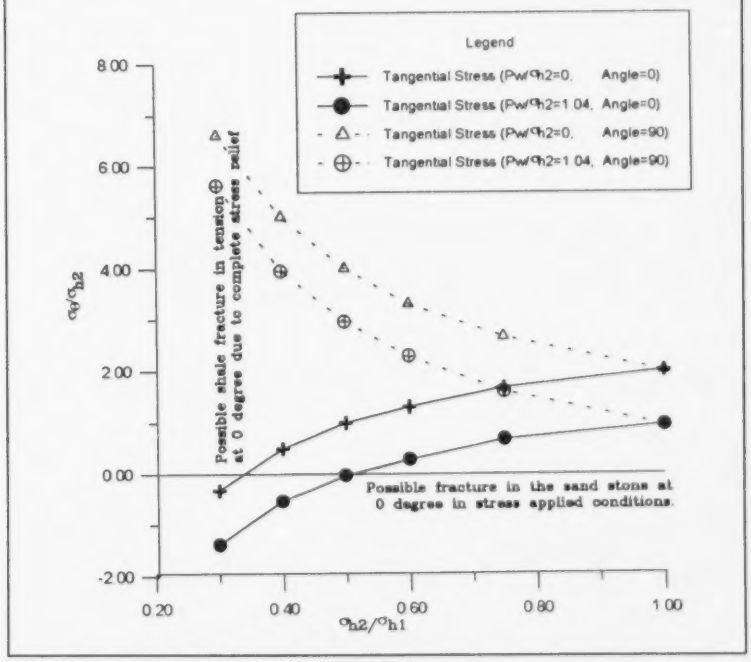

Chapter 5

ANALYTICAL MODEL OF RADIUS OF POTENTIAL FRACTURE REGION

STEADY-STATE FLOW

The objective of this chapter is to develop a mathematical model for calculating the radius of the potential fracturing region. First, a brief description of steadystate flow is presented, and then information presented in Chapter 4 is combined with steady-state flow conditions to develop the model.

5.1 Steady-State Flow

Steady-state flow occurs when the pressure distribution and rate remain constant with time. It is assumed that this condition has already been attained. The system which resembles steady-state flow is the one where injection in any zone is replaced with an equal mass of fluid production. Water injection in a producing field where complete voidage replacement is maintained should come close to meeting this requirement.

Consider one-dimensional, radially symmetrical, steady-state incompressible flow, and assume that the well pressure is represented by p_W and the pressure at the external boundary r_e by p_e, and that the wellbore radius r_W is very small compared to the radius of the injection zone; that is, $r_w << r_e$. The pressure distribution is given by:

$$p(r) = p_w + \frac{p_e - p_w}{\log \frac{r_e}{r_w}} \log \frac{r}{r_w} \qquad (5.1)$$

5.2 Analytical Model

When the pore pressure in the permeable injection zone is greater than the minimum horizontal stress in the bounding layer, and a surface defect exists at the interface, then the high pore pressure in the injection zone is transmitted to the bounding layer and may trigger a fracture. The parameters used for calculating the radius of the potential fracture region are given in Table 5.1.

5.2.1 Isotropic Stress Field, Stress Applied and Steady-State Flow Conditions.

The pore pressure distribution in the injection zone was calculated using Equation 5.1, and the radial and tangential stresses were calculated using Equations 4.1 and 4.2. The stresses and pressure plotted as shown in Figures 5.1 and 5.2. Referring to Figure 5.1, the increase in the injection pressure $\left(p_w / \sigma_e = 1.04\right)$ at the face of the wellbore (bottom hole) resulted in a pore pressure higher than the horizontal stresses in the confining layer only as far as $3r_w$. The pore pressure in the region away from the wellbore was always lower than the combined stresses (original horizontal stress + tangential stresses). Therefore the fracture may not occur in this region so long as the injection pressure does not increase. When the injection pressure increases to $p_w / \sigma_e = 1.27$, that is, 27% greater than the stress in the confining layer, the radius of the fracture region, r_f, increases approximately to $20r_w$. At the boundary of the potential fracture region, the pore pressure profile in the injection zone intersects the tangential stress profile in the confining layer; hence, pore pressure and tangential stresses are equal at this point. Setting $r = r_f$ at the boundary , then

$$\sigma_\theta = p(r_f) \tag{5.2}$$

Therefore noting $r_w << r_e$ and equating Equations 4.1 and 5.1

$$p_w + \frac{p_e - p_w}{\log \frac{r_e}{r_w}} \log \frac{r_f}{r_w} = -\frac{\sigma_w r_w^2 - \sigma_e r_e^2 + \frac{r_w^2 r_e^2}{r_f^2}(\sigma_w - \sigma_e)}{r_e^2 - r_w^2} \tag{5.3}$$

where

$$p_w \equiv \sigma_w \tag{5.4}$$

Normalizing with respect to the far field stress, σ_e, and solving for r_f gives the radius of the potential fracture region when the tangential stress and steady-state pore pressure are equel:

$$r_f = r_w \exp\left(\frac{A}{C} - \frac{B}{C r_f^2}\right) \tag{5.5}$$

where:

$$A = 1 - \frac{\sigma_w}{\sigma_e} \tag{5.6}$$

$$B = r_w^2\left(\frac{\sigma_w}{\sigma_e} - 1\right) \tag{5.7}$$

and

$$C = \frac{\frac{p_e - p_w}{\sigma_e}}{\log \frac{r_e}{r_w}} \tag{5.8}$$

Similarly the pore pressure profile in the injection zone intersects the radial stress profile in the confining layer, at the boundary of the fracture region, as shown in Figure 5.2. Thus the pore pressure and radial stresses are equal at this point. Again setting $r = r_f$ at the boundary;

$$\sigma_r = p(r_f) \tag{5.9}$$

Therefore noting $r_w << r_e$ and equating Equations 4.2 and 5.1

$$p_w + \frac{p_e - p_w}{\log \frac{r_e}{r_w}} \log \frac{r_f}{r_w} = \frac{\sigma_e r_e^2 - \sigma_w r_w^2 + \frac{r_w^2 r_e^2}{r_f^2}(\sigma_w - \sigma_e)}{r_e^2 - r_w^2} \tag{5.10}$$

Where $p_w \equiv \sigma_w$ as given in Equation 5.4

Normalizing with respect to the far field stress and solving for r_f gives the radius of potential fracture for radial stress and steady-state flow conditions:

$$r_f = r_w \exp\left(\frac{A}{C} + \frac{B}{C r_f^{\,2}}\right) \tag{5.11}$$

where

$$A = 1 - \frac{\sigma_w}{\sigma_e} \tag{5.12}$$

$$B = r_w^2\left(\frac{\sigma_w}{\sigma_e} - 1\right) \tag{5.13}$$

and

$$C = \frac{\frac{p_e - p_w}{\sigma_e}}{\log\frac{r_e}{r_w}} \tag{5.14}$$

5.2.2 Isotropic Stress Field, Stress Relief and Steady-State Flow Conditions

By setting σ_w / σ_e equal to the pressure in the annulus and keeping it constant, Equations 5.4 and 5.7 can be used to calculate the radius of the potential fracture region under stress relief conditions. Therefore, by setting $\sigma_w / \sigma_e = 0$ and then 0.5, the radius of the potential fracture region can be calculated for the two cases mentioned in Section 4.3.2. In this case $p_W \neq \sigma_e$ and stresses in the confining layer are not affected by the well pressure.

5.2.3 Anisotropic Stress Field, Stress Applied and Steady-State Flow Conditions

Radial stresses under this condition increase with an increase in pressure. Therefore the confining layer will not fracture under the influence of radial stresses as shown in Figure 5.3 and a model for radial stresses and anisotropic conditions is not developed. However, the tangential stresses decrease with an increase in well pressure. To develop the analytical model for the radius of the potential fracture region, the stress distribution in the confining layer and pore pressure distribution in the injection zone were calculated using Equations 4.5 and 5.1, respectively. The stresses and pressure were plotted as shown in Figure 5.4. Again, at the boundary of the fracturing region, $r = r_f$ and the pore pressure and tangential stress are equal.

Therefore equating Equations 4.5 and 5.1

$$p_w + \frac{p_e - p_w}{\log \frac{r_e}{r_w}} \log \frac{r_f}{r_w} = \frac{1}{2}\left(\sigma_{h_1} + \sigma_{h_2}\right) + \frac{r_w^2}{2r_f^2}\left(\sigma_{h_1} + \sigma_{h_2} - 2\sigma_w\right) - \frac{1}{2}\left(\sigma_{h_1} - \sigma_{h_2}\right)\left(1 + \frac{3r_w^4}{r_f^4}\right)\cos 2\theta \tag{5.15}$$

where

$$p_w \equiv \sigma_w$$

Normalizing with respect to the minimum horizontal stress and solving Equation 5.15 for r_f gives the radius of potential fracture region :

$$r_f = r_w \exp\left[\frac{A}{2Cr_f^2} - \frac{B}{C} + \frac{D}{C}\cos 2\theta + \frac{DE}{Cr_f^4}\cos 2\theta\right] \tag{5.16}$$

where

$$A = r_w^2\left[\frac{\sigma_{h1}}{\sigma_{h2}} - \frac{2\sigma_w}{\sigma_{h2}} + 1\right] \tag{5.17}$$

$$B = \frac{p_w}{\sigma_{h2}} - \frac{1}{2}\left[\frac{\sigma_{h1}}{\sigma_{h2}} + 1\right] \tag{5.18}$$

$$C = \frac{\frac{p_e - p_w}{\sigma_{h2}}}{log\frac{r_e}{r_w}} \tag{5.19}$$

$$D = -\frac{1}{2}\left[\frac{\sigma_{h1}}{\sigma_{h2}} - 1\right] \tag{5.20}$$

and

$$E = 3r_w^4 \tag{5.21}$$

5.2.4 Anisotropic Stress Field, Stress Relief and Steady-State Flow Conditions

Radial stresses are zero at the wellbore wall under complete stress relief conditions. However, physically realistic solutions begin at the wellbore radius, where the stress profile in the confining layer and the pore pressure distribution in the injection zone are such that the radial stress remains higher than the pore pressure, as shown in Figure 5.5. Therefore again the confining layer is not fractured due to radial stress. The radius of potential fracture region using tangential stresses can be calculated by setting σ_w / σ_e equal to the annulus pressure as discussed in Section 5.2.2.

The mathematical models developed in Equations 5.5, 5.11 and 5.16 are implicit, and can be solved using the Newton Raphson method.

TABLE 5.1

INJECTION ZONE AND CONFINING LAYER PARAMETERS USED FOR STEADY STATE FLOW CONDITIONS

Radius of well, r_w	0.1 m
Radius of affected domain, r_e	50 m
Initial Injection zone pressure, p_e	1) $.7\sigma_e$ 2) $.8\sigma_e$
Far field stress, σ_e	1 Pa
Injection pressure, p_w	$1.04\sigma_e \leq p_w \leq 1.27\sigma_e$

Figure 5.1 – Steady-State Flow and Tangential Stresses in Isotropic Stress Field

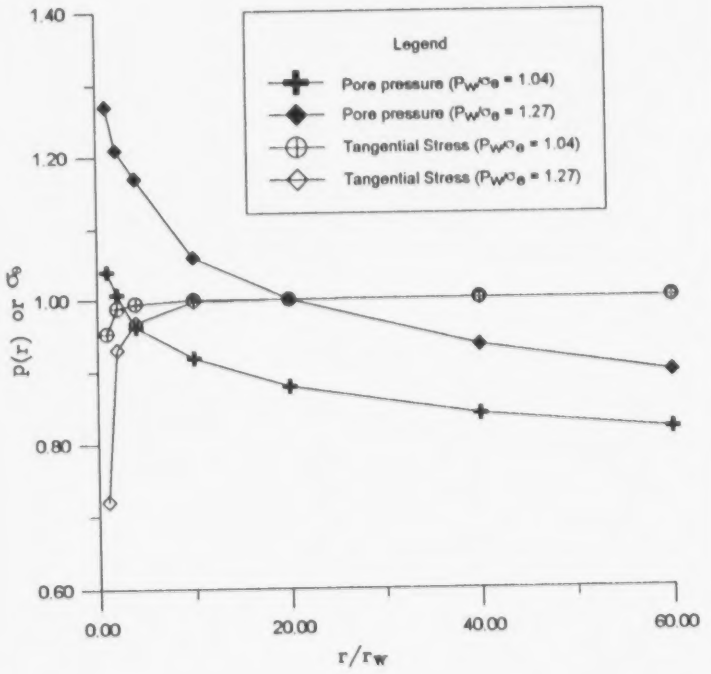

Figure 5.2 – Steady-State Flow and Radial Stresses in Isotropic Stress Field

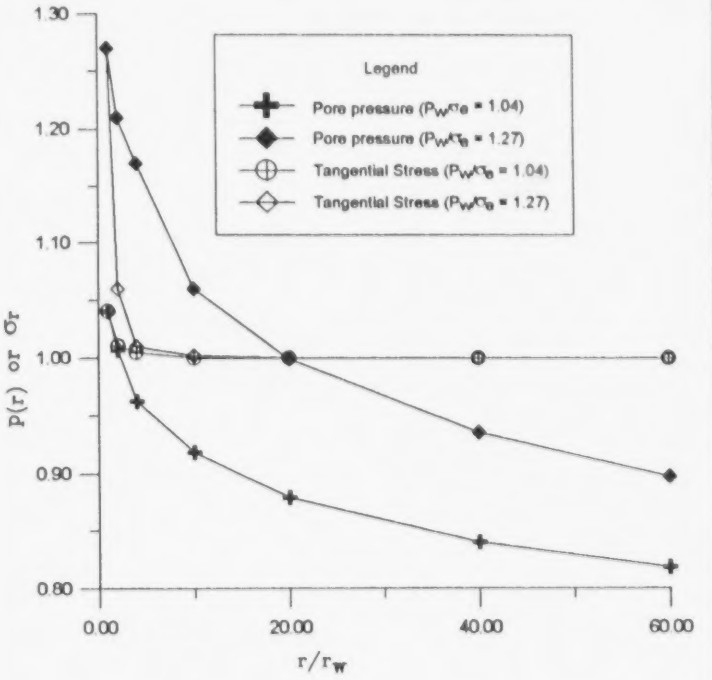

Figure 5.3 – Steady–State Flow and Radial Stresses in Anisotropic Stress Field

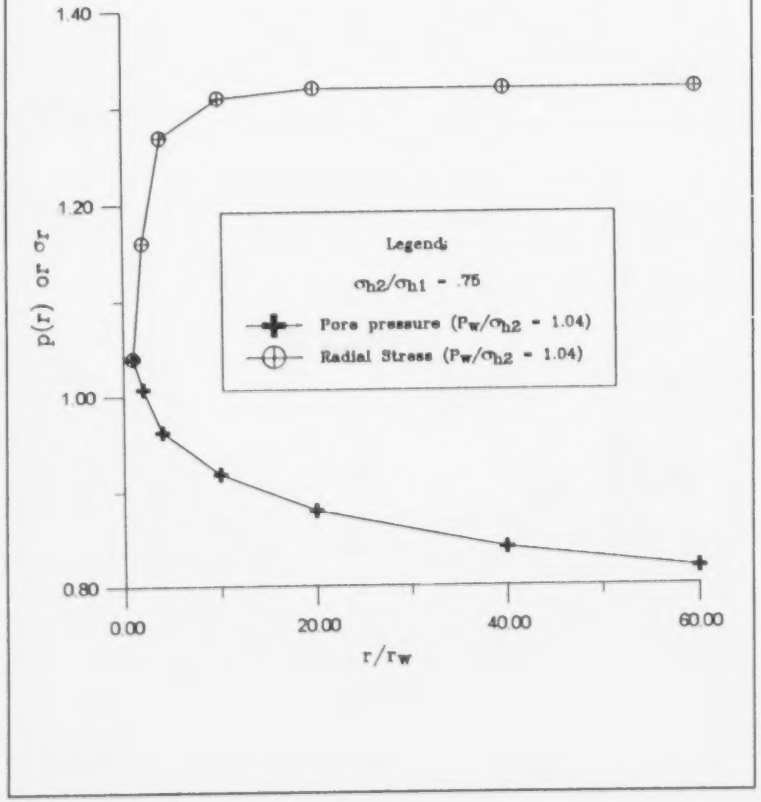

Figure 5.4 – Steady–State Flow and Tangential Stresses in Anisotropic Stress Field

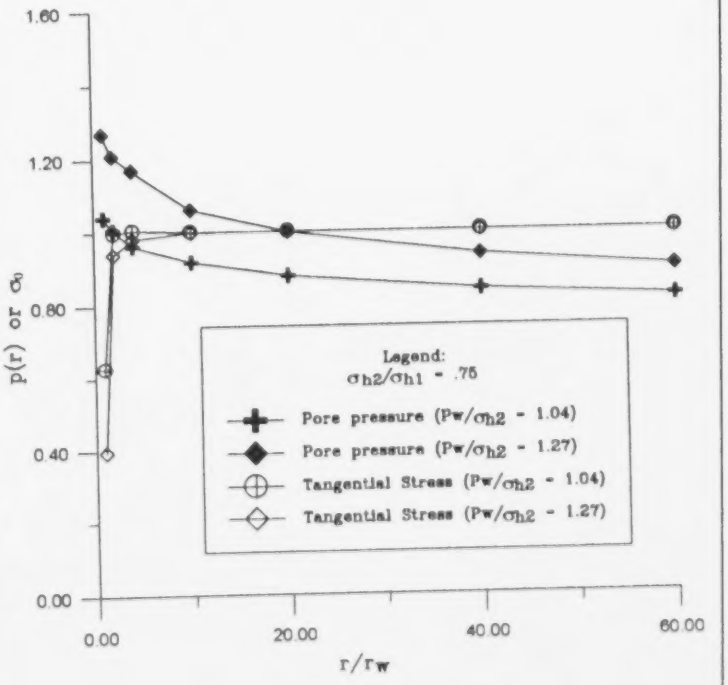

Figure 5.5 – Steady–State Flow and Radial Stresses in Complete Stress Relief Conditions Anisotropic Stress Field

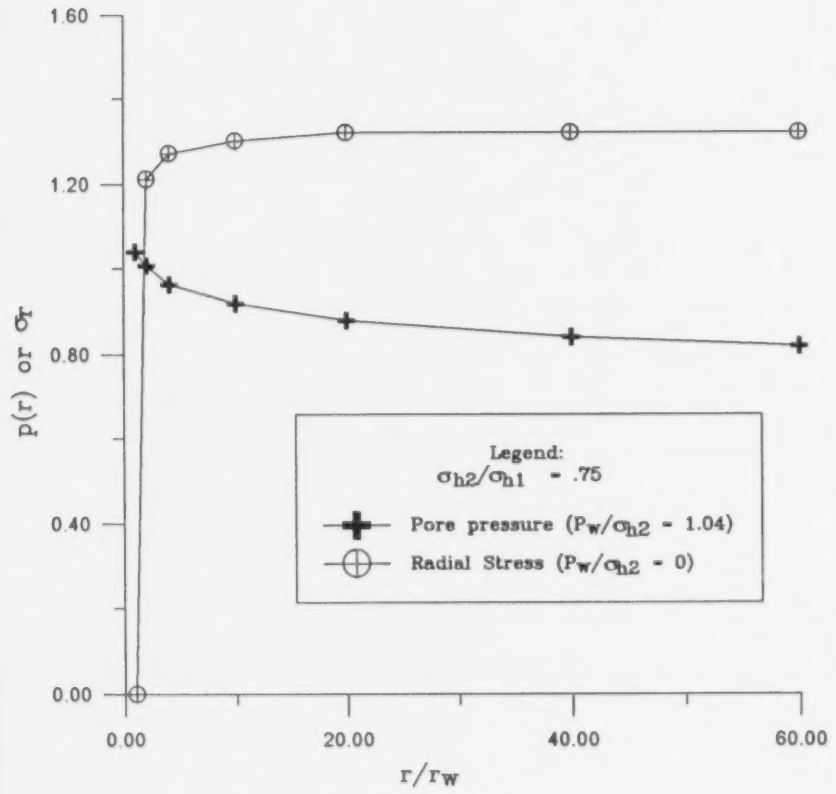

Chapter 6

ANALYTICAL MODEL OF RADIUS OF POTENTIAL FRACTURE REGION

TRANSIENT FLOW

The effect of rate and time cannot be determined with the models developed in Chapter 5. Moreover, they cannot be used if a compressible or slightly compressible fluid is injected. To consider these factors transient flow conditions are used to develop the models for the radius of the potential fracture region.

6.1 Transient Flow

Transient flow is where the pressure at any point changes with time. In one case, the rate is kept constant at the well and the pressure distribution is calculated at various times in the reservoir, referred to as the constant terminal rate boundary condition. On the other hand, if the wellbore pressure is kept constant and the rate is allowed to change, then one has a constant terminal pressure boundary condition. The latter case is more useful for water influx problems. In this chapter a constant terminal rate is assumed for the transient flow boundary condition.

One dimensional, radially symmetrical conditions are considered. The wellbore pressure is given by p_w and the external boundary pressure by P_i. It is assumed that the wellbore radius r_w is very small compared to the radius of the external boundary, r_e, so that the pressure at the wellbore does not affect the external boundary pressure. A variety of solutions for calculating pressure in the reservoir or at the wellbore under transient flow conditions are available in the literature. The solution given by Matthews and Russell (1967) is used in this chapter. The following initial and boundary conditions were assumed by the authors:

$p = p_i$ at $t = 0$ for all r

$p = p_i$ at $r = \infty$ for all t

and

$$\left.\frac{\partial p}{\partial r}\right|_{r_w} = \frac{q\mu}{2\pi kh}\frac{1}{r_w}$$

The pressure distribution in the reservoir as function of distance and time is given by

$$p(r,t) = p_i + \frac{q\mu}{4\pi kh}\mathrm{E}i\left(\frac{\phi\mu c r^2}{4kt}\right) \tag{6.1}$$

and the wellbore pressure is given by

$$p_w = p_i + \frac{q\mu}{4\pi kh}\ln\frac{4kt}{\gamma\phi\mu c r_w^{\,2}} \tag{6.2}$$

6.2 Analytical Model

The analytical model for the radius of the potential fracture region was solved for the values given in Table 6.1. The results are discussed in the following sections.

6.2.1 Isotropic Stress Field, Stress Applied and Transient Flow Conditions.

The pore pressure distribution in the injection zone was calculated using Equation 6.1. Radial and tangential stresses were calculated using Equations 4.1 and 4.2. Following the procedure outlined in Section 5.2.1, the results are plotted in Figures 6.1 and 6.2. Pore pressure and tangential stresses are equal at the boundary of the potential fracture region. Let the radius of the boundary be r_f.

Therefore,

$$r = r_f \tag{6.3}$$

and

$$\sigma_\theta = p(r_f, t) \tag{6.4}$$

Therefore noting $r_w << r_f$ and equating Equations 4.1 and 6.1

$$p_i + \frac{q\mu}{4\pi kh} \mathrm{E}i\left(\frac{\phi\mu c r_f^{\,2}}{4kt}\right) = -\frac{\sigma_w r_w^{\,2} - \sigma_e r_e^{\,2} + \frac{r_w^{\,2} r_e^{\,2}}{r_f^{\,2}}(\sigma_w - \sigma_e)}{r_e^{\,2} - r_w^{\,2}} \tag{6.5}$$

Similarly, the pore pressure profile in the injection zone intersects the radial stress profile in the confining layer, at the boundary of fracturing region, as shown in Figure 6.2. Therefore, equating Equations 4.2 and 6.1

$$p_i + \frac{q\mu}{4\pi kh} \mathrm{E}i\left(\frac{\phi\mu c r_f^{\,2}}{4kt}\right) = \frac{\sigma_e r_e^{\,2} - \sigma_w r_w^{\,2} + \frac{r_w^{\,2} r_e^{\,2}}{r_f^{\,2}}(\sigma_w - \sigma_e)}{r_e^{\,2} - r_w^{\,2}} \tag{6.6}$$

where

$$\sigma_w \equiv p_w = p_i + \frac{q\mu}{4\pi kh} \ln \frac{4kt}{\gamma\phi\mu c r_w^{\,2}} \tag{6.7}$$

Dividing Equations 6.5 and 6.6 by σ_e to normalize them with respect to the far field stress, and then solving for r_f gives the radius of potential fracture region.

For isotropic tangential stresses;

$$r_f = \left[-\frac{C}{A + B\,\mathrm{E}i\left(D r_f^{\,2}\right)}\right]^{\frac{1}{2}} \tag{6.8}$$

and for isotropic radial stresses;

$$r_f = \left[\frac{C}{A + B\,\mathrm{E}i\left(Dr_f^{\,2}\right)} \right]^{\frac{1}{2}} \tag{6.9}$$

where

$$A = \frac{p_i}{\sigma_e} - 1 \tag{6.10}$$

$$B = \frac{q\mu}{4\pi hk\sigma_e} \tag{6.11}$$

$$C = r_w^{\,2}\left[\frac{\sigma_w}{\sigma_e} - 1 \right] \tag{6.12}$$

and

$$D = \frac{\phi\mu c}{4kt} \tag{6.13}$$

Referring to Figure 4.3, near the wellbore, the tangential stress is substantially lower than the radial stress; therefore, it controls the tensile fracture. Away from the wellbore both tangential and radial stresses tend to the far field stress value. However, the value of the tangential stress is slightly less than the radial stress; therefore it has more influence in controlling the tensile fracture.

6.2.2 Isotropic Stress Field, Stress Relief and Transient Flow Conditions

By setting σ_w / σ_e equal to the pressure in the annulus and keeping it constant, Equations 6.5 and 6.6 can be used to calculate the radius of the potential fracture region under stress relief conditions. Therefore by considering $\sigma_w / \sigma_e = 0$ and 0.5, the radius of the potential fracture region can be

calculated for the two cases mentioned in Section 4.3.2. In this case p_w is not equal σ_w, and the stresses in the confining layer are not affected by the well pressure. Therefore Equation 6.7 is not used. However, the wellbore pressure is calculated for the pore pressure distribution using Equation 6.2 and is discussed with the results in Chapter 8.

6.2.3 Anisotropic Stress Field, Stress Applied, and Transient Flow Conditions

When the stress field is anisotropic, only the tangential stresses permit the creation of a potential fracture region under the stress applied or stress relief conditions, as discussed in Sections 5.2.3 and 5.2.4. The pore pressure distribution in the injection zone and the stress profile in the confining layer are shown in Figure 6.3. Assuming $r = r_f$ at the boundary of the fracture region, and equating Equations 4.5 and 6.1

$$p_i + \frac{q\mu}{4\pi kh} Ei\left[\frac{\phi\mu c r_f^{\,2}}{4kt}\right] = \frac{1}{2}(\sigma_{h1} + \sigma_{h2}) + \frac{r_w^{\,2}}{2r_f^{\,2}}(\sigma_{h1} + \sigma_{h2} - 2\sigma_w) - \frac{1}{2}(\sigma_{h1} - \sigma_{h2})\left[1 + \frac{3r_w^{\,4}}{r_f^{\,4}}\right] cos\, 2\theta \tag{6.14}$$

Where $\sigma_w \equiv p_w$ as given in Equation 6.7

Dividing equation 6.14 by σ_e and solving for r_f gives the radius of potential fracture region for anisotropic tangential stress and transient flow conditions

$$r_f = \left[\frac{A}{B + CEi(Hr_f^{\,2}) - D\left(1 + \frac{G}{r_f^{\,4}}\right)}\right]^{\frac{1}{2}} \tag{6.15}$$

where

$$A = \frac{r_w^2}{2}\left(\frac{\sigma_{h1}}{\sigma_{h2}} - \frac{2\sigma_w}{\sigma_{h2}} + 1\right) \tag{6.16}$$

$$B = \frac{p_i}{\sigma_{h2}} - \frac{1}{2}\left(\frac{\sigma_{h1}}{\sigma_{h2}} + 1\right) \tag{6.17}$$

$$C = \frac{q\mu}{4\pi hk\sigma_{h2}} \tag{6.18}$$

$$D = -\frac{1}{2}\left[\frac{\sigma_{h1}}{\sigma_{h2}} - 1\right]\cos 2\theta \tag{6.19}$$

$$G = 3r_w^4 \tag{6.20}$$

and

$$H = \frac{\phi\mu c}{4kt} \tag{6.21}$$

6.2.4 Anisotropic Stress Field, Stress Relief and Transient Flow Conditions

The radius of the potential fracture region under stress relief using tangential stresses can be calculated by setting σ_w / σ_e equal to the annulus pressure as discussed in Sections 5.2.2 and

5.2.4 and 6.2.2. Therefore Equation 6.7 is not used. However, the wellbore pressure is calculated for a constant rate using Equation 6.2 and is discussed with the results in Chapter 8.

The mathematical models developed in Equations 6.8, 6.9 and 6.15 are implicit equations and can be solved using the Newton Raphson method.

TABLE 6.1

INJECTION ZONE AND CONFINING LAYER PARAMETERS USED FOR TRANSIENT AND PSEUDOSTEADY-STATE FLOW CONDITIONS

INJECTION ZONE AND CONFINING LAYER

Largest horizontal stress, σ_{h1}	1·32 σ_{h2}
Least horizontal stress, σ_{h2}	1 Pa
Radius of well, r_w	0·1 m
Radius of affected domain, r_e	50 m

INJECTION ZONE

Initial Injection zone pressure, p_i	1) 0·7 σ_{h2} 2) 0.8 σ_{h2}
Porosity, ϕ	0·25
Permeability, k	9.8692E-14 m^2
Injection fluid viscosity, μ	1 m Pa.s
Compressibility, c	10^{-6} to 10^{-9} Pa^{-1}
Height, h	10 m
Time, t	1 to10000 hours

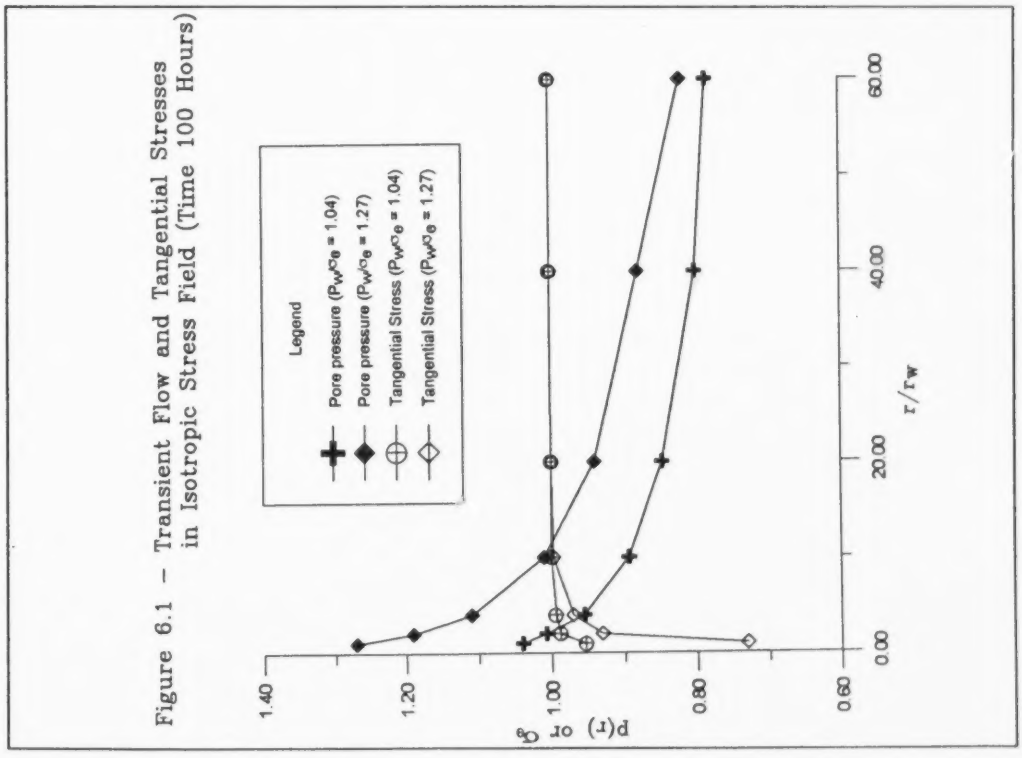

Figure 6.1 – Transient Flow and Tangential Stresses in Isotropic Stress Field (Time 100 Hours)

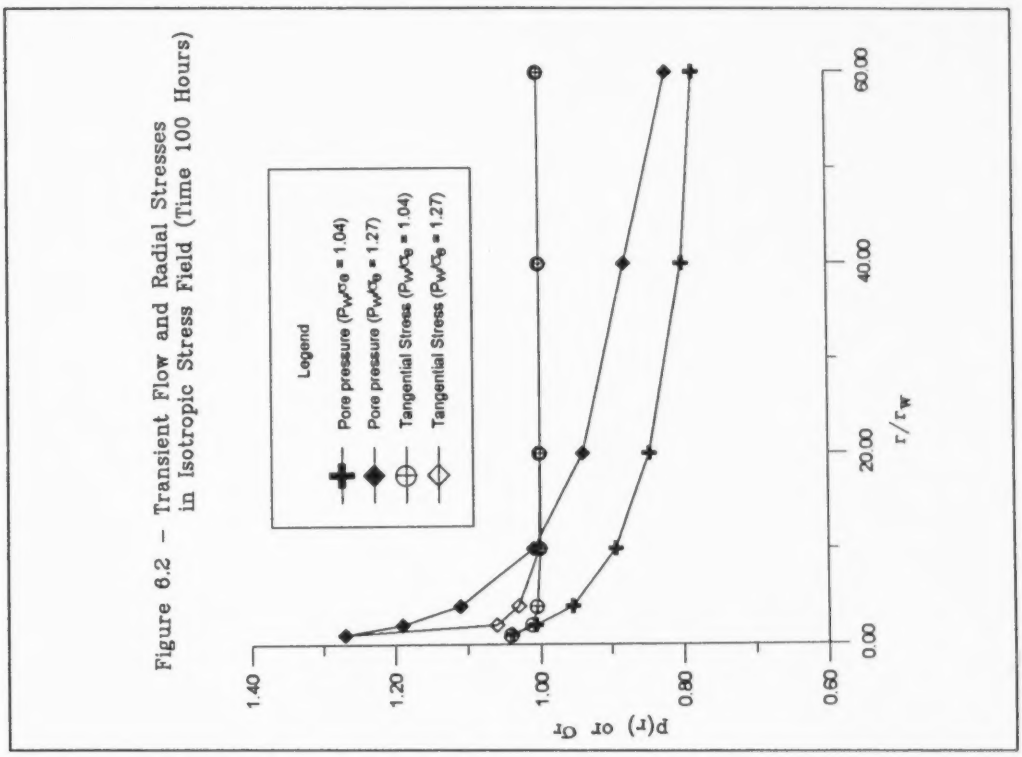

Figure 6.2 – Transient Flow and Radial Stresses in Isotropic Stress Field (Time 100 Hours)

Figure 6.3 – Transient Flow and Tangential Stresses in Anisotropic Stress Field (Time 100 Hours)

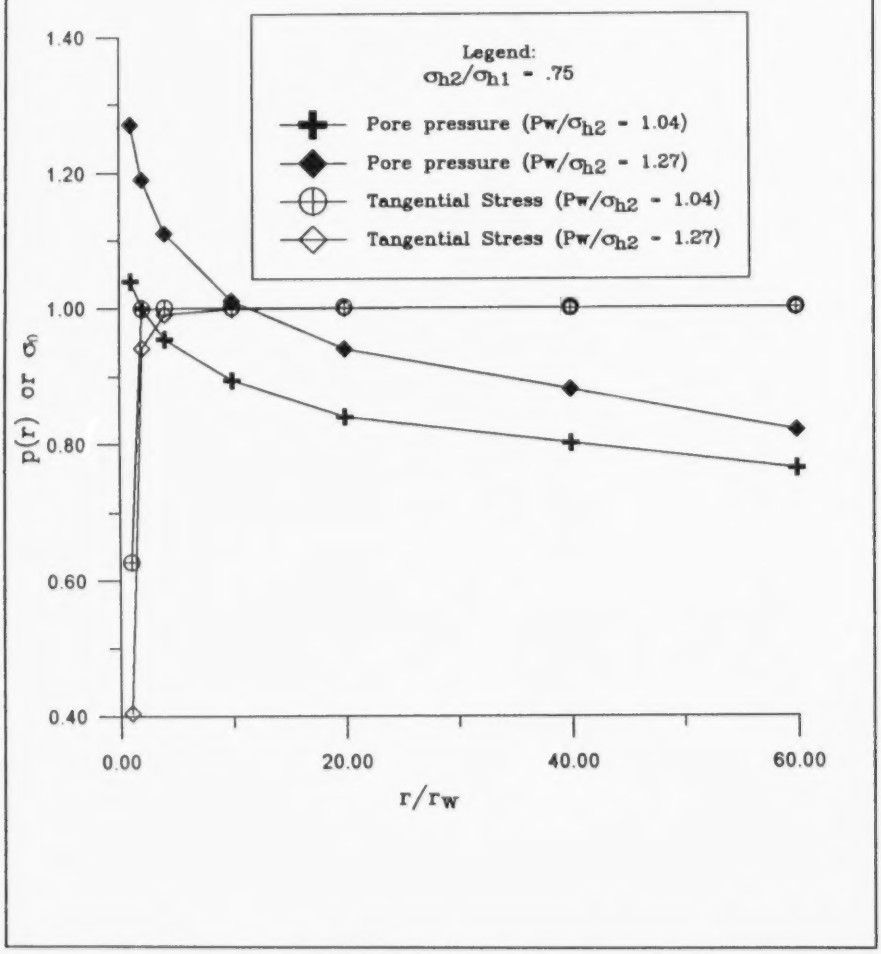

Chapter 7

ANALYTICAL MODEL OF RADIUS OF POTENTIAL FRACTURE REGION

PSEUDOSTEADY-STATE FLOW

In the previous chapter for transient flow, the well was assumed to be located in a very large reservoir so that the flow from or to the well was not affected by the external boundary. The time for this assumption is finite. As soon as the flow begins to be affected by the external boundary it is no longer in a transient state. In this chapter, the model for the radius of the potential fracture region is developed considering the effect of the external boundary conditions; that is, under pseudosteady-state flow conditions.

7.1 Pseudosteady-State Flow

As soon as the pressure disturbance has been felt throughout the reservoir including at the external boundary, the reservoir is no longer infinite-acting and the pressure distribution is not governed by transient radial flow. At this point a new assumption is made to include the external boundary conditions. The initial condition remains the same as in transient flow, and the flow rate is again treated as constant at the wellbore. However, the new condition at the outer boundary of the injection zone is that of no-flow. Therefore, under stabilized conditions the injection zone pressure increases with time. A system resembling pseudosteady-state flow is where industrial waste is disposed of in a relatively small formation or in a large reservoir area over an extended period of time. The pressure in such formations increases with time and should be monitored.

Several solutions for pseudosteady-state flow are available in the literature. The solution given by Matthews and Russell (1967) is used in this chapter. The authors assumed the following initial and boundary conditions:

$p = p_i$ at $t = 0$ for all r

$$\left.\frac{\partial p}{\partial r}\right|_{r_e} = 0$$

and

$$\left.\frac{\partial p}{\partial r}\right|_{r_w} = \frac{q\mu}{2pkh}\frac{1}{r_w}$$

Assuming $r_w << r_e$ and neglecting higher order terms in the Bessel function expansion in the solution, the pressure in the reservoir is given by

$$p(r,t) = p_i + \frac{q\mu}{2\pi kh}\left[\frac{r_D^{\,2}}{2r_{eD}^{\,2}} + \frac{2t_{Dw}}{r_{eD}^{\,2}} + \ln\frac{r_{eD}}{r_D} - \frac{3}{4}\right] \tag{7.1}$$

and the wellbore pressure is given by

$$p_w = p_i + \frac{q\mu}{2\pi kh}\left[\frac{2t_{Dw}}{r_{eD}^{\,2}} + \ln r_{eD} - \frac{3}{4}\right] \tag{7.2}$$

where

$$r_{eD} = \frac{r_e}{r_w} \tag{7.3}$$

$$r_D = \frac{r}{r_w} \tag{7.4}$$

and

$$t_{Dw} = \frac{kt}{\phi \mu c r_w^2} \tag{7.5}$$

Equation 7.1 shows that, although the reservoir pressure increases with time, the pressure gradients are a function only of flow rate and do not change with time.

7.2 Analytical Model

The parameters given in Table 6.1 are used again here to generate typical results for the radius of the potential fracture region.

7.2.1 Isotropic Stress Field, Stress Applied and Pseudosteady-State Flow Conditions.

The pore pressure distribution in the injection zone was calculated using Equation 7.1. Radial and tangential stresses were calculated using Equations 4.1 and 4.2. Referring to Figure 7.1, the pore pressure and tangential stresses are equal at the boundary of the potential fracture region. Assuming $r = r_f$ and $r_D = r_{fD}$ at the boundary and equating Equations 4.1 and 7.1

$$p_i + \frac{q\mu}{2\pi kh}\left[\frac{r_{fD}^2}{2r_{eD}^2} + \frac{2t_{Dw}}{r_{eD}^2} + \ln\left(\frac{r_{eD}}{r_{fD}}\right) - \frac{3}{4}\right] = -\frac{\sigma_w r_w^2 - \sigma_e r_e^2 + \frac{r_w^2 r_e^2}{r_f^2}(\sigma_w - \sigma_e)}{r_e^2 - r_w^2}, \tag{7.6}$$

Similarly radial stresses and pore pressure are equal at the extent of the potential fracture region in Figure 7.2. Therefore equating Equations 4.2 and 7.1

$$p_i + \frac{q\mu}{2\pi kh}\left[\frac{r_{fD}^{\ 2}}{2r_{eD}^{\ 2}} + \frac{2t_{Dw}}{r_{eD}^{\ 2}} + \ln\left(\frac{r_{eD}}{r_{fD}}\right) - \frac{3}{4}\right] = \frac{\sigma_e r_e^{\ 2} - \sigma_w r_w^{\ 2} + \frac{r_w^{\ 2} r_e^{\ 2}}{r_f^{\ 2}}(\sigma_w - \sigma_e)}{r_e^{\ 2} - r_w^{\ 2}} \qquad (7.7)$$

where

$$\sigma_w \equiv p_w = p_i + \frac{q\mu}{2\pi kh}\left[\frac{2t_{Dw}}{r_{eD}^{\ 2}} + \ln r_{eD} - \frac{3}{4}\right] \qquad (7.8)$$

Dividing Equations 7.6 and 7.7 by σ_e to normalize them with respect to the far field stress, and solving for r_f gives the radius of potential fracture region.

For isotropic tangential stresses,

$$r_f = r_w \exp\left[\frac{E}{Br_f^{\ 2}} + \frac{A}{B} + \frac{Cr_f^{\ 2}}{r_w^{\ 2}} + D\right] \qquad (7.9)$$

and for isotropic radial stresses,

$$r_f = r_w \exp\left[-\frac{E}{Br_f^{\ 2}} + \frac{A}{B} + \frac{Cr_f^{\ 2}}{r_w^{\ 2}} + D\right] \qquad (7.10)$$

where

$$A = \frac{p_i}{\sigma_e} - 1 \qquad (7.11)$$

$$B = \frac{q\mu}{2\pi kh\sigma_e} \tag{7.12}$$

$$C = \frac{1}{2r_{eD}^{\ 2}} \tag{7.13}$$

$$D = \left[\frac{2t_{Dw}}{r_{eD}^{\ 2}} + \ln(r_{eD}) - \frac{3}{4}\right] \tag{7.14}$$

and

$$E = r_w^{\ 2}\left[\frac{\sigma_w}{\sigma_e} - 1\right] \tag{7.15}$$

Referring to Figure 4.4, near the wellbore, the tangential stress is substantially lower than the radial stress; therefore, it controls the tensile fracture. Away from the wellbore both tangential and radial stresses tend to the far field value; However, the value of the tangential stress is still less than that of the radial stress. Therefore, it has more influence in controlling the tensile fracture.

7.2.2 Isotropic Stress Field, Stress Relief and Pseudosteady-State Flow Conditions

By setting σ_w / σ_e equal to the pressure in the annulus and keeping it constant, Equations 7.9 and 7.10 can be used to calculate the radius of the potential fracture region under stress relief conditions. In this case p_W is not equal σ_e and stresses in the confining layer are not affected by the well pressure, as discussed in Section 6.2.2. Therefore Equation 7.8 is not used. However, the wellbore pressure is calculated for the pore pressure distribution using Equation 7.2 and is discussed with the results in Chapter 8.

7.2.3 Anisotropic Stress Field, Stress Applied, and Pseudosteady-State Flow Conditions

When the stress field is anisotropic, only the tangential stresses are sufficiently altered to permit a fracture in the confining layer as discussed earlier. The pore pressure distribution in the injection zone and the stress profile in the confining layer is shown in Figure 7.3. Therefore at the boundary of fracturing region, and equating Equations 4.5 and 7.1

$$p_i + \frac{q\mu}{2\pi kh}\left[\frac{r_{fD}^{\ 2}}{2r_{eD}^{\ 2}} + \frac{2t_{Dw}}{r_{eD}^{\ 2}} + \ln\left(\frac{r_{eD}}{r_{fD}}\right) - \frac{3}{4}\right]$$
$$= \frac{1}{2}(\sigma_{h1} + \sigma_{h2}) + \frac{r_w^{\ 2}}{2r_f^{\ 2}}(\sigma_{h1} + \sigma_{h2} - 2\sigma_w) - \frac{1}{2}(\sigma_{h1} - \sigma_{h2})\left[1 + \frac{3r_w^{\ 4}}{r_f^{\ 4}}\right]\cos 2\theta \qquad (7.16)$$

Where $\sigma_w \equiv p_w$, as given in Equation 7.7

Dividing Equation 7.16 by σ_{h2} to normalize with respect to far field stress, and solving for r_f gives the radius of the potential fracture region when pseudosteady-state and anisotropic tangential stresses are used.

$$r_f = r_w \exp\left[-\frac{E}{Br_f^{\ 2}} - \frac{G}{Br_f^{\ 4}} + \frac{A}{B} + \frac{Cr_f^{\ 2}}{r_w^{\ 2}} + D\right] \qquad (7.17)$$

where

$$A = \frac{p_i}{\sigma_{h2}} - \frac{1}{2}\left[\frac{\sigma_{h1}}{\sigma_{h2}} + 1\right] + \frac{1}{2}\left[\frac{\sigma_{h1}}{\sigma_{h2}} - 1\right]\cos 2\theta \qquad (7.18)$$

$$B = \frac{q\mu}{2\pi kh\sigma_{h2}} \tag{7.19}$$

$$C = \frac{1}{2\,r_{eD}{}^2} \tag{7.20}$$

$$D = \left[\frac{2t_{Dw}}{r_{eD}{}^2} + \ln r_{eD} - \frac{3}{4}\right] \tag{7.21}$$

$$E = \frac{r_w{}^2}{2}\left[\frac{\sigma_{h1}}{\sigma_{h2}} - \frac{2\sigma_w}{\sigma_{h2}} + 1\right] \tag{7.22}$$

and

$$G = -\frac{3r_w{}^4}{2}\left[\frac{\sigma_{h1}}{\sigma_{h2}} - 1\right]\cos 2\theta \tag{7.23}$$

7.2.4 Anisotropic Stress Field, Stress Relief and Pseudosteady-State Flow Conditions

The radius of the potential fracture region using tangential stresses can be calculated by setting σ_w/σ_e equal to the annulus pressure as discussed in Section 5.2.2 and 5.2.4 and 6.2.2. Therefore Equation 7.8 is not used. However, the wellbore pressure is calculated for this pore pressure distribution using Equation 7.2 and is discussed with the results in Chapter 8.

The mathematical models developed in Equations 7.9, 7.10 and 7.17 are nonlinear and cannot be solved analytically. These equations can be solved using the Newton Raphson or some other iterative method.

Figure 7.1 – Pseudosteady-State Flow and Tangential Stresses in Isotropic Stress Field (Time 1 Hour)

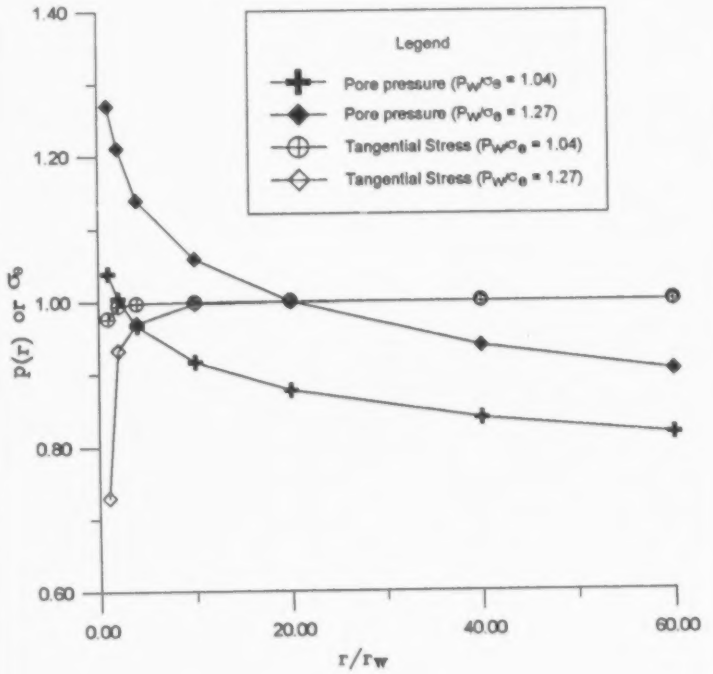

Figure 7.2 – Pseudosteady-State Flow and Radial Stresses in Isotropic Stress Field (Time 1 Hour)

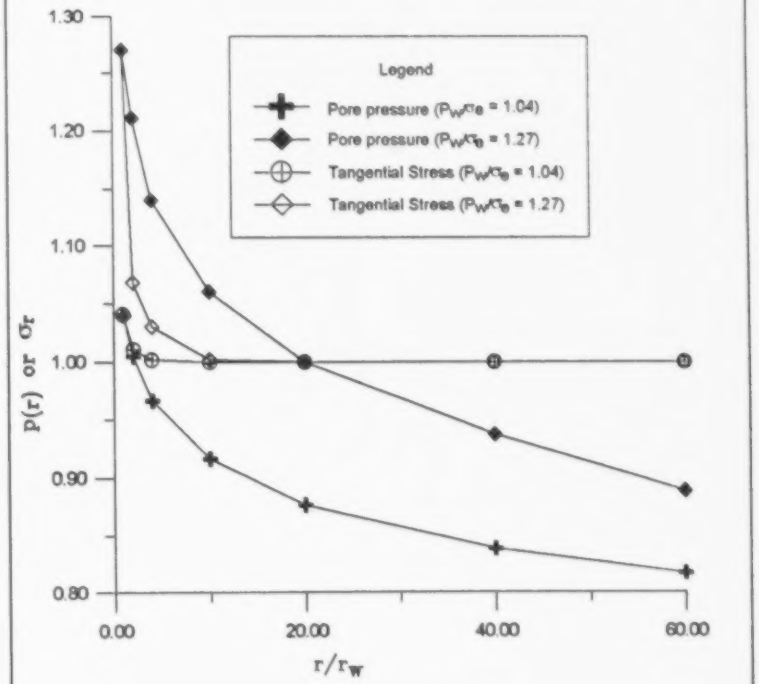

Figure 7.3 – Pseudosteady–State Flow and Tangential Stresses in Anisotropic Stress Field (Time 1 Hours)

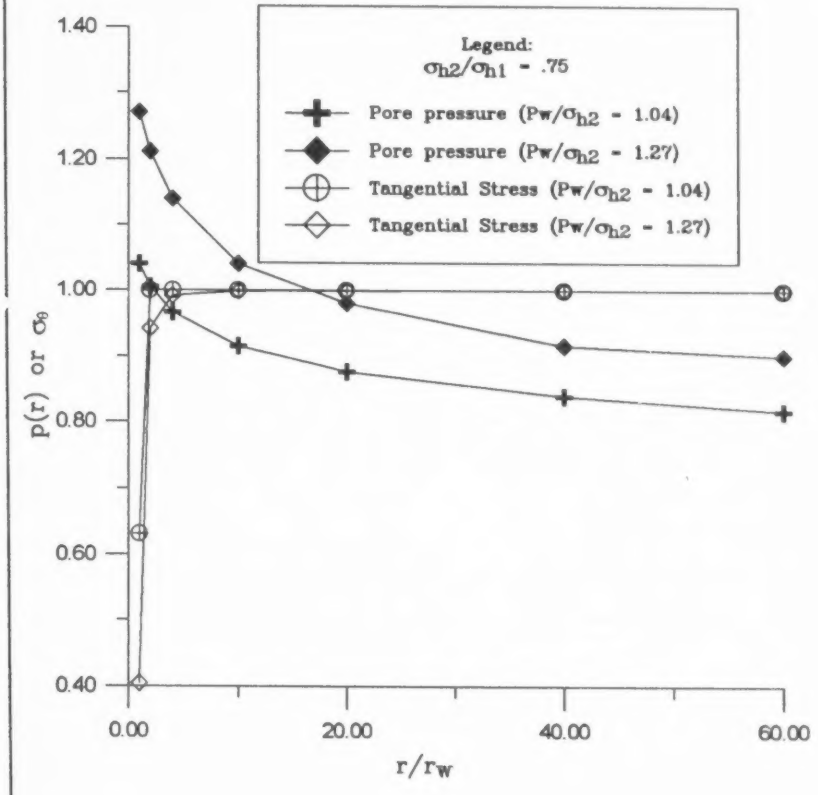

Chapter 8

INVESTIGATION OF THE LIMITS OF THE REGION OF POTENTIAL FRACTURE

The analytical expressions for the radius of potential fracture region were developed for steady-state, transient and pseusosteady-state flow conditions. In this chapter, curves are developed to interpret these expressions for the radius of the potential fracture region. The effect of different parameters is also examined.

Hubbert and Willis (1957) suggested that formation breakdown occurs according to Equation 4·7, in the plane $\theta = 0$. Figure 4·8 showed that the fracture first becomes possible in the plane $\theta = 0$. In the plane $\theta = \pi / 2$ the tangential stresses are higher. As discussed in Chapter 2 many authors suggested that the breakdown pressure is greater than the fracture extension pressure. The difference in definition between fracture initiation from a pre-existing crack and breakdown pressure has been the motivation for this study.

If there is no defect or crack in the injection zone, then the pressure required to initiate a fracture in this zone is equal to or greater than the breakdown pressure. If a crack exists in the confining layer at the interface, then the high pore pressure can be transmitted into the confining layer without creating any fracture in the injection zone. As the pressure in the crack becomes higher than the minimum horizontal stresses, the crack extends, and if the fracture toughness of the material can be considered to be zero, the fracture can break through into the overlying formation.

8.1 Effect of Injection and Injection Zone Pressure

As the pore pressure increases, a volumetric expansion occurs. Under in-situ conditions, a volume change can not occur because the permeable injection zone is bounded by impermeable rock. Thus the attempted increase in strain is converted into an increase in stress (Cleary, 1980). The increase

in stress is lateral over a large area. As the pressure in the injection zone increases, the pore pressure becomes higher than the horizontal stress in the confining layer over a large area and the radius of the potential fracture region will increases.

When pressure is applied in the wellbore, radial and tangential stresses are developed. It has been discussed in the previous chapters that when the stress field is anisotropic, only the tangential stresses are effective in creating a fracture. Curves were developed to determine the effect of injection pressure and injection zone pressure on the extent of the potential fracture region for isotropic, and anisotropic stress fields and for different well completions. The parameters given in the Table 5.1 and 6.1 were used and time periods of 100 hour and 1 hours were used for transient and pseudosteady-state flow conditions respectively.

8.1.1 Isotropic Stress Field and Stress Applied Conditions

To investigate the effect of injection zone pressure on the extent of the potential fracture region various injection pressures and far field stress ratios were considered. Injection zone pressure to far field stress ratios of 0.7 and 0.8 were used. The results for tangential stress are combined with the results of the anisotropic stress field to be discussed later. The results for radial stress are shown in Figures 8.1, 8.2 and 8.3 for steady-state, transient, and pseudosteady-state flow conditions, respectively. It is obvious that as the ratio of injection pressure to far field stress p_w / σ_e, increases, the radius of the potential fracture region increases. Considering Figure 8.1 for steady-state flow conditions, as the value of p_w / σ_e increases from 1.04 to 1.27 at an injection zone pressure to far field stress ratio (p_e / σ_e) of 0.8, the value of the potential fracture region increases from 2.7 to 37 wellbore radii. Since the wellbore radius is 0.1m or 10 cm, which is approximately equal to a 4" wellbore, the maximum radius of the potential fracture region is only 3.7 m.

As the ratio of injection zone pressure to far field stress (p_e / σ_e) increases, the radius of the potential fracture region increases for a given injection pressure. Also, for a given far field stress ratio in the confining layer, the extent of the potential fracture region depends on the pressure in the underlying injection zone. Thus for a high-pressured aquifer the radius of the potential fracture

region is greater. A high (p_e / σ_e) ratio represents the physical situation of a high-pressured shallow aquifer, and a low ratio represents the situation of a normally pressured deep aquifer. The injection pressure limit for a high pressure aquifer is very low compared to a normally pressured aquifer.

8.1.2 Isotropic Stress Field and Stress Relief Conditions

When the completion packer is set below the confining layer, then stress relief conditions prevail, depending on the annulus pressure, as discussed in Section 4.3.2. In this situation, the stresses in the confining layer are reduced in the vicinity of the wellbore. Therefore, maintaining the original injection pressure results in an increase in the radius of the fracture region. The radii of the potential fracture regions were calculated at complete stress relief $(\sigma_w / \sigma_e = 0)$ and partial stress relief $(\sigma_w / \sigma_e = 0.5)$ conditions. The curves were developed for various injection pressures, and injection zone pressure to far field stress ratios (p_e / σ_e) of 0.7 and 0.8. The results are shown in Figures 8.4 to 8.6 for steady-state, transient, and pseudosteady-state flow conditions, respectively. Near the wellbore the radius of the potential fracture region at $p_e / \sigma_e = 0.7=$ and 0.8 are same. It appears from the curves that an increase in the stresses due to high injection zone pressure is compensated by a decrease in the radial stresses due to the stress relief conditions. Away from the wellbore the radial stresses approach the far field values and the effect of the injection zone pressure dominates; therefore, the radius of fracture region is much higher at $p_e / \sigma_e = 0.8$ as compared to $p_e / \sigma_e = 0.7$.

8.1.2.1 Effect of Stress Relief Near the Wellbore

Since the stress relief conditions only affect the region near the wellbore, the radius of the fracture region was plotted near the wellbore to determine the effect of complete and partial stress relief conditions. According to Equation 4.4, the radial stresses at the wellbore are equal to the wellbore pressure; therefore, under complete stress relief conditions, the radial stresses at the wellbore are zero. The stresses are reduced in the vicinity of the wellbore and are less than the stresses under partial stress relief conditions. Therefore, for the same injection pressure, the radius of the potential fracture region is higher under the complete relief condition as compared to that under the partial stress relief conditions, provided that the p_e / σ_e ratio is the same. Figures 8.7 to 8.9 show the

results for steady-state, transient, and pesudosteady-state flow conditions respectively. The radius of the potential fracture region increases with an increase in injection zone pressure. Similar behaviour has been noted under all three flow conditions.

8.1.3 Anisotropic Stress Field and Stress Applied Conditions

The radius of the potential fracture region was calculated using tangential compressive stresses for various injection pressures. Injection zone pressure to minimum horizontal stress ratios of 0·7 and 0·8 were used. The results for the isotropic stress field were combined with the anistropic stress field and are presented in Figures 8·9 to 8·12 for steady-state, transient, and pseudosteady-state flow conditions, respectively. A minimum to maximum horizontal stress ratio of 0·7 was used to incorporate the effect of anisotropy. For a given injection pressure, the radius of the fracture region increases with an increase in injection zone pressure to minimum horizontal stress ratio. The effect of anisotropy results in a slight reduction of r_f near the wellbore, provided that the injection pressure and the p_e / σ_{h2} ratio are kept constant. Away from the wellbore, tangential stresses tend to approach the minimum horizontal stress value and r_f is same for both the isotropic and the anisotropic stress field. The p_e / σ_{h2} ratio seems to be the dominant factor in calculating the radius of the potential fracture region. Therefore, the injection zone pressure or the magnitude of the minimum horizontal stress σ_{h2}, has more influence on the radius of fracturing region than the stress field around the wellbore.

8.1.4 Anisotropic Stress Field and Stress Relief Conditions

When the stress field is isotropic, the tangential stress is a maximum at the wellbore; away from the wellbore it approaches the value of the far field stress. According to Equation 4.3, the maximum normalized tangential stress at the wellbore, σ_θ / σ_e, under complete stress relief conditions, is 2. When the stress field is anisotropic, the tangential stresses will again be maximum at the wellbore but will be less than under isotropic stress field. Therefore, under the stress relief conditions, a higher injection rate is required to initiate a fracture near the wellbore. Under transient and pseudosteady-state flow conditions an injection pressure ratio (p_e / σ_{h2}) of 1.19 is required to initiate a fracture, compared to 1.04 under the stress applied conditions. Away from

the wellbore the tangential stress approaches the minimum horizontal stress. Therefore, for a given injection pressure, depending on the degree of anisotropy, r_f is slightly less for anisotropic stress field compared to that for an isotropic stress field, provided that p_w and the p_e / σ_e ratio are kept constant. These results are shown in Figures 8.13 to 8.15 for steady-state, transient, and pseudosteady-state flow conditions. As the p_e / σ_e ratio increases r_f increases.

Similar behaviour has been observed for the partial stress relief condition $(\sigma_w / \sigma_e = 0.5)$. The results are shown in Figures 8.16 through 8.18.

8.1.4.1 Effect of Stress Relief Near the Wellbore

Since the stress relief conditions affect the stresses only near the wellbore, r_f was calculated using tangential stresses for an isotropic stress field and plotted as shown in Figures 8.19 to 8.21. Under the complete stress relief conditions, the tangential stresses at the wellbore are maximum and are higher than the stresses in the partial stress relief conditions. The stresses approach the far field values as distance increases away from the wellbore. Therefore, keeping p_w and the p_e / σ_e ratio constant, the radius of the potential fracture region is higher for partial stress relief conditions. The radius of the potential fracture region increases with an increase in injection zone pressure. Therefore the injection zone pressure is a dominant factor in calculating the radius of the potential fracture region. The effect of the p_e / σ_e ratio was negligible near the wellbore when radial stresses were used in Section 8.1.2.1. Further away from the wellbore, as the effect of the stress relief conditions on the tangential stresses decreases, r_f converges to the same value for different degrees of stress relief.

The results were not plotted for anisotropic conditions $\sigma_{h2} / \sigma_{h1} = 0.7$ because it has been established in the previous section that the radius of the potential fracture region is only slightly less than when the stress field is isotropic.

8.2 Effect of Stress Contrast

When the horizontal stress contrast increases, a tensile zone is created in the region surrounding the wellbore. The rock may be fractured in tension at a high horizontal stress contrast. To determine the effect of stress contrast on the radius of the potential fracture region, the horizontal stress ratio was varied from 1 to 0.5. As discussed in Chapter 4, under the stress applied condition, the injection zone fractures in tension at a horizontal stress ratio of 0.5; therefore, horizontal stress ratios of less than 0.5 are not considered.

8.2.1 Anisotropic Stress Field and Stress Applied Conditions

The radius of the potential fracture region was calculated for three different injection pressures at each stress ratio and plotted for steady-state, transient and pseudosteady-state flow conditions as shown in Figures 8.22 to 8.24. The radius of the fracture region was almost the same at all stress ratios. However, r_f increases with an increase in the injection pressure. Therefore, stress contrast is not a dominant factor in controlling the radius of the potential fracture region.

8.2.2 Anisotropic Stress Field and Stress Relief Conditions

The confining layer will breaks in tension when the horizontal stress ratio is 0.3 or less under the complete stress relief condition, as discussed in Chapter 4. Therefore water injection or waste disposal is not desirable at a stress ratio of 0.3 or less. The stress relief conditions across the confining layer prevail when the packer is set below the confining layer. However, across the injection zone stress applied conditions always exist, and under the stress applied conditions the

injection zone fractures at a stress ratio of 0.5. If the same horizontal stresses are assumed in the injection zone and confining layer, then a formation with a stress ratio of less than 0.5 may never be attained across the confining layer in field applications. Therefore, the stress ratio was varied between 1 and 0.5 to study the effect of stress contrast on the radius of the potential fracture.

The radius of the potential fracture region was calculated for three different injection pressures at each stress ratio under complete and partial stress relief conditions and plotted for steady-state, transient and pseudosteady-state flow conditions as shown in Figures 8.25 to 8.27. Again the stress contrast does not affect the radius of the potential fracture region.

8.3 Effect of Packer Setting Depth

The prime purpose of a downhole packer is to provide a seal between the tubing and casing to prevent vertical movement of fluids in the annulus past the sealing point. The packers help prevent casing leaks and improve wellbore integrity. If the packer is set above the confining layer then the wellbore integrity is still effectively maintained but stress applied conditions prevail across the confining layer. So, for a given injection pressure, the radius of the potential fracture region is greater than it would be for stress relief conditions. To ensure stress relief conditions across the confining layer so that the potential fracture region becomes smaller for a given injection pressure, the packer must be set below the confining layer.

8.4 Effect of Injection Rate

Guo et al. (1993) suggested that the fracturing pressure depends on the injection rate and on the minimum horizontal stress. The effect of rate on the radius of the potential fracture region was studied for transient and pseudosteady-state flow conditions. The results for isotropic radial and tangential stresses and anisotropic tangential stress $\sigma_{h2}/\sigma_{h1} = 0.7$ for various rates and $p_e/\sigma_e = .7$ are shown in Figures 8.28 and 8.29. As the rate increases, the well pressure increases and in turn the pore pressure in the injection zone increases as discussed above. Hence the radius of potential fracture region increases. Near the wellbore, the stresses in the confining layer are

distinctly affected by the well pressure and away from the wellbore the stresses tend to approximate the far field values. Thus the radius of the fracture region at lower wellbore pressures is slightly higher for an isotropic stress field than for an anisotropic stress field. These results are consistent with other results as discussed in Section 8.1.3.

8.5 Effect of Injection Time

As the injection time increases the pore pressure in the injection zone increases; therefore, the radius of the potential fracture region increases. The results for transient and pseudosteady-state are shown in Figures 8.30 and 8.31. These results are consistent with other results discussed in Section 8.1.3 and 8.5. Increasing the time increases the pressure in the injection zone at a much faster rate for pseudosteady-state flow because of the no flow external boundary condition. Therefore, increasing the time from one hour to 2.5 hours in the pseudosteady-state case resulted in a radius of potential fracture region higher than after 10000 hours under transient flow conditions, keeping all other reservoir parameters constant.

8.6 Effect of Injection Zone Porosity, Fluid Viscosity and Compressibility

As the porosity-viscosity-compressibility product $\phi\mu c$ is increased in Equation 6.1 for transient flow conditions, the pore pressure decreases. Therefore increasing $\phi\mu c$ decreases the radius of the potential fracture region. The results for transient and pseudosteady-state flow are shown in Figures 8.32 and 8.33.

Figure 8.1 – Radius of Potential Fracture Region
Steady-State Flow and Radial Stresses in
Isotropic Stress Field

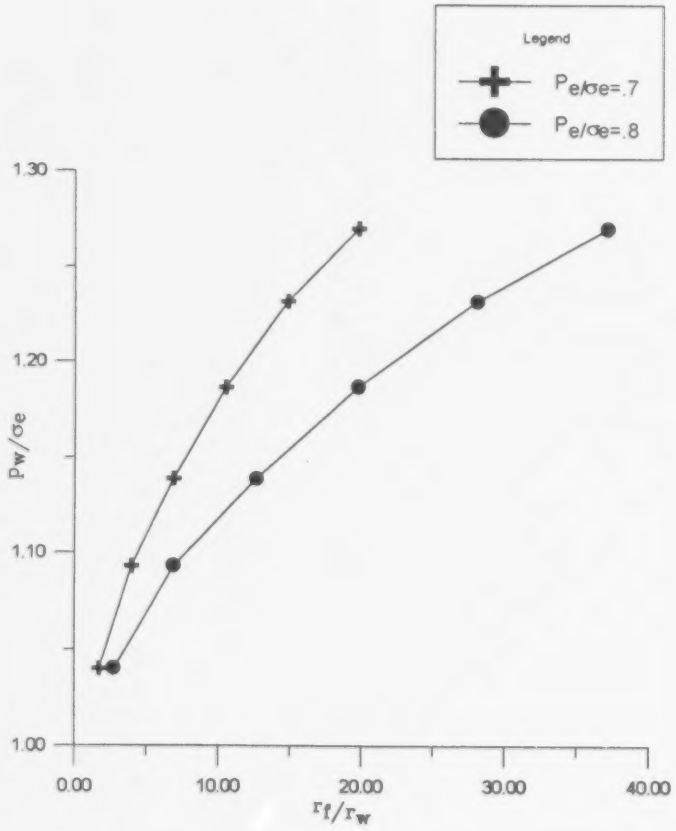

Figure 8.2 – Radius of Potential Fracture Region
Transient Flow and Radial Stresses in
Isotropic Stress Field (Time 100 Hours)

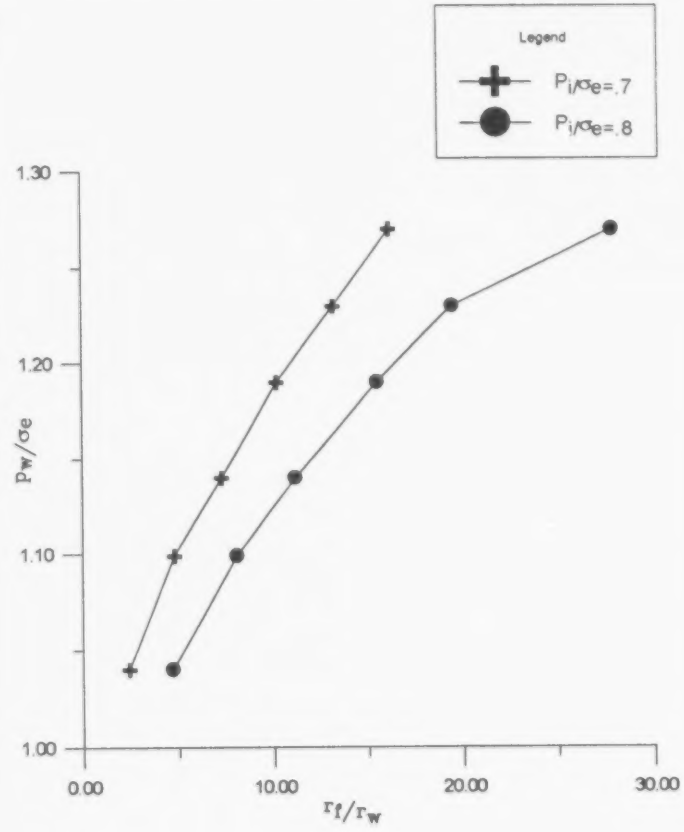

Figure 8.3 – Radius of Potential Fracture Region Pseudosteady–State Flow and Radial Stresses in Isotropic Stress Field (Time 1 Hour)

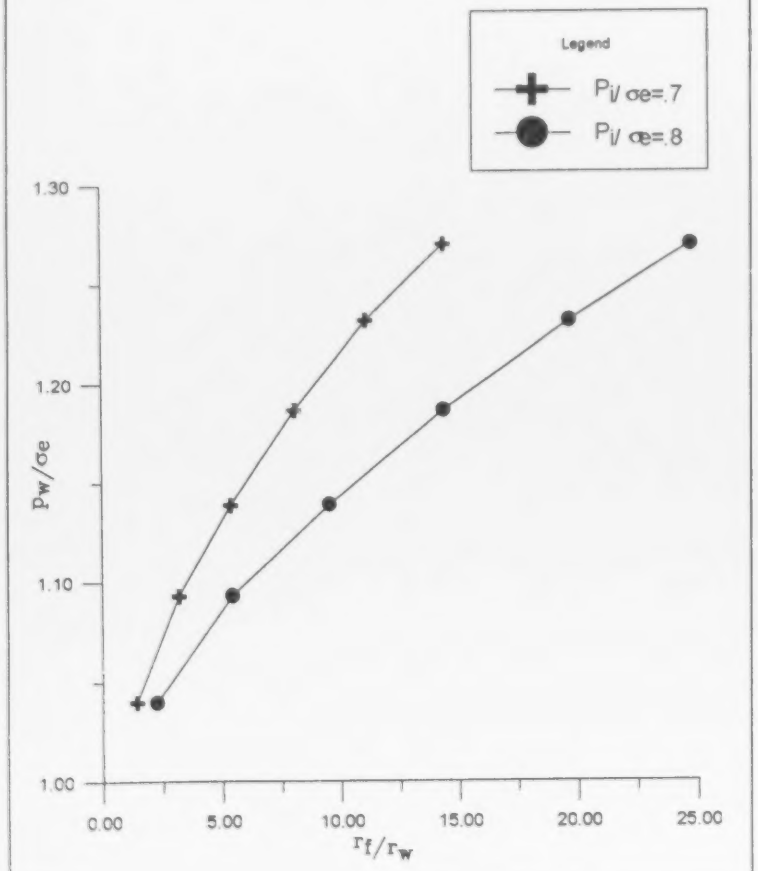

Figure 8.4 – Radius of Potential Fracture Region Steady–State Flow and Radial Stresses in Complete and Partial Stress Relief Conditions

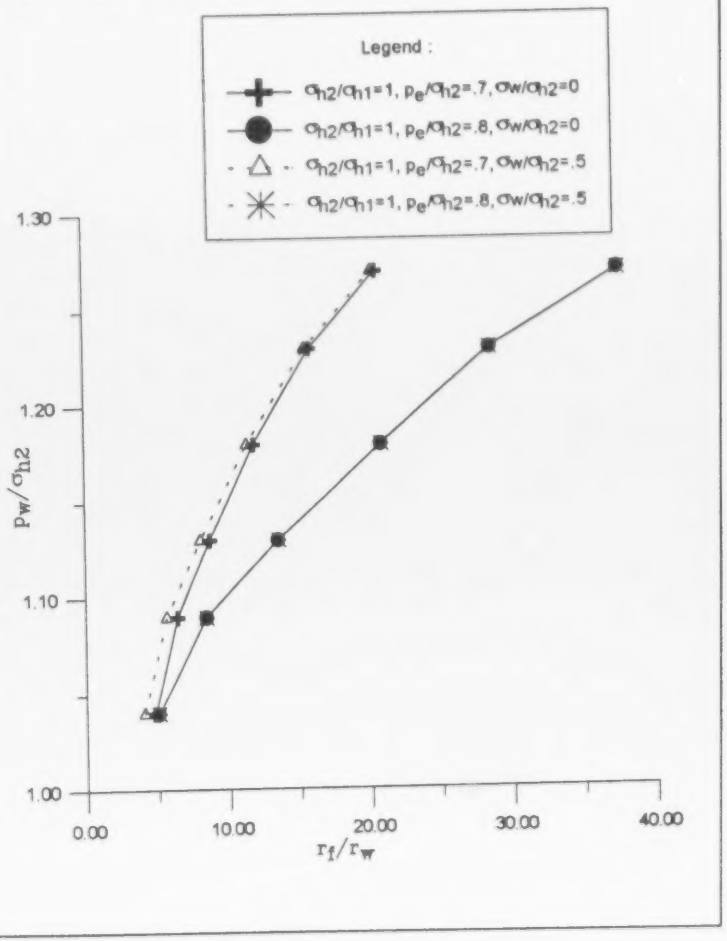

Figure 8.5 – Radius of Potential Fracture Region Transient Flow and Radial Stresses in Complete and Partial Stress Relief Conditions(Time 100 hours)

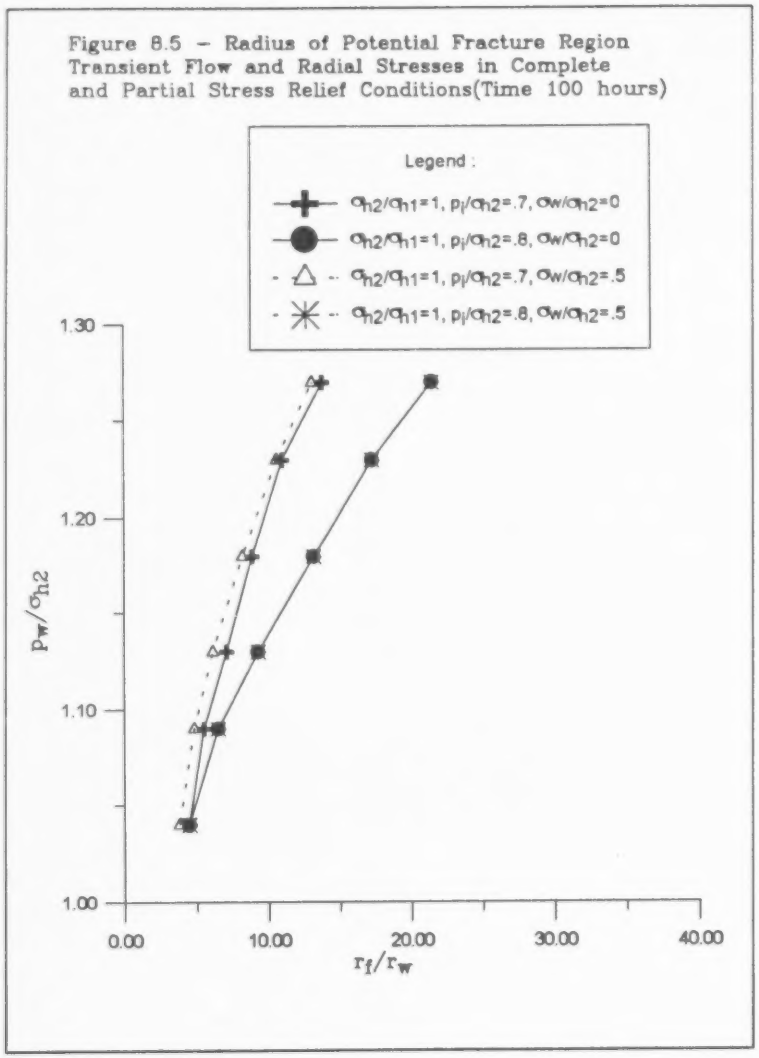

Figure 8.6 – Radius of Potential Fracture Region Pseudosteady–State Flow and Radial Stresses in Complete and Partial Stress Relief Conditions (Time 1 hour)

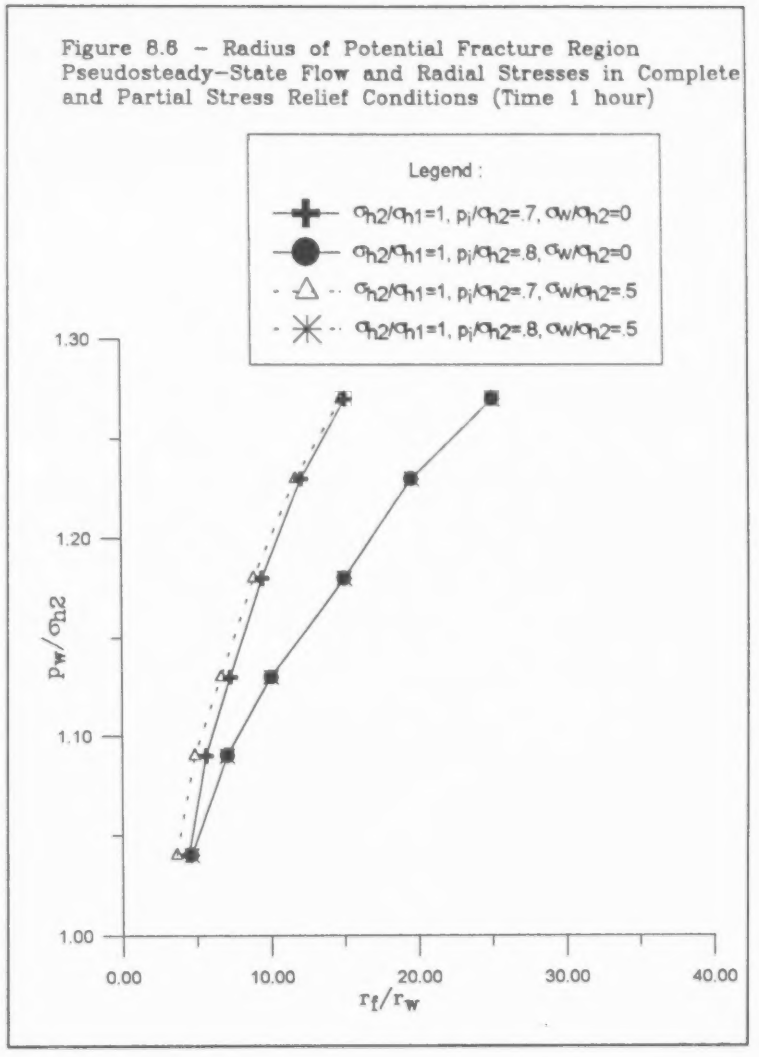

Figure 6.7 – Comparison of Radius of Potential Fracture Region Near Wellbore in Complete and Partial Stress Relief Conditions Steady-state Flow and Radial Stresses

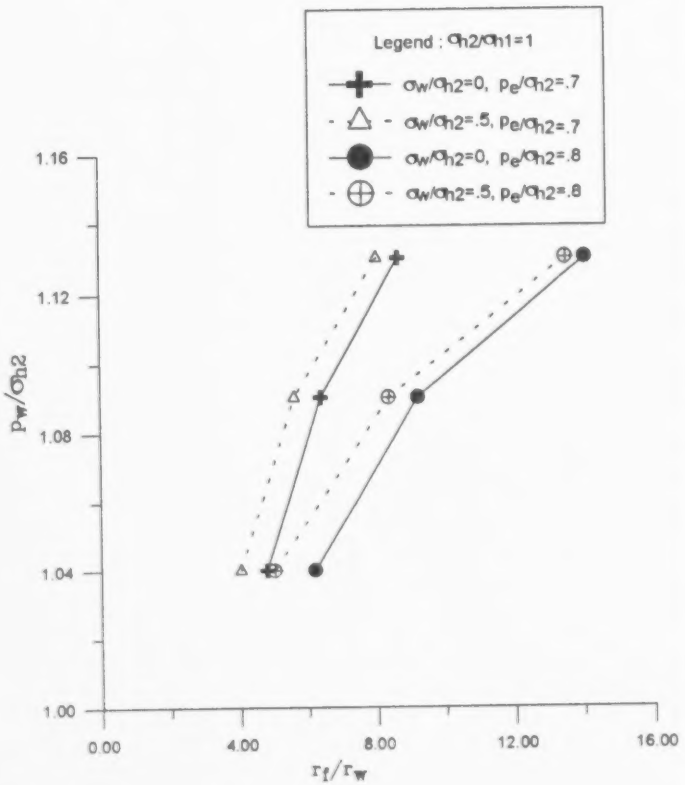

Figure 6.8 – Comparison of Radius of Potential Fracture Region Near Wellbore in Complete and Partial Stress Relief Conditions Transient Flow and Radial Stresses (Time 100 hours)

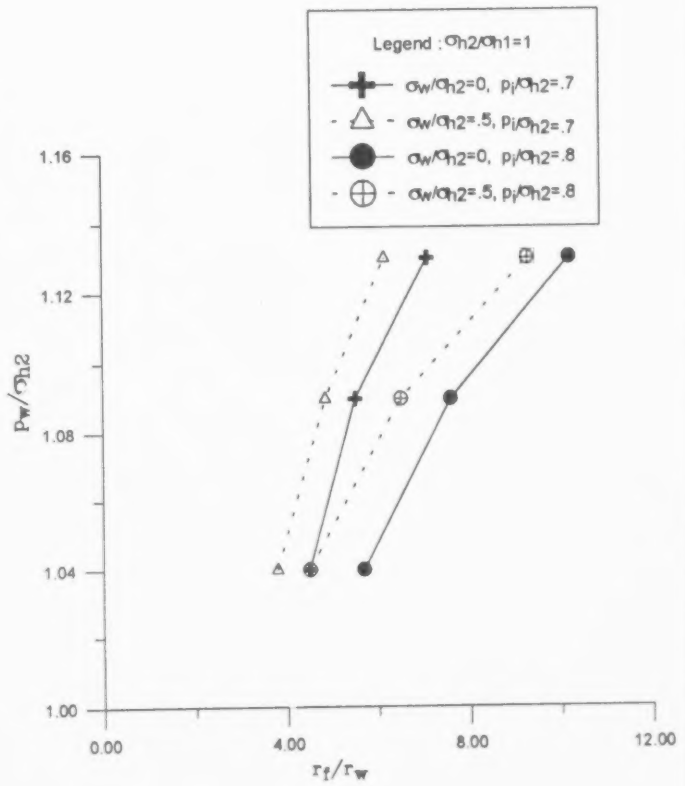

Figure 8.9 – Comparison of Radius of Potential Fracture Region Near Wellbore in Complete and Partial Stress Relief Conditions Pseudosteady–State Flow and Radial Stresses (Time 1 hours)

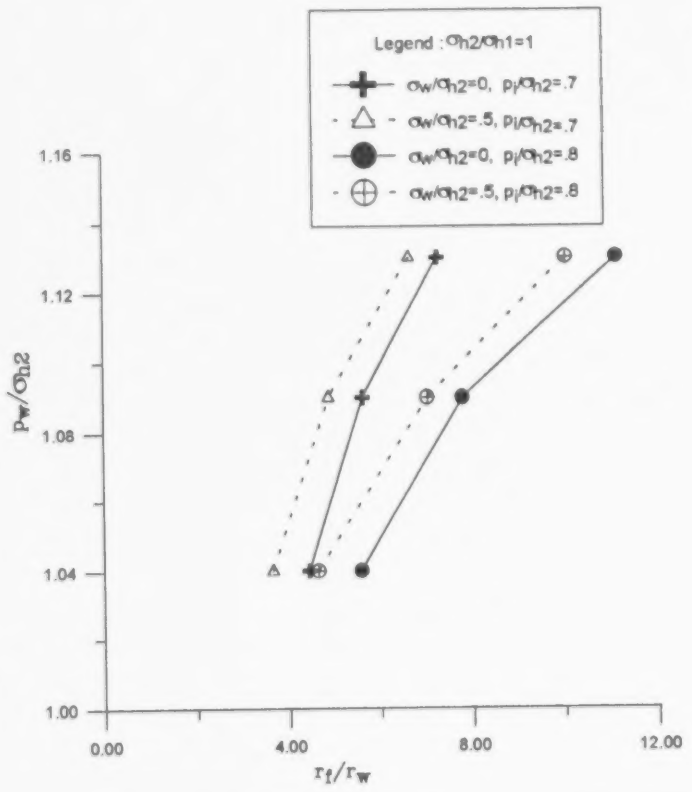

Figure 8.10 – Radius of Potential Fracture Region Effect of Stress Contrast and Injection Zone Pressure Steady–State Flow and Tangential Stresses

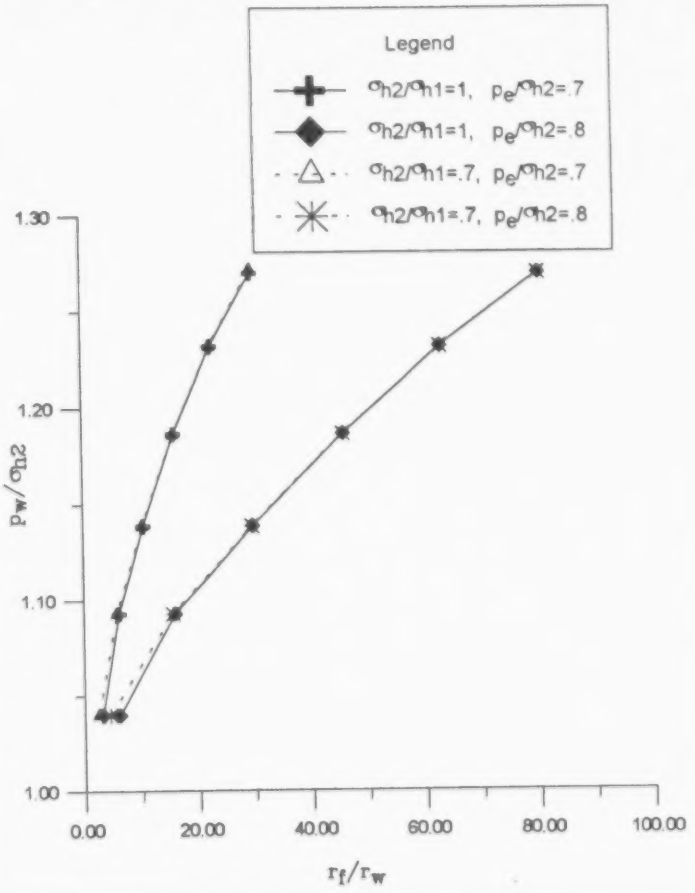

Figure 8.11 – Radius of Potential Fracture Region
Effect of Stress Contrast and Injection Zone Pressure
Transient Flow and Tangential Stresses(Time 100 Hours)

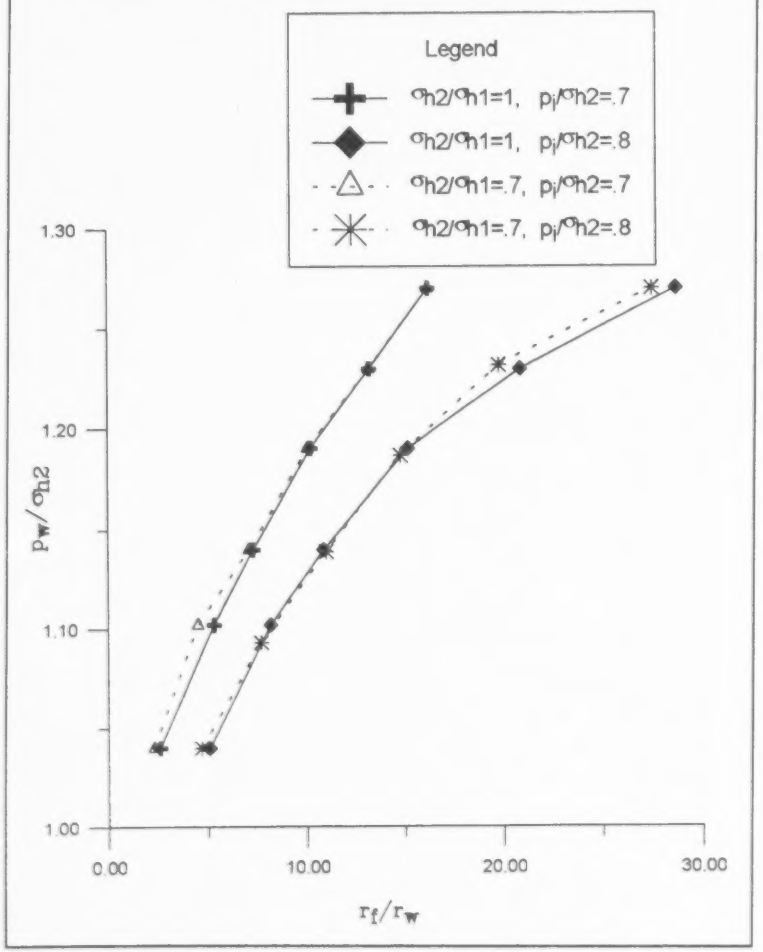

Figure 8.12 – Radius of Potential Fracture Region
Effect of Stress Contrast and Injection Zone Pressure
Pseudosteady–State Flow and Tangential Stresses
(Time 1 Hour)

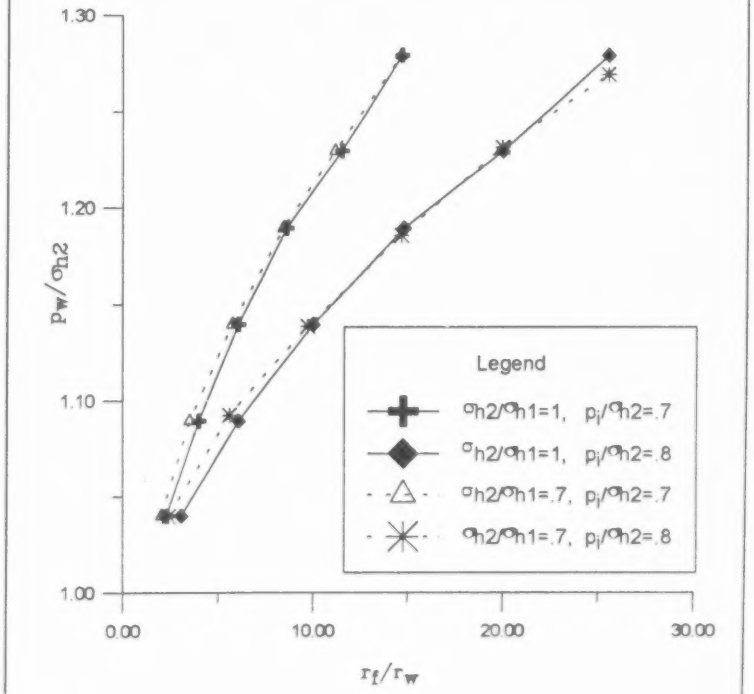

Figure 8.13 – Radius of Potential Fracture Region
Effect of Stress Contrast and Injection Zone Pressure
Steady-State Flow and Tangential Stresses in
Complete Stress Relief Conditions

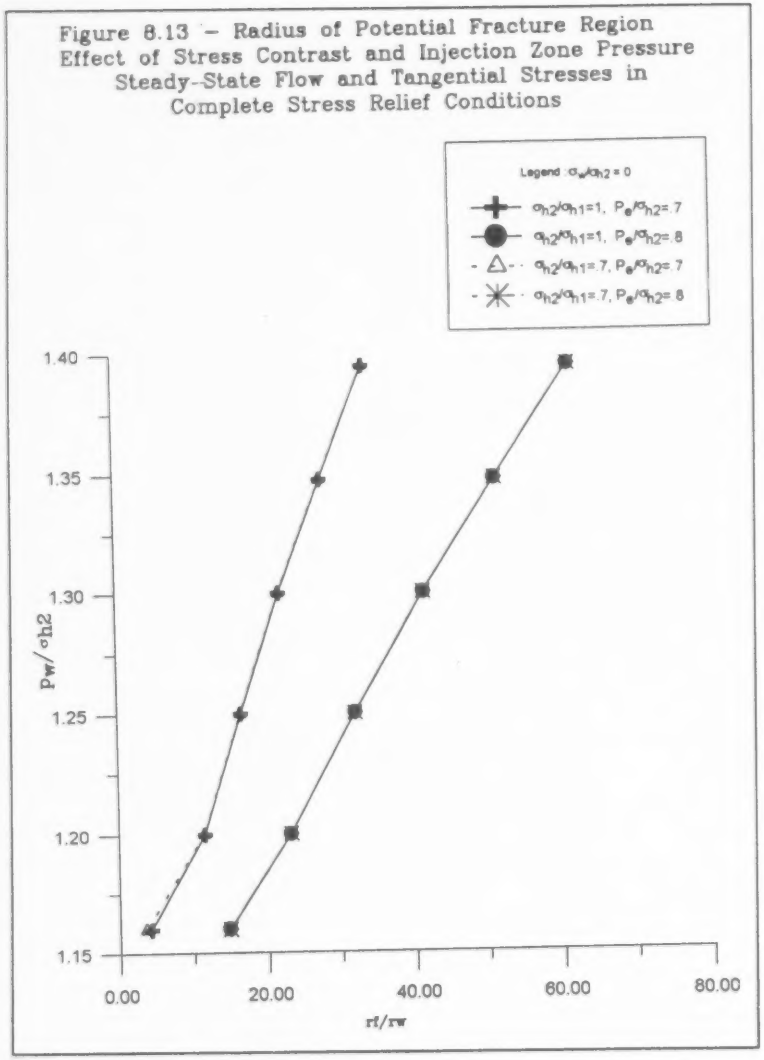

Figure 8.14 – Radius of Potential Fracture Region
Effect of Stress Contrast and Injection Zone Pressure
Transient Flow and Tangential Stresses in
Complete Stress Relief Conditions

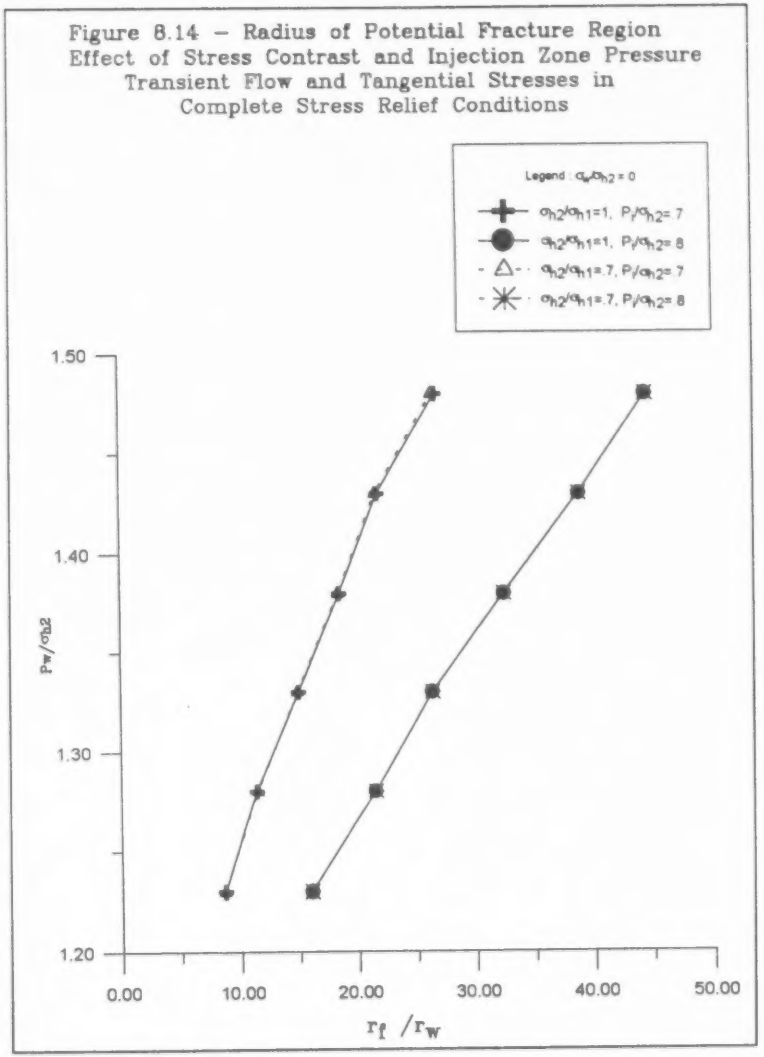

Figure 8.15 – Radius of Potential Fracture Region
Effect of Stress Contrast and Injection Zone Pressure
Pseudosteady-State Flow and Tangential Stresses in
Complete Stress Relief Conditions (Time 1 Hours)

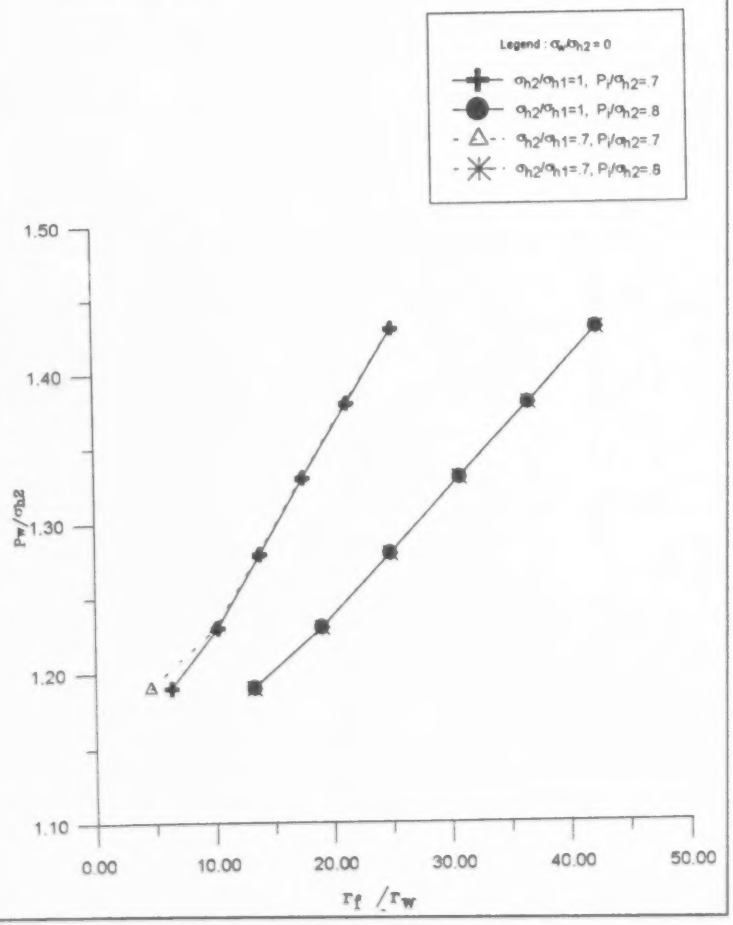

Figure 8.16 – Radius of Potential Fracture Region
Effect of Stress Contrast and Injection Zone Pressure
Steady-State Flow and Tangential Stresses in
Partial Stress Relief Conditions

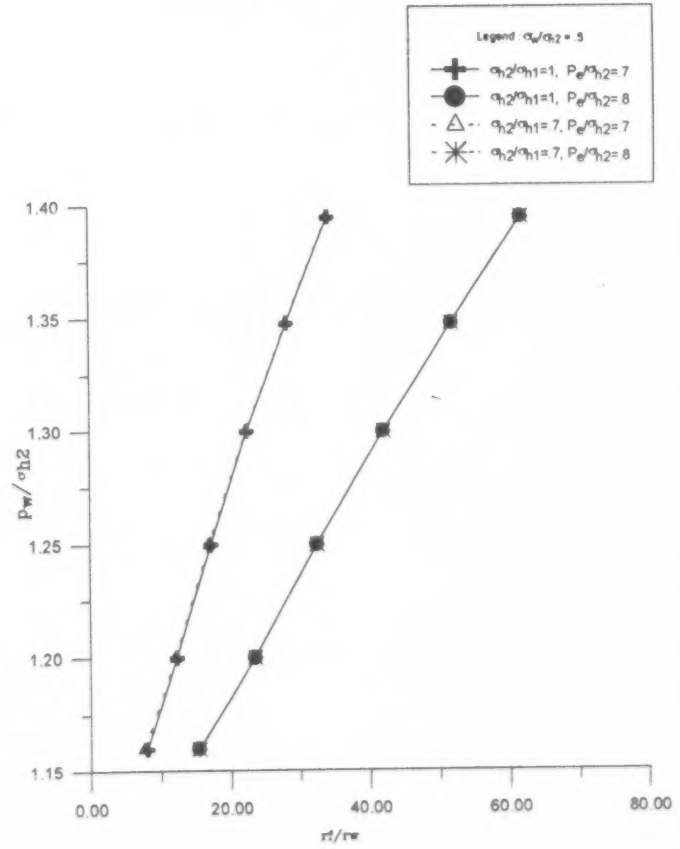

Figure 8.17 – Radius of Potential Fracture Region
Effect of Stress Contrast and Injection Zone Pressure
Transient Flow and Tangential Stresses in
Partial Stress Relief Conditions(Time 100 Hours)

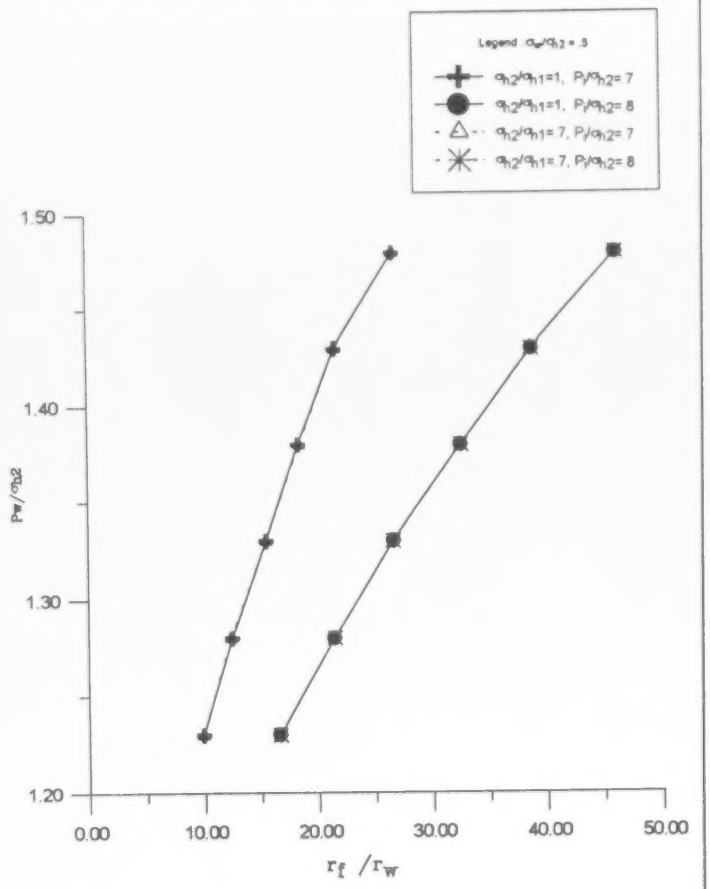

Figure 8.18 – Radius of Potential Fracture Region
Effect of Stress Contrast and Injection Zone Pressure
Pseudosteady–State Flow and Tangential Stresses in
Partial Stress Relief Conditions (Time 1 Hours)

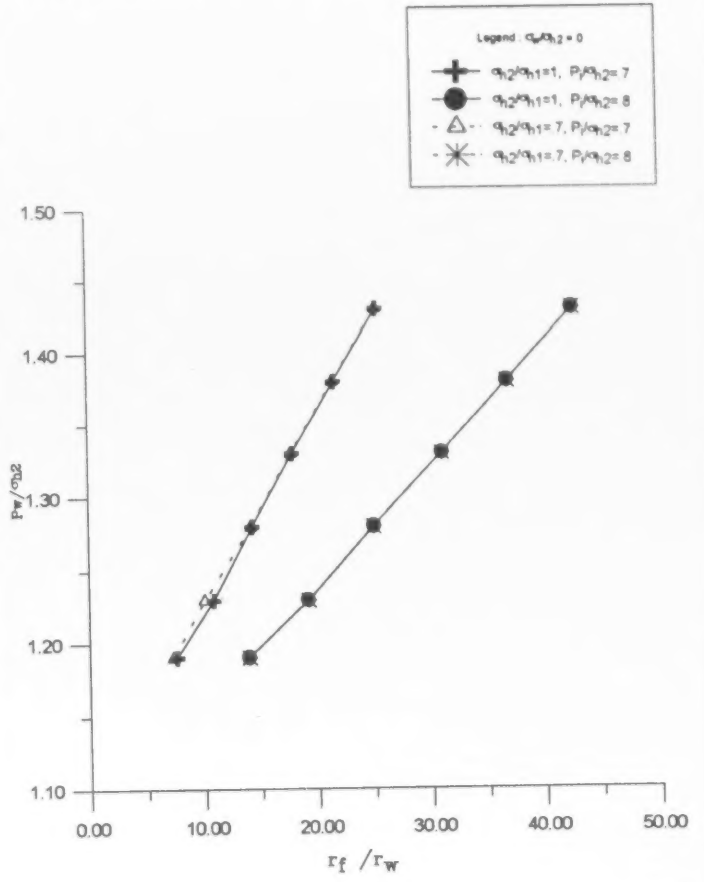

Figure 8.19 – Comparison of Radius of Potential Fracture Region Near Wellbore in Complete and Partial Stress Relief Conditions Steady-State Flow and Tangential Stresses

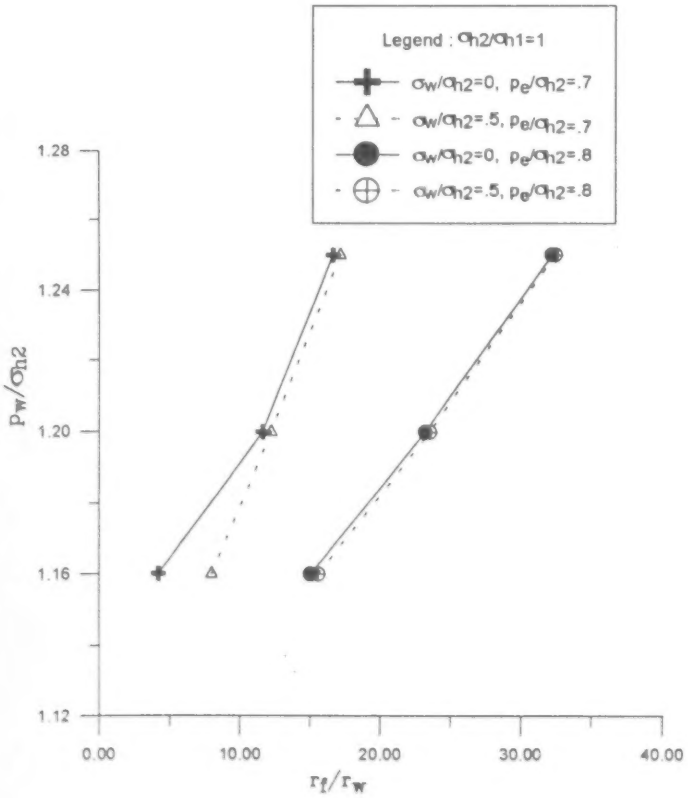

Figure 8.20 – Comparison of Radius of Potential Fracture Region Near Wellbore in Complete and Partial Stress Relief Conditions Transient Flow and Tangential Stresses (Time 100 hours)

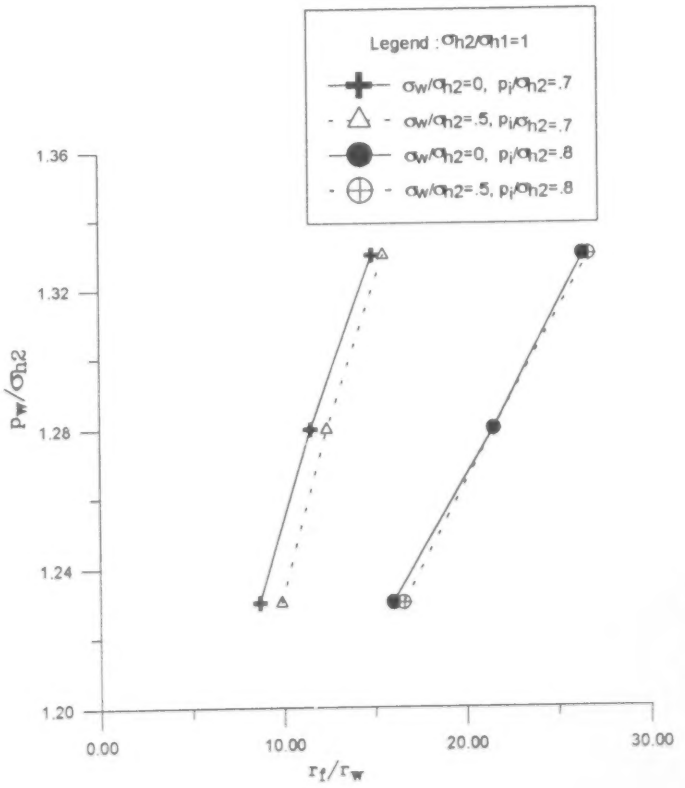

Figure 8.21 – Comparison of Radius of Potential Fracture Region Near Wellbore in Complete and Partial Stress Relief Conditions Pseudosteady–State Flow and Tangential Stresses (Time 1 hours)

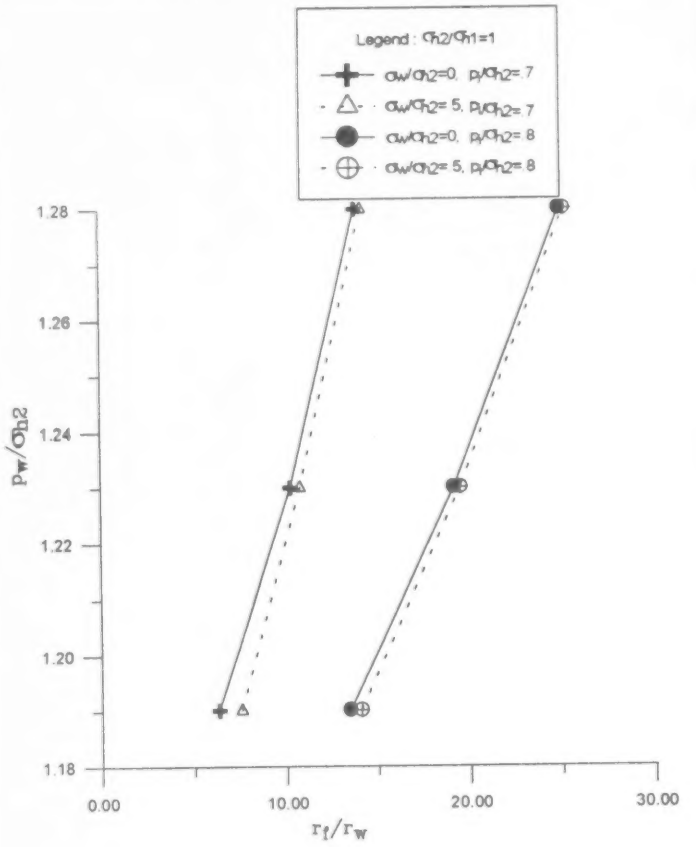

Figure 8.22 – Effect of Horizontal Stress Contrast and Injection Pressure, Steady–State Flow and Tangential Stresses

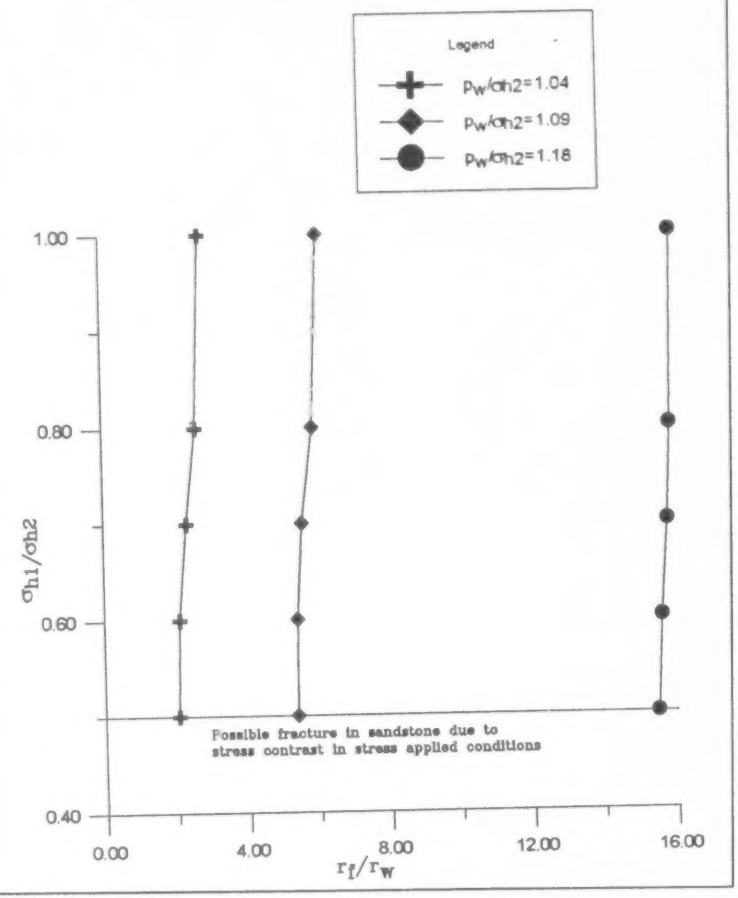

Figure 8.23 –Effect of Horizontal Stress Contrast and Injection Pressure, Transient Flow and Tangential Stresses (Time 100 Hours)

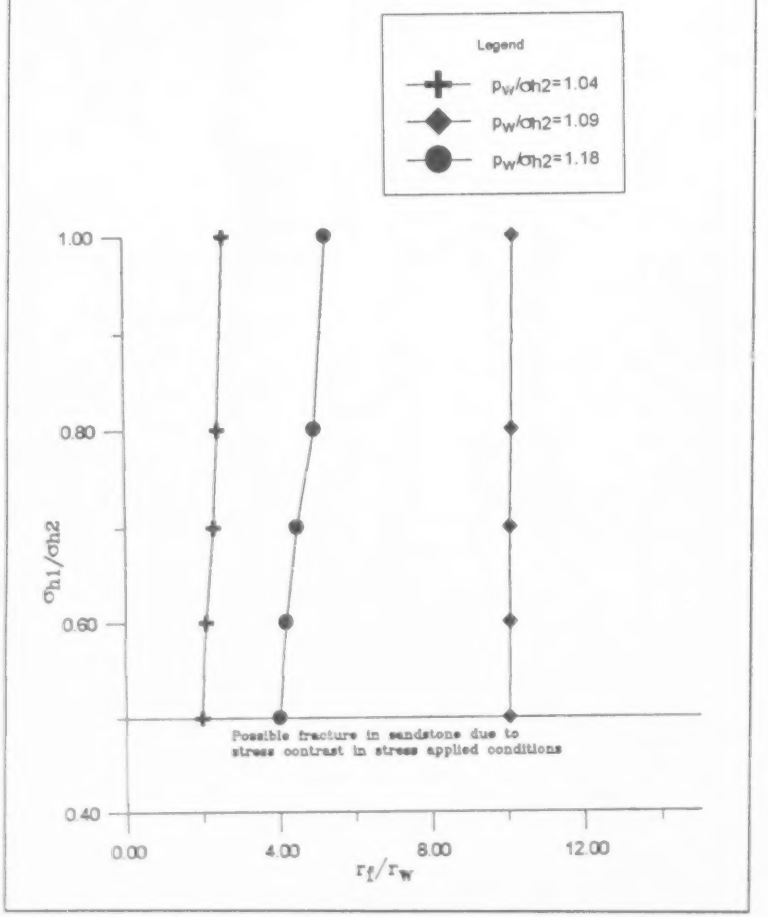

Figure 8.24 –Effect of Horizontal Stress Contrast and Injection Pressure, PseudoSteady–State Flow and Tangential Stresses (Time 1 Hour)

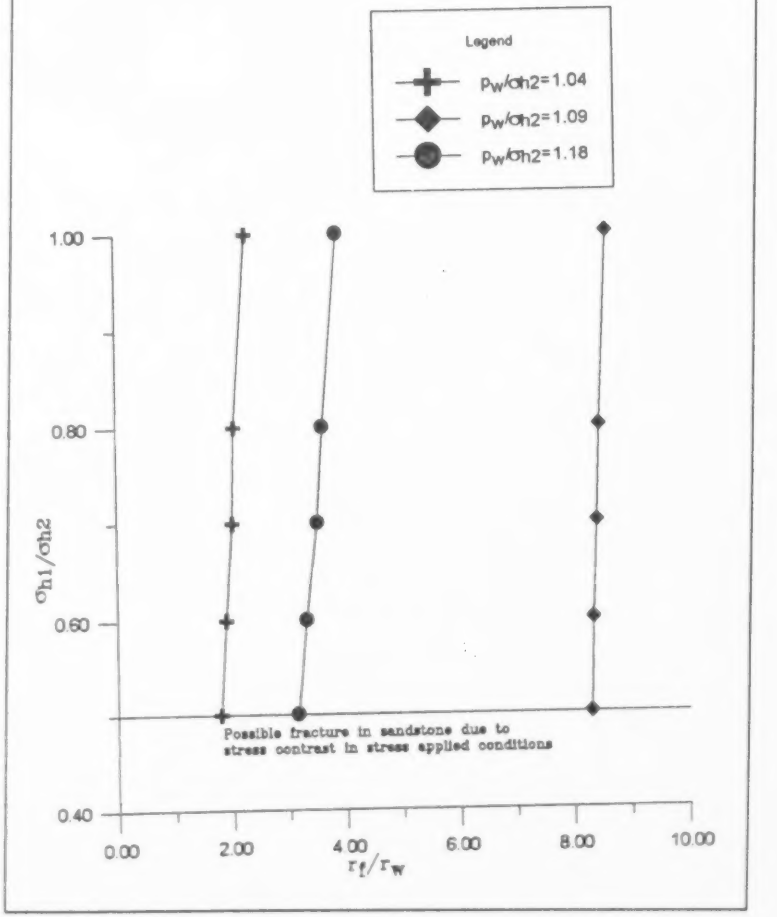

Figure 8.25 – Effect of Horizontal Stress Contrast and Injection Pressure, Steady–State Flow and Tangential Stresses in Complete and Partial Stress Relief Conditions

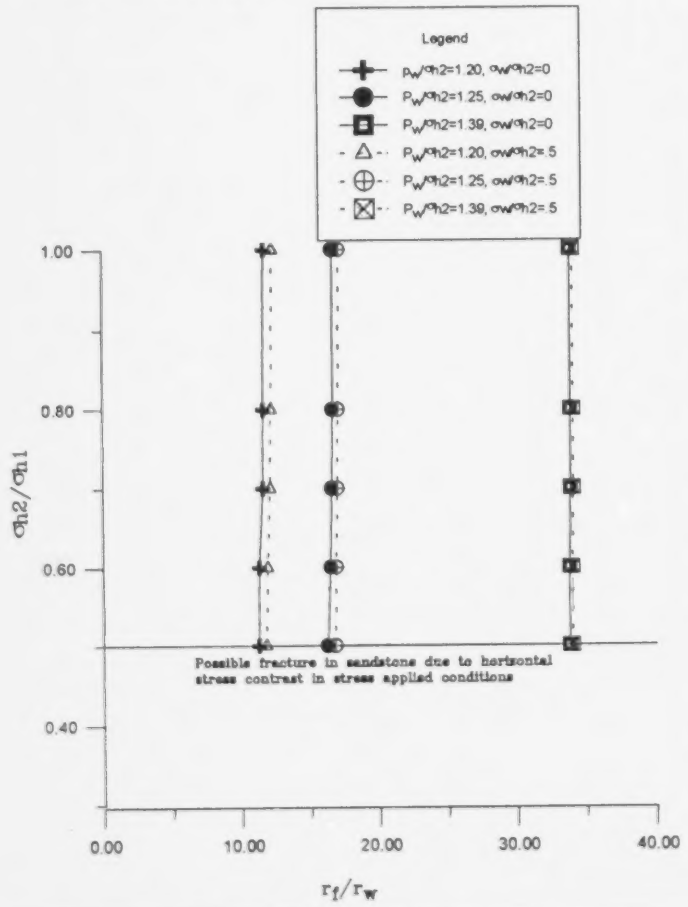

Figure 8.26 – Effect of Horizontal Stress Contrast and Injection Pressure, Transient Flow and Tangential Stresses in Complete and Partial Stress Relief Conditions (Time 100 Hours)

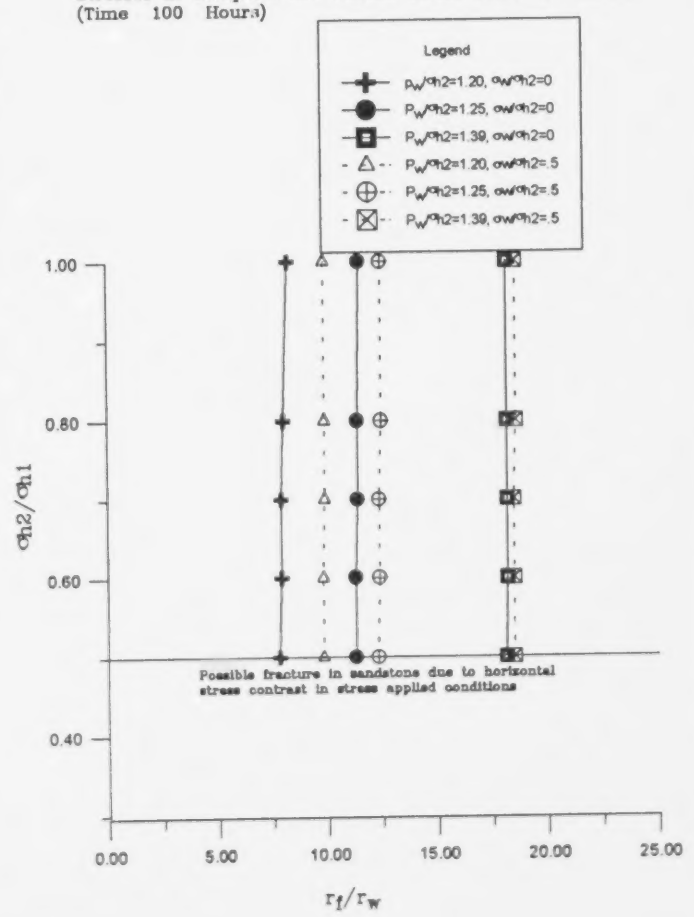

Figure 8.27 – Effect of Horizontal Stress Contrast and Injection Pressure, Pseuodsteady-State Flow and Tangential Stresses in Complete and Partial Stress Relief Conditions (Time 1 Hour)

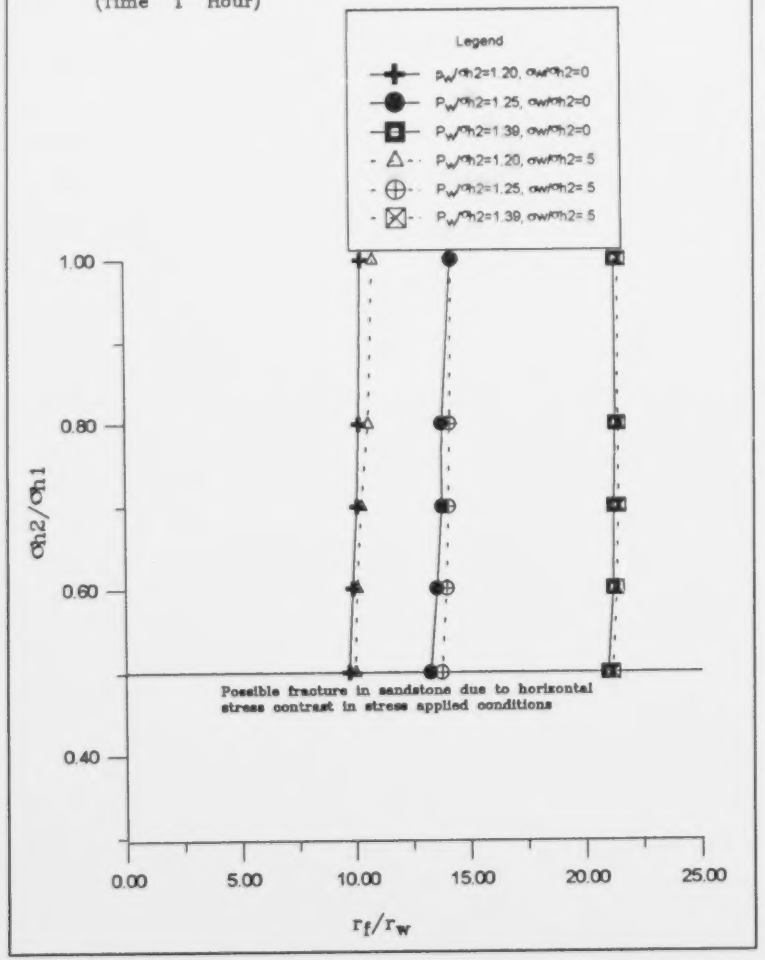

Figure 8.28 – Effect of Rate on the Radius of Potential Fracture Region, Transient Flow (Time 100 Hours)

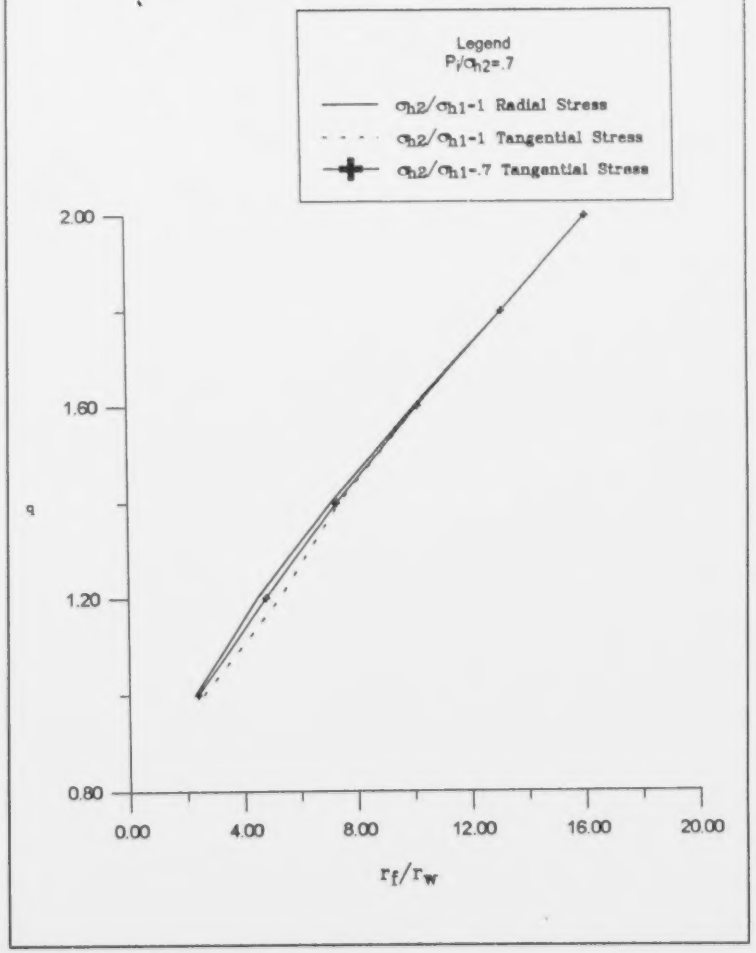

Figure 8.29 – Effect of Rate on the Radius of Potential Fracture Region, Pseudosteady–State Flow Conditions (Time 1 Hours)

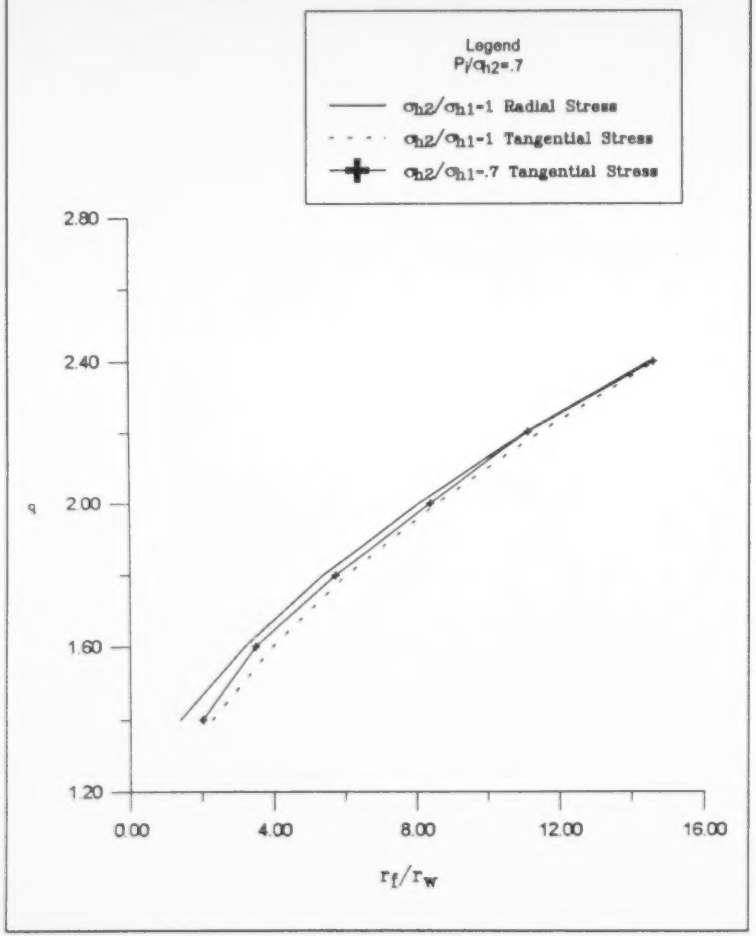

Figure 8.30 – Effect of Time on the Radius of Potential Fracture Region. Transient Flow Conditions

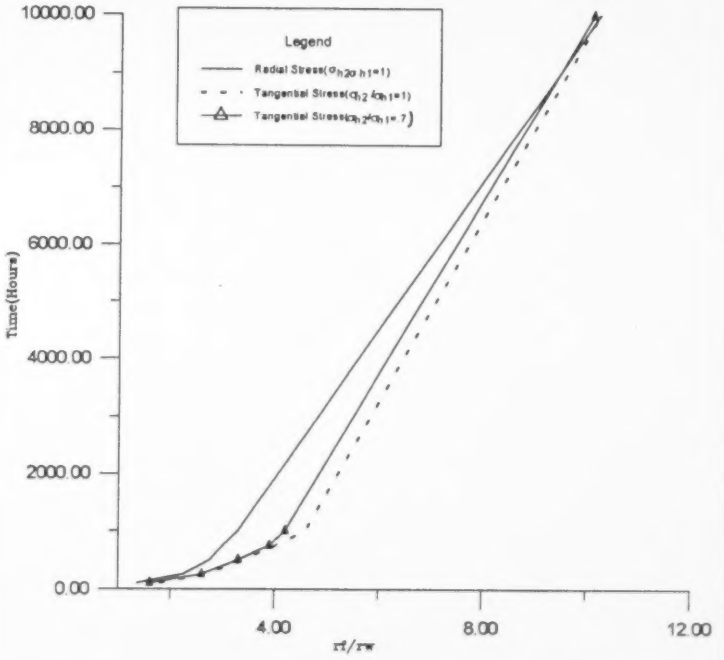

Figure 8.31 – Effect of Time on the Radius of Potential Fracture Region Pseudosteady–State Flow Conditions

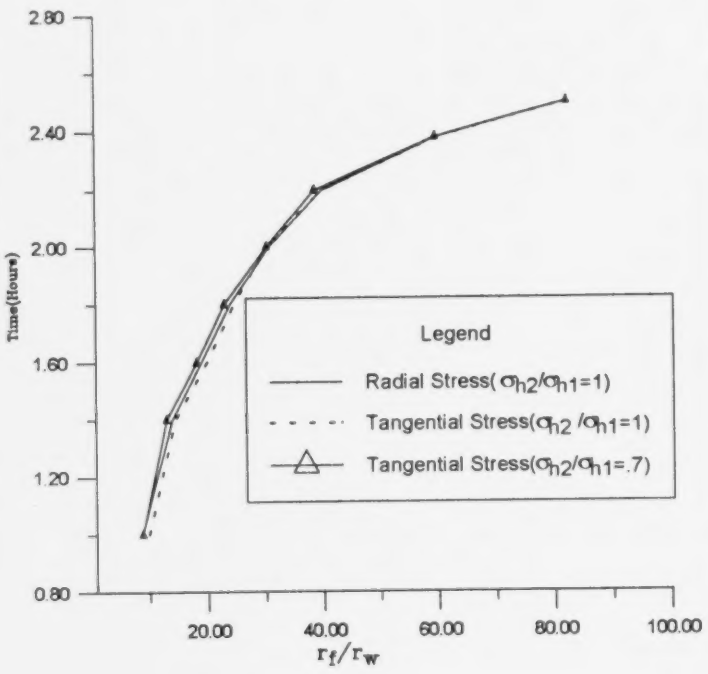

Figure 8.32 – Effect of Porosity, Viscosity and Compressibility on the Radius of Potential Fracture Region, Transient Flow (Time 100 Hours)

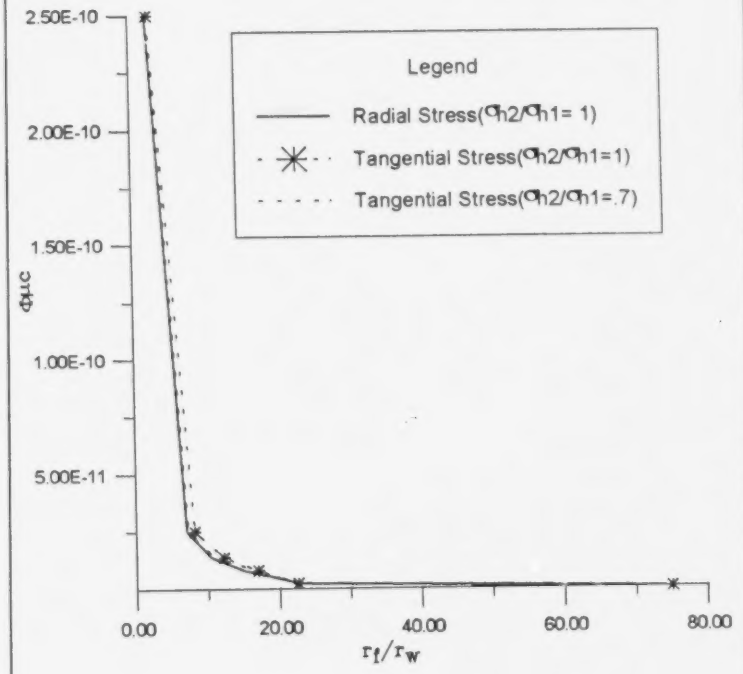

Figure 8.33 – Effect of Porosity, Viscosity and Compressibility on the Radius of Potential Fracture Region, Pseudosteady–State Flow Conditions (Time 1 Hour)

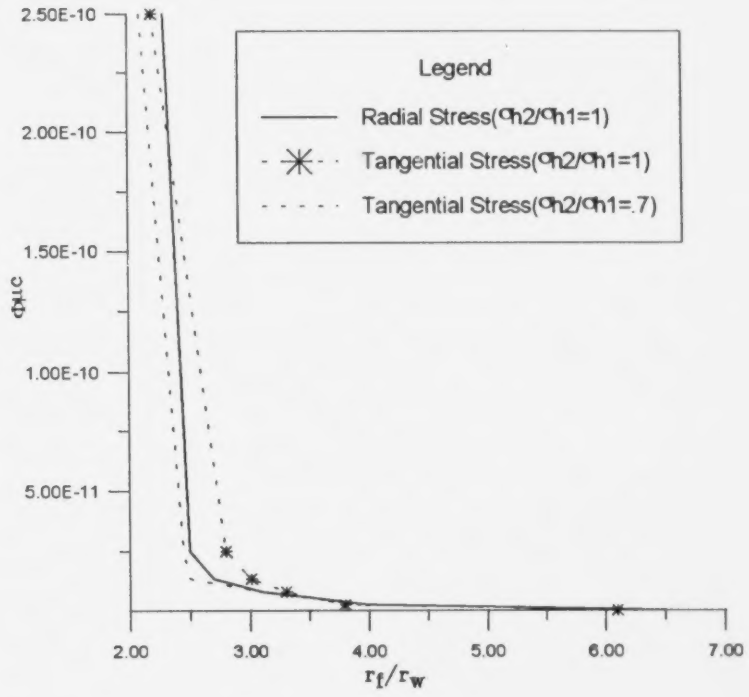

Chapter 9

CONCLUSIONS AND RECOMMENDATIONS

The main focus in this study has been identifying the potential fracture region that may develop when the wellbore injection pressure is higher than the minimum horizontal stress in the confining layer during injection and disposal operations. The models for calculating the radius of the potential fracture region were developed for steady-state, transient and pseudosteady-state flow conditions and the effects of different parameters on the extent of the potential fracture region were examined. The equations used were independent of material properties, therefore the effect of different material properties on the radius of potential fracture region has not been examined at this time.

9.1 Conclusions

The following conclusions may be drawn from this prelimenary study of fracturing in the confning layer:

1) The boundary of the region in which a fracture may occur in the confining layer can be determined if the injection zone pressure and far field stresses in the confining layer are known.

2) The radius of the potential fracture region depends on the ratio of the injection zone pressure and far field stress in the confining layer. Thus, the radius of the potential fracture region for a high-pressure shallow aquifer is the same as for a normally pressured deep aquifer.

3) The radius of the fracture region depends on the injection pressure and rate. Therefore, increasing the injection pressure or the rate increases the radius of the fracture region when the ratio of the injection zone pressure to the far field stress is kept constant.

4) The increase in the ratio of injection zone pressure to far field stress does not affect radial stresses near the wellbore under complete stress relief conditions when the stress field is isotropic. Away from the wellbore the radius of the potential fracture region increases with an increase in this ratio.

5) Only tangential stress changes permit the extension of a pre-existing crack in the confining layer when the stress field is anisotropic.

6) The radius of the potential fracture region, at low wellbore injection pressures, depends on packer setting depth and the annulus pressure above the packer. When the packer is set below the confining layer and a small annulus pressure is maintained, the radius of the potential fracture region decreases compared to when the packer is set above the confining layer and wellbore pressure can be transmitted directly to the confining layer.

7) The radius of the potential fracture region is not affected significantly by the horizontal stress contrast. Only a slight reduction in the radius has been observed with an increase in the anisotropy.

8) The injection zone fractures in tension when the minimum to maximum horizontal stress ratio is 0.5. Therefore it is not desirable to inject or dispose waste at this or any lower horizontal stress ratio.

9) The radius of the potential fracture region increases with injection time for pseudosteady-state and transient flow. However, the rate of increase is slower than for changes in the injection rate.

9.2 Recommendations

This preliminary study shows that there is a potential problem in 90% fracture pressure limit, set by Energy Resources Conservation Board, However, the results require experimental varification in the laboratory before applying them in the field. Therefore, we have the following recommendations:

1) Verify the results obtained by this study through the controlled experiments in the field or in the laboratory.

2) Study the effect of mechanical properties, strength properties and fracture toughness on the radius of potential fracture region and on the fracture propagation in the confining layer.

BIBLIOGRAPHY

Anderson, G.D., and Larson, D.B.(1978): "Laboratory Experiments on Hydraulic Fracture Growth Near an Interface," Proc. 19th U.S. Symposium on Rock Mechanics, Nevada, (May). pp. 332-342.

Boone, T.J., and Detournay, E.(1990): "Response of a Vertical Hydraulic Fracture Intersecting a Poroelastic Formation Bounded by Semi-Infinite Impermeable Elastic Layers," Inter-national Journal of Rock Mechanics, Mining Science and Geomechanics, (October). pp. 189-197.

Bradley,W.B.(1979): "Failure of Inclind Boreholes," Journal of Energy Resources Technical Transaction, ASME, (June). pp. 232-239.

Carmichael, R.S.(1982): *Hand Book of Physical Properties of Rocks*, **2**, CC Press, Florida, pp. 325-327

Cleary, M.P.(1978): "Primary Factors Governing Hydraulic Fractures in Heterogeneous Stratified Porous Formation," Paper 78-Pet-47, Presented at the ASME Energy Technological Conference, Houston, Texas (November). pp. 1-12.

Cleary, M.P.(1980): "Analysis of Mechanisms and Procedures for Producing Favorable Shapes of Hydraulic fractures," Paper SPE 9260, Presented at the SPE 55th Annual Fall Technical Conference, Dallas (September). pp. 1-16.

Daneshy, A.A.(1978): "Hydraulic Fracture Propagation in Layered Formation," Society of Petroleum Engineers Journal, (February).

Eekelen, H.A.(1980): "Hydraulic Fracture Geometry: Fracture Containment in Layered Formation," Paper SPE 9261, Presented at the SPE 55th Annual Fall Technical Conference, Dallas, (September). pp. 341-349.

Fjaer, E., Holt, R. M., Horsrud, P., Raaen, A. M., and Risnes, R.(1992): *Petroleum Related Rock Mechanics*, Elsevier press. pp. 116-124, 242-245 and 274-278.

Garon, A.M., Lin, C.Y., and Dunayevsky,V.A.(1988): "Simulation of Thermally Induced Water Flood Fracturing In Prudhoe Bay,"Paper SPE 17417, Presented at the SPE California Regional Meeting, Long Beach, (March). pp. 193-204.

Guo, F., Morgenstern, N.R., and Scott, J.D.(1993): "An Experimental Investigation into Hydraulic Fracture Propagation." International Journal of Rock Mechanics, Mining Science and Geomechanics Abstract. pp.1-35.

Hagoort, J., Weatherill, B.D., and Settari, A.(1978): "Modeling the propagation of water flood Induced Hydraulic Fractures," SPE Paper 7412 presented at SPE annual Technical Conference And Exhibition, Housten, Texas(August). pp. 293-303.

Haimson, B.C., and Fairhurst, C.(1969): "Hydraulic Fracturing in Porous-Permeable Materials", Journal of Petroleum Technology, (July). pp. 811-817.

Hardy, R.M.: *Engineering Problems Involving Pre consolidated Clay Shale*, (1959). pp. 1-3

Hubbert, M.K., and Willis, D.G.(1957): "Mechanics of Hydraulic fracturing," Trans. of AIME. **210** (February). pp. 153-163.

Jaeger, J.C., and Cook, N.G.W.(1979): *Fundamental of Rock Mechanics*, Chapman and Hall Press London. pp.186-188.

Kry, P.R., and Gronseth, J.M.(1982): "In Situ Stresses and Hydraulic Fracturing In the Deep Basin," Paper 82-3321 presented at the 33rd Annual Technical Meeting of the Petroleum Society of CIM, Calgary, (June).

Matthews, C.S., and Russel,D.G.(1967): "Mathematical Basis for Pressure Analysis Methods" ' Chapter 2 in Pressure Buildup and Flow Tests in Wells'. SPE monograph **1** (April). pp. 4-13.

Nolte, K.G.(1988): "Fracture Design Consideration Based on Pressure Analysis," Society of Petroleum Engineering Journal, (February). pp. 22-30.

Peterson, M.S.(1978): *Experimental Rock Deformation The Brittle Field*, Springer-Verlag Press, Berlin. pp. 16-46.

Robarts, A.(1977): *Geotechnology, An Introductory Text For Students and Engineers*, Pergamon Press Oxford. pp. 17-21

Rosepiler, M.J.(1979): "Determination of Principal Stresses and Confinement of Hydraulic Fractures In Cotton Valley," Paper SPE 8405, Presented at the SPE 54th Annual Fall Technical Conference, Las Vagas, Nevada (September). pp. 1-10.

Scott, P.P., Bearden, W.G., and Howard,G.C.(1953): "Rock Rupture as Affected by Fluid Properties," Transaction AIME (January). pp. 111-124.

Sidney, J.G., Griffin, R.M., and Pratt, H.R.(1973): "Stress-Strain and Failure Properties of a Porous Shale," Paper SPE 4242, Presented at the SPE Sixth Conference on Drilling and Rock Mechanics, Austin, Texas (January). pp. 117-128.

Simonson, E.R., Abou-sayed, A.S., and Clifton.R.J.(1976): "Containment of Massive Hydraulic Fractures," Paper SPE 6089, Presented at the SPE 51th Annual Technical Conference, and Exhibition, New Orleans (October). pp. 27-32.

Teufel, L.W., and Clark, J.A.(1984): "Hydraulic Fracture propagation in Layerd Rock: Experimental Studies of Fracture Containment," Society of Petroleum Engineers Journal (February). pp. 19-32.

Vutukuri. V.S., and Lama, R.D.(1978): *Hand Book on Mechanical Properties of Rocks*, **1**, Trans Tech Publication, Clausthal, Germany. pp. 104-106.

Vutukuri, V.S., and Lama, R.D.: *Hand Book on Mechanical Properties of Rocks*, **4**, Trans Tech Publication, Clausthal, Gremany. pp. 225-232

Veatch, R.W.(1983): "Overview of Current Hydraulic Fracturing Design and Treatment Technology-Part 1," Journal of Petroleum Technology, (April). pp. 677-687.

Veatch, R.W.(1983): "Overview of Current Hydraulic Fracturing Design and Treatment Technology-Part 2," Journal of Petroleum Technology, (May). pp 853-864.

Warpinski, N. R., Branggan, P., and Wilmer, R.(1985): "In-Situ Stress Measurements at U.S. DOE's Multiwell Experiment Site, Mesaverde Group, Rifle, Colorado," Journal of Petroleum Technology, (March). pp. 527-536.

Warpinski, N.R., Schmidt, R.A., and Northrop, D.A.(1980): "In Situ Stresses: The Predominant Influence on Hydraulic Fracture Containment," Paper SPE 8932, Presented at the SPE/DOE Symposium on Unconventional Gas Recovery, Pittsburg, Pennsylvania (May). pp. 83-94.

Whitehead, W.S., Holditch, S.A., and Hunt,E.R.(1987): "The effect of Lithology and Reservoir Pressure on the In-Situ Stresses in Waskom (Travis Peak) Field," Paper SPE 16403, Presented at the SPE/DOE Symposium on Low Permeability Reservoirs, Denver, Colorado (May). pp. 139-151.

Wyman, R.E., Holditch, S.A, and Randolph, P.L.(1980): "Analysis of an Elmworth Hydraulic Fracture in Alberta," Journal of Petroleum Technology, (September). pp. 1621-1630.

APPENDIX

C
C FORTRAN PROGRAMS USED IN THE STUDY
C
```
C**********************************************************************
C     PROGRAMS FOR STRESS PROFILE IN THE CONFINING LAYER
C
C**********************************************************************
C
C     RADIAL STRES IN ISOTROPIC STRESS FIELD
C     --------------------------------------
C
C
      OPEN(1,FILE='DATA.CON',STATUS='OLD')
      OPEN(2,FILE='DATA.BEH',STATUS='NEW')
      SIGE=1.0
      PW=1.04
      SIGW=PW
      RE=50
      RW=.1
      DO 20 I=I,20
      READ(1,*) R1
      WRITE(*,*) R1
      R=R1*RW
      WRITE(*,*) R
      SIGR=((SIGE*(RE**2))-(SIGW*(RW**2))+(((RW**2)*(RE**2))/R**2)
     + *(SIGW-SIGE))/((RE**2)-(RW**2))
      SIGR1=SIGR/SIGE
      WRITE(2,*) R,SIGR,SIGR1
20    CONTINUE
      END
C
C
C     RADIAL STRESS IN ANISOTROPIC STRESS FIELD
C     -----------------------------------------
C
C
      OPEN(1,FILE='DATA.CON',STATUS='OLD')
      OPEN(2,FILE='DATA.BEH',STATUS='NEW')
C     REQUIRE NO OF DATA POINTS AT THE TOP OF THE INPUT FILE
C     e.g IN THIS PROGRAM 20 SHOULD BE AT THE TOP OF INPUTFILE
      SGMAX=1.32
      SGMIN=1.00
      PW=1.04
      SIGW=PW
      RE=50.0
      RW=.1
      COSTH=1
      DO 10 I=I,20
      READ(1,*) R1
      WRITE(*,*) R1
      R=R1*RW
C     R=.1
C     WRITE(*,*) R
      S1=(SGMAX+SGMIN)/2
C     WRITE(*,*) SGMAX,SGMIN,PW,RW,R
      S2=((-SGMAX-SGMIN+(2*PW))/2)*(RW**2/R**2)
      S3=(((SGMAX-SGMIN)/2)*(1-((4*(RW**2))/(R**2))+(3*(RW**2)
     + *(RW**2))/((R**2)*(R**2)))*COSTH)
      SIGR=S1+S2+S3
      SIGR1=SIGR/SGMIN
      WRITE(2,*) R,SIGR,SIGR1
10    CONTINUE
      END
C
```

```
C
C       TANGENTIAL STRESS IN ISOTROPIC STRESS FIELD
C       -------------------------------------------
C
C
        OPEN(1,FILE='DATA.CON',STATUS='OLD')
        OPEN(2,FILE='DATA.BEH',STATUS='NEW')
        SIGE=1.0
        PW=1.04
        SIGW=PW
        RE=50
        RW=.1
        DO 20 I=I,20
        READ(1,*) R1
        WRITE(*,*) R1
        R=R1*RW
        WRITE(*,*) R
        SIGT=-((SIGW*(RW**2))-(SIGE*(RE**2))+(((RW**2)*(RE**2))/R**2)
     + *(SIGW-SIGE))/((RE**2)-(RW**2))
        SIGT1=SIGT/SIGE
        WRITE(2,*) R,SIGT,SIGT1
20      CONTINUE
        END
C
C
C       TANGENTIAL STRESS IN ANISOTROPIC STRESS FIELD
C       ---------------------------------------------
C
C
        OPEN(1,FILE='DATA.CON',STATUS='OLD')
        OPEN(2,FILE='DATA.BEH',STATUS='NEW')
C       REQUIRE NO OF DATA POINTS AT THE TOP OF THE INPUT FILE
C       e.g IN THIS PROGRAM 20 SHOULD BE AT THE TOP OF INPUTFILE
        SGMAX=1.325
        SGMIN=1.0
        PW=0.00
        SIGW=PW
        RE=50.0
        RW=.1
        COSTH=1
        DO 10 I=I,20
        READ(1,*) R1
C       WRITE(*,*) R1
        R=R1*RW
C       R=.1
        WRITE(*,*) R
        S1=(SGMAX+SGMIN)/2
C       WRITE(*,*) SGMAX,SGMIN,PW,RW,R
        S2=((SGMAX+SGMIN-(2*PW))/2)*(RW**2/R**2)
        S3=((SGMAX-SGMIN)/2)*(1+((3*(RW**2)
     + *(RW**2))/((R**2)*(R**2)))*COSTH)
        SIGT=S1+S2-S3
        SIGT1=SIGT/SGMIN
        WRITE(2,*) R,SIGT,SIGT1
10     CONTINUE
        END
C



C
```

```
C*********************************************************************
C   PROGRAMS FOR PORE PRESSURE PROFILE IN THE INJECTION ZONE AND
C   FOR THE RADIUS OF POTENTIAL FRACTURE REGION
C*********************************************************************
C
C
C     STEADY-STATE FLOW CONDITIONS
C     ============================
C
C
C     PORE PRESSURE PROFILE
C     ---------------------
C
C
      REAL PR,RW
      INTEGER R1
      OPEN(1,FILE='DATA.CON',STATUS='OLD')
      OPEN(2,FILE='DATA.BEH',STATUS='NEW')
      SIG2=1.0
      PW=1.04
      PE=.7
      RW=.1
      Re=50.
C     R1=1,2,4,10,20,40
      WRITE(*,*) 'R1'
      DO 10 I=1,22
      READ(1,*) R1
      WRITE(*,*) R1
      R=R1*RW
      WRITE(*,*) R
      PR=PW+((Pe-PW)/(LOG(Re/RW)))*lOG(R/RW)
      PR1=PR/SIG2
      WRITE(2,*)R,PR,PR1
10    CONTINUE
      END
C
C
C
C     RADIUS OF POTENTIAL FRACTURE REGION: TANGENTIAL STRESSES
C     --------------------------------------------------------
C
C
C
      IMPLICIT REAL*8 (A-H,O-Z)
      EPS=1.0D-8
      SIG2=1.0
      SIG1=1/.7
C     SIGMAW=0
      RE=50.0
      RW=0.1
      PW=1.04
      PE=.7
      X=SIG1/SIG2
      Y=PW/SIG2
      Z=PE/SIG2
      COSTH=1
      WRITE(*,*) 'GUESS, PW, PE EQS'
      READ(*,*) R,PW,PE,J
      SIGMAW=PW
      A=(((SIG1/SIG2)-(2*SIGMAW/SIG2))+1)*RW**2
      B=PW/SIG2-((SIG1/SIG2+1)/2)
      C=(PE-PW)/DLOG(RE/RW)*SIG2
      D=-((SIG1/SIG2)-1)/2
      E=3*(RW**4)
```

```
      WRITE(*,*) A,B,C,D,E,SIGMAW
      DO 5 I=1,100
      IF(J.EQ.1) THEN
      F=-A/(2*R**2)-(D*(1+(E/R**4)))*COSTH+C*DLOG(R/RW)+B
      DF=(A/R**3)+C/R+(4*D*E/R**5)*COSTH
      ELSE
      F=R-RW*DEXP((A/(2*C*R**2))-(B/C)+(D/C)+D*E/(C*(R**4)))
      DF=1-RW*DEXP((A/(2*C*R**2))-(B/C)+(D/C)+D*E/(C*(R**4)))*
     +(-A/(C*R**3)-(4*D*E/(C*(R**5))))
      ENDIF
      IF(DABS(F).LE.EPS) THEN
      GO TO 10
      ELSE
      R=R-F/DF
      ENDIF
    5 CONTINUE
   10 WRITE(*,*) R,F,I,Y,Z
      STOP
      END
C
C
C     RADIUS OF POTENTIAL FRACTURE REGION:RADIAL STRESSES
C     ---------------------------------------------------
C
C
      IMPLICIT REAL*8 (A-H,O-Z)
      EPS=1.0D-8
      SIGMAE=1
      SIGMAW=0
      RE=50.0
      RW=.1
      PW=1.04
      PE=.7
      WRITE(*,*) 'GUESS, PW, PE EQS'
      READ(*,*) R,PW,PE,J
      SIGMAW=PW
C     A=-PW/SIGMAE+(1-(SIGMAW*(RW**2)/(SIGMAE*(RE**2))))
      A=1-PW/SIGMAE
      B=((SIGMAW/SIGMAE)-1)*RW**2
      C=(PE-PW)/DLOG(RE/RW)*SIGMAE
      DO 5 I=1,100
      IF(J.EQ.1) THEN
      F=A+B/R**2-C*DLOG(R/RW)
      DF=-2.0*B/R**3-C/R
      ELSE
      F=R-RW*DEXP(A/C+B/(C*R**2))
      DF=1+RW*DEXP(A/C+B/(C*R**2))*2*B/(C*R**3)
      ENDIF
      IF(DABS(F).LE.EPS) THEN
      GO TO 10
      ELSE
      R=R-F/DF
      ENDIF
      D=PW/SIGMAE
      E=PE/SIGMAE
    5 CONTIN E
   10 WRITE(*,*) R,F,I,D,E
      STOP
      END
C
C
```

```
C
C     TRANSIENT FLOW CONDITIONS
C     =========================
C
C     PORE PRESSURE PROFILE
C     ---------------------
C
C
      REAL K,MU
      SIG2=1.0E06
      PHI=.25
      MU=1.0E-3
      C=1.0E-9
      K=9.862E-14
      T=3600.*100
      PI=.7E06
      RW=.1
      RE=50.0
      Q=.01196
      H=10.0
      GAM=1.78
      WRITE(*,*) 'GUESS'
      READ(*,*) R1
      R=R1*RW
      WRITE(*,*) R
      X=(PHI*MU*C*(R**2))/(4*K*T)
      EIX=X
      WRITE(*,*) R,X
C     DO 5 I=1,10
      IF(X.LE..01) THEN
      PR=PI+((Q*MU/(4*3.14*K*H))*LOG((4*K*T)/(GAM*PHI*MU*C*(R**2))))
      PR1=PR/SIG2
      ELSE
      WRITE(*,*) EIX
      WRITE(*,*) 'VALUE OF EIX'
      READ(*,*) EIX
      PR2=PI+((Q*MU/(4*3.14*K*H))*EIX)
      PR3=PR2/SIG2
      ENDIF
C  5  CONTINUE
      WRITE(*,*) PR,PR1,PR2,PR3
      STOP
      END
C
C
C
C     RADIUS OF POTENTIAL FRACTURE REGION: TANGENTIAL STRESSES
C     --------------------------------------------------------
C
C
C
      IMPLICIT REAL*8 (A-H,O-Z)
      REAL*8 MU,H
      EPS=1.0D-8
      SIGMAE=1.0
C     SIGMAW=0
      PI=.7
      Q1=.01196
      H=10.0
      PHI=.25
      MU=1.0D-3
      C=1.0D-6
      PER=9.862D-14
      T=3600.0*100
```

```
      RW=.1
      RE=50.0
      WRITE(*,*) 'GUESS,Q2'
      READ(*,*) R,Q2
      Q=Q1*Q2
      D=PI/SIGMAE-1
      E=(Q*MU/(4*3.14*PER*H*SIGMAE))/1.0E06
      PW=PI+E*(DLOG(4*PER*T/(1.78*PHI*MU*C*RW**2)))
      SIGMAW=PW
      WRITE(*,*) PW
      G=(SIGMAW/SIGMAE-1)*(RW**2)
      DO 35 I=1,200
      A=(PHI*MU*C*(R**2))/(4*PER*T)
      EIA=EI(A)
      F=D+E*EIA+(G/(R**2))
      DF=-E*(DEXP(-A)/A)-(2*G/(R**3))
      IF (DABS(F).LE.EPS) THEN
      GO TO 37
      ELSE
      R=R-F/DF
      ENDIF
   35 CONTINUE
   37 WRITE(*,*) R,F,I
      STOP
      END
C
C
C
      FUNCTION EI(A)
C=====================================================================
C
C
C                    SIMPSON'S 1/3 + 3/8 ALGORITHM
C                ( Good for both odd or even datapoints )
C
C=====================================================================
      IMPLICIT REAL*8 (A-H,O-Z)
      DIMENSION F(2010)
      B=10.5
      NP=2000
      NS=NP-1
      H=(B-A)/NS
      DO 5 J=1,NP
      X=A+(J-1)*H
      F(J)=DEXP(-X)/X
   5  CONTINUE
      J=1
      IF(NS/2*2.EQ.NS) THEN
      K=NS
      ELSE
      T=(3.*H/8.)*(F(NP-3)+3.*F(NP-2)+3.*F(NP-1)+F(NP))
      IF(NS.EQ.3) GO TO 25
      K=(NS-3)
      ENDIF
      DO 10 J=1,K,2
      T=T+(H/3.)*(F(J)+4.*F(J+1)+F(J+2))
   10 CONTINUE
   25 EI=T
      RETURN
      END
C
```

```
C
C     RADIUS OF POTENTIAL FRACTURE REGION:RADIAL STRESSES
C     ---------------------------------------------------
C
C
      IMPLICIT REAL*8 (A-H,O-Z)
      REAL*8 MU,H
      EPS=1.0D-8
      SIGMAE=1.0
C     SIGMAW=0
      PI=.7
      Q1=.01196
      H=10.0
      PHI=.25
      MU=1.0D-3
      C=1.0D-9
      PER=9.862D-14
      T=3600.0*100
      RW=.1
      RE=50.0
      WRITE(*,*) 'GUESS,Q2'
      READ(*,*) R,Q2
      Q=Q1*Q2
      D=PI/SIGMAE-1
      E=(Q*MU/(4*3.14*PER*H*SIGMAE))/1.0E06
      PW=PI+E*(DLOG(4*PER*T/(1.78*PHI*MU*C*RW**2)))
      SIGMAW=PW
      WRITE(*,*) PW
      G=(SIGMAW/SIGMAE-1)*(RW**2)
      DO 35 I=1,200
      A=(PHI*MU*C*(R**2))/(4*PER*T)
      EIA=EI(A)
      F=D+E*EIA-(G/(R**2))
      DF=-E*(DEXP(-A)/A)+(2*G/(R**3))
      IF (DABS(F).LE.EPS) THEN
      GO TO 37
      ELSE
      R=R-F/DF
      ENDIF
 35   CONTINUE
 37   WRITE(*,*) R,F,I
      STOP
      END
C
C
C
      FUNCTION EI(A)
C=====================================================================
C
C
C                  SIMPSON'S 1/3 + 3/8 ALGORITHM
C              ( Good for both odd or even datapoints )
C
C=====================================================================
      IMPLICIT REAL*8 (A-H,O-Z)
      DIMENSION F(2010)
      B=10.5
      NP=2000
      NS=NP-1
      H=(B-A)/NS
      DO 5 J=1,NP
      X=A+(J-1)*H
      F(J)=DEXP(-X)/X
 5    CONTINUE
```

```
      J=1
      IF(NS/2*2.EQ.NS) THEN
      K=NS
      ELSE
      T=(3.*H/8.)*(F(NP-3)+3.*F(NP-2)+3.*F(NP-1)+F(NP))
      IF(NS.EQ.3) GO TO 25
      K=(NS-3)
      ENDIF
      DO 10 J=1,K,2
      T=T+(H/3.)*(F(J)+4.*F(J+1)+F(J+2))
   10 CONTINUE
   25 EI=T
      RETURN
      END
C
C
C
C     PSEUDO STEADY STATE FLOW CONDITIONS
C     ===================================
C
C
C
C     PRESSURE PROFILE
C     ----------------
C
C
      REAL K,MU,A,B,D,E
      OPEN(1,FILE='DATA.CON',STATUS='OLD')
      OPEN(2,FILE='DATA.BEH',STATUS='NEW')
      SIG2=1.0E06
      PHI=.25
      MU=1.0E-3
      C=1.0E-9
      K=9.862E-14
      T=3600.0
      PI=.7E6
      RW=.1
      RE=50.0
      Q=.01196
      H=10.0
C     WRITE(*,*) 'GUESS'
C     READ(*,*) R1
      DO 5 I=1,24
      READ(1,*) R1
      R=R1*RW
      WRITE(*,*) R
      RD=R/RW
      RED=RE/RW
      TDW=K*T/(PHI*MU*C*(RW**2))
C     Q=QW*(RE**2-R**2/(RE**2-RW**2))
      WRITE(*,*) TDW
      A=(Q*MU/(2*3.14*K*H))
      B=2/(RED**2)
      D=((RD**2)/4)+TDW
      E=LOG(RED/RD)
C     WRITE(*,*) A,B,D,E
      F=A*((B*D)+E-3/4)
      PR=PI+(A*((B*D)+E-3/4))
      PR1=PR/SIG2
      WRITE(2,*) R,PR,PR1
    5 CONTINUE
      STOP
      END
C
```

```
C
C     RADIUS OF POTENTIAL FRACTURE REGION:TANGENTIAL STRESSES
C     -------------------------------------------------------
C
C
C

      IMPLICIT REAL*8 (A-H,O-Z)
      REAL*8 MU,K,G,PR
      EPS=1.0D-8
      SIG1=1.428
      SIG2=1.0
      RE=50.0
      RW=0.1
C     PW=0
      PI=.7
      COSTH=1
      PHI=.25
      MU=1.0D-3
      C=1.0D-6
      K=9.862E-14
      T=3600.0
      Q1=.01196
      HT=10.0
      WRITE(*,*) 'GUESS,Q2,EQS'
      READ(*,*) R,Q2,J
      Q=Q1*Q2
C     RD=R/RW
      RED=RE/RW
      TDW=K*T/(PHI*MU*C*(RW**2))
      WRITE(*,*) TDW
      A=PI/SIG2-((SIG1/SIG2+1)/2.)+((SIG1/SIG2-1)/2.)*COSTH
      B=Q*MU/(2.*3.14*K*HT*SIG2)/1.0E06
      H=1./(2.*RED**2)
      D=2.*TDW/RED**2+DLOG(RED)-.75
      PW=PI+(B*D)
      SIGMAW=PW
      E=0.5*(SIG1/SIG2-((2.*SIGMAW)/SIG2)+1)*RW**2
      G=-1.5*(SIG1/SIG2-1)*RW**4*COSTH
      WRITE(*,*) A,B,H,D,E,G,PW
      DO 5 I=1,100
      IF(J.EQ.1) THEN
      F=A+((B*H*(R**2))/(RW**2))+(B*D)-(B*DLOG(R/RW))-E/(R**2)-
     + (G/(R**4))
      DF=((2*B*H*R)/(RW**2))-(B/R)+((2*E)/(R**3))+((4*G)/(R**5))
      ELSE
      F=R-RW*DEXP(((-E/(R**2))-(G/(R**4))+(A)+(B*H*(R**2))/(RW**2)+
     +(B*D))/B)
      DF=1-RW*DEXP(((-E/(R**2))-(G/(R**4))+(A)+(B*H*(R**2))/(RW**2)+
     +(B*D))/B)*(((2*E/(R**3))+(4*G/(R**5))+(2*B*H*R/(RW**2)))/B)
      ENDIF
      IF(DABS(F).LE.EPS) THEN
      GO TO 10
      ELSE
C     WRITE(*,*) R,F,DF,I
      R=R-F/DF
      ENDIF
      Y=PW/SIG2
      Z=PI/SIG2
    5 CONTINUE
   10 WRITE(*,*) R,F,I,Y,Z
C 10 WRITE(*,*) R,F,I
      STOP
      END
```

```
C
C
C     RADIUS OF POTENTIAL FRACTURE REGION:RADIAL STRESSES
C     ---------------------------------------------------
C
C
C
      IMPLICIT REAL*8 (A-H,O-Z)
      REAL*8 MU,K,G,PR,HT,H
      EPS=1.0D-8
      SIGMAE=1.0
      RE=50.0
      RW=0.1
C     PW=1.04
      PI=.7
      COSTH=1
      PHI=.25
      MU=1.0E-3
      C=1.0E-7
      K=9.862E-14
      T =3600.0
      Q1=.01196*1.4
      HT=10.0
      WRITE(*,*) 'GUESS,Q2'
      READ(*,*) R,Q2
      Q=Q1*Q2
C     RD=R/RW
      RED=RE/RW
      TDW=K*T/(PHI*MU*C*(RW**2))
      A=1-PI/SIGMAE
      B=Q*MU/(2.*3.14*K*HT*SIGMAE)/1.0E06
      H=1./(2.*RED**2)
      D=2.*TDW/RED**2+DLOG(RED)-.75
      PW=PI+(B*D)
      SIGMAW=PW
      E=(SIGMAW/SIGMAE-1)*RW**2
      WRITE(*,*) E
      DO 5 I=1,100
      F=R-RW*DEXP(-E/(B*(R**2))+(A/B)+((H*(R**2))/(RW**2))+D)
      DF=1-RW*DEXP(-E/(B*(R**2))+(A/B)+((H*(R**2))/(RW**2))+D)*
     +(2*E/(B*(R**3))+2*H*R/(RW**2))
      IF(DABS(F).LE.EPS) THEN
      GO TO 10
      ELSE
      R=R-F/DF
      ENDIF
    5 CONTINUE
   10 WRITE(*,*) R,F,I
      STOP
      END
```